Development and Assessment of Metal Containing Drugs as Model Radiopharmaceuticals for Cancer Treatment

by

Phillipus Chrisstoffel Willem van der Berg

A dissertation submitted to meet the requirements for the degree of

Magister Scientiae

in the

Department of Chemistry

Faculty of Natural- and Agricultural Sciences

at the

University of the Free State

Supervisor: Prof. Hendrik G. Visser

Co-Supervisor: Prof. Andreas Roodt

January 2013

Acknowledgements

I wish to express my gratitude to the following:

First and foremost, I would like the thank my God and Heavenly Father for the countless blessings that You have bestowed on me and for allowing me to understand great and unsearchable things which I did not know. The honour and the glory of all belong to You for I am nothing without You.

Thank you to Prof. Andreas Roodt for all his guidance and encouragement. Your endless enthusiasm for chemistry makes learning chemistry an adventure. It is an honour to be known as one of your students.

To Prof. Hendrik G. Visser, thank you for all your guidance, patience, endurance, leadership and perseverance throughout the course of this work. Your patience and willingness to give advice when things just don't go as planned is what kept me motivated throughout my studies.

Thank you to all my colleagues in the Inorganic group for all their computer skills and patience when having to explain something several times. Every one of you contributed to the success of this study in some way and for that I thank you.

To my parents, Karel and Cecilia van der Berg, and my brother, Karel van der Berg, and my two sisters, Annelie Deetlifts and Theresa Walldick, without your love, support, faith, sacrifices, understanding and continuous encouragement this would not be possible.

The financial assistance from the University of the Free State, NTeMBI, NRF/THRIP and Sasol towards this research is hereby gratefully acknowledged.

Table of contents

Table of contents

Table of contents

Table of contents

Abbreviations and Symbols

Abbrevaition	Meaning
SPECT	Single photon emission computed tomography
PET	Positron emission tomography
DNA	Deoxyribonucleic acid
BFCA	Bifunctional chelate approach
NRU	National Research Universal
HFR	High Flux Reactor
DOTA	1,4,7,10-tetraazacyclododecane-1,4,7,10-teraacetic acid
NOTA	1,4,7-triazacyclonane-1,4,7-triacetic acid
EDTA	Ethylenediaminetetraacetic acid
DTPA	Diethylene triamine pentaacetic acid
TAME Hex	Tris(aminomethyl)ethane-*N*,*N*,*N'*,*N'*,*N''*,*N''*-hexaacetic acid
TATE	(Tyr^3)octreotate
hEGF	Human epidermal growth factor
FDG	^{18}F-fluorodeoxyglucose
LET	Linear energy transfer
NHS	N-hydroxysuccinimide
NCl	National Cancer Institute
γ	Gamma
α	Alpha
β	Beta
A	Absorbance (theoretical)
A_{obs}	Observed absorbance
nm	Nanometre
mmol	Millimol
g	Gram
Å	Armstrong
IR	Infra Red
ν	IR stretching frequency
NMR	Nuclear Resonance Spectroscopy
XRD	X-Ray diffractometry
UV/Vis spectroscopy	Ultraviolet/Visible spectroscopy
MeV	Millielectronvolt
µl	Microliter
µM	Micromolar
di-Mebpb	*N*,*N'*-(4,5-Dimethyl-1,2-phenylene)bis(pyridine-2-carboxamide)
bpb	*N*,*N'*-(1,2-phenylene)bis(pyridine-2-carboxamide)
$[Ga(bpb)(H_2O)_2]NO_3 \cdot CH_3OH$	[Ga(*N*,*N'*-(1,2-phenylene)bis(pyridine-2-carboxamide))$(H_2O)_2$]$NO_3 \cdot CH_3OH$
$[Ga(di\text{-}Mebpb)(H_2O)_2]NO_3$	[Ga(*N*,*N'*-(4,5-Dimethyl-1,2-phenylene)bis(pyridine-2-carboxamide))$(H_2O)_2$]NO_3

Abbreviations and Symbols

[Au(bpb)]Cl	[Au((*N*,*N'*-(1,2-phenylene)bis(pyridine-2-carboxamide))]Cl
[(Mebpb)toluene]	3,4-Bis(pyridine-2-carboxamido)toluene
dmbpy	4,4'-dimethylbipyridine
TPP	5,10,15,20-tetraphenylporphin
terpy	2,2':6',2"-terpyridine
Z	Number of molecules in a unit cell
k_x	Rate constant for a forward equilibrium reaction
k_{-x}	Rate constant for a backward equilibrium reaction
K_x	Equilibrium constant for an equilibrium reaction
K_{obs}	Observed rate constant
ppm	(Unit of chemical shift) parts per million
MeOH	Methanol
DMSO	Dimehtylsulfoxide
λ	UV/Vis wavelength
$\Delta H^{\neq}$	Entalpy of activation
$\Delta S^{\neq}$	Entropy of activation
M	$mol.dm^{-3}$
TMS	Tetramethylsilane
MTT	(3-(4,5-dimethylthazol-2-yl)-2,5-diphenyl tetrazolium bromide)
FDA	Food and drug administration

Abstract

This research focuses on the development of new teatradentate carboxamide ligands and their coordination to gallium(III) and gold(III). The solid state characteristics and reactivity studies in solution of these model compounds would give more insight into the behaviour of radiopharmaceuticals for cancer treatment.

The crystallographic characterization of two carboxamide ligands, di-Mebpb and bpb and two metal complexes, $[Ga(bpb)(H_2O)_2]NO_3 \cdot CH_3OH$ and [Au(bpb)]Cl, is fully discussed and compared to literature in Chapter 5. The ligand, di-Mebpb crystallizes in a non-centrosymmetric, monoclinic *Cc* space group, with four molecules per unit cell. The ligand, bpb crystallizes in a centrosymmetric monoclinic $P2_1/c$ space group, with four molecules in the unit cell. The dihedral angles between the central phenyl ring and the two picoline rings for the di-Mebpb ligand, is calculated as 57.06(5) ° and 22.05(8) °, respectively and the dihedral angle between the central phenyl ring and the two picoline rings of the bpb ligand are calculated as 57.82(4) ° and 17.96(7) °, respectively. $[Ga(bpb)(H_2O)_2]NO_3 \cdot CH_3OH$ crystallizes in a centrosymmetric, orthorhombic *Pbca* space group, with four molecules per unit cell while the [Au(bpb)]Cl, complex crystallizes in a centrosymmetric, triclinic $P\bar{1}$ space group, with two molecules per unit cell. The octahedron around the gallium(III) ion is somewhat distorted as indicated by the large bite angle of N1-Ga-N4 (115.03(1) °) and the small bite angle of O4-Ga-O3 (161.62(1) °). The gold(III) complex crystallizes in a distorted square planar formation with the gold(III) deviating 0.0518(3) Å from the plane formed by the four coordinating nitrogen atoms (N1-N2-N3-N4) and the bond angles of N-Au-N range from 81.8(2) ° to 111.9(2). °.

A kinetic investigation was conducted to follow the rate at which methanol is substituted from a *trans*-$[Ga(bpb)(CH_3OH)_2]^+$ complex with 4-methylpyridine as entering ligand. The proposed substitution mechanism is postulated to involve two distinguishable reaction steps. The equilibrium constant, K_1, for the first methanol substitution was obtained as ~1 M^{-1} from the overall equilibrium constant, $K_{overall}$, which was determined as 44(2) M^{-1}. The equilibrium constants, K_2 and K_3, were determined as 5.8(1) M^{-1} and 6(1) M^{-1}, respectively at 25.0 °C.

Abstract

The rate constant for the second substitution step, k_3, was determined as 8.5(1) x 10^{-4} (s^{-1}) which is much slower than what was expected at 25.0 °C. A large negative $\Delta S^{\neq}$ value of -122(10) (J K^{-1}.mol^{-1}) was determined for the forward reaction (k_3), which suggests an associative mechanism for the MeOH substitution with 4-mepy as entering ligand, but high pressure kinetic studies are required to investigate this fully.

Cell studies were performed on two newly synthesized compounds, di-Mebpb and $[Ga(bpb)(H_2O)_2]NO_3 \cdot CH_3OH$. These compounds were tested on oesophageal cancer cell lines which showed promising results towards inhibition, however it was not reactive enough to be considered as active substance for inhibition, with respective IC_{50} values of 3.796 µM and 2.285 µM for di-Mebpb and $[Ga(bpb)(H_2O)_2]NO_3 \cdot CH_3OH$.

Opsomming

Hierdie navorsing fokus op die ontwikkeling van nuwe tetradentate karboksamied ligande en hulle koördinasie aan gallium(III) en goud(III). Die vaste toestand eienskappe en reaktiwiteit studies in oplossing van hierdie model komplekse bied `n dieper insig in die gedrag van radiofarmaseutika vir kanker behandeling.

Die kristallografiese eienskappe van twee karboksamied ligande, di-Mebpb en bpb, en twee metal komplekse, $[Ga(bpb)(H_2O)_2]NO_3 \cdot CH_3OH$ en [Au(bpb)]Cl, word volledig bespreek en met literatuur vergelyk in Hoofstuk 5. Die ligand di-Mebpb kristalliseer in die nie-sentrosimmetriese, monokliniese *Cc* ruimtegroep, met vier molecule per eenheidsel. Die ligand bpb kristalliseer in die sentrosimmetriese, monokliniese $P2_1/c$ ruimtegroep, met vier molecule per eenheidsel. Die dihedriese hoeke tussen die sentrale feniel ring en die twee pikolien ringe in die di-Mebpb ligand is bereken as 57.06(5) ° en 22.05(8) °, onderskeidelik, en dihedriese hoeke tussen die sentrale feniel ring en die twee pikolien ringe in die bpb ligand is bereken as 57.82(4) ° en 17.96(7) °, onderskeidelik. $[Ga(bpb)(H_2O)_2]NO_3 \cdot CH_3OH$ kristalliseer in die sentrosimmetriese, ortorombiese *Pbca* ruimtegroep, met vier molecule per eenheidsel, terwyl die [Au(bpb)]Cl kompleks in die sentrosimmetriese, $P\bar{1}$ ruimtegroep kristalliseer, met twee molecules per eenheidsel. Die octa hedron rondom die gallium(III) ioon is effens vervorm, soos aangedui deur die groot bythoek van N1-Ga-N4 (115.03(1) °) en die klein bythoek van O4-Ga-O3 (161.62(1) °. Die goud(III) kompleks kristalliseer in `n vervormde vierkantig planêre vormasie met `n uitwyking van 0.0518(3) Å vir die goud(III) atom uit die vlak gevorm deur die vierkoördinerende stikstof atome (N1-N2-N3-N4) en bindingshoeke van N-Au-N wat wissel van 81.8(2) ° tot 111.9(2) °.

`n Kinetiese ondersoek is uitgevoer om die tempo waarteen methanol uit *trans*-$[Ga(bpb)(CH_3OH)_2]^+$ vervang word deur 4-metielpiridien vas te stel. Die voorgestelde uitruilings meganisme behels twee onderskeibare reaksie stappe. Die ewewigskonstante, K_1, vir die eerste methanol substitusie is vasgestel as ~1 M^{-1} uit die algehele ewewigskonstante, $K_{algeheel}$, wat vasgestel is as 44(2) M^{-1}. Die ewewigskonstantes, K_2 and K_3, is vasgestel as onderskeidelik 5.8(1) M^{-1}en 6(1) M^{-1} teen 25.0 °C.

Opsomming

Die tempo konstante vir die tweede substitusie stap, k_3, is vasgestel as 8.5(1) x 10^{-4}(s^{-1}), wat aansienlik stadiger is as wat verwag is teen 25.0 °C. `n Groot negatiewe $\Delta S^{\neq}$ waarde van -122(10) ($J.K^{-1}.mol^{-1}$) is vasgestel vir die voorwaarts se reaksie ($k_3$), wat `n assosiatiewe meganisme vir die MeOH substitusie deur 4-mepy as inkomende ligand voorstel, maar hoë-druk kinetiese studies word benodig om dit volledig te ondersoek.

Sel studies is uitgevoer op twee nuut vervaardigde verbindings, di-Mebpb en $[Ga(bpb)(H_2O)_2]NO_3 \cdot CH_3OH$. Hierdie verbindings is getoets op esofagiale kanker sel lyne en het belowende resultate getoon ten opsigte van inhibisie, maar was met onderskeie IC_{50} waardes van 3.796 en 2.285 vir di-Mebpb en $[Ga(bpb)(H_2O)_2]NO_3 \cdot CH_3OH$ nie reaktief genoeg om as aktiewe komplekse vir inhibisie oorweeg te word nie.

1 Introduction and Aim

1.1 Introduction

The global burden of cancer continues to increase because of aging, the growth of the world population and cancer-causing behaviours, such as smoking. GLOBOCAN estimate that approximately 12.7 million cancer cases and 7.6 million cancer deaths were reported in 2008. Breast cancer is the most commonly diagnosed and the leading cause of death amongst females, accounting for 23 % of the total cancer cases and 14 % of total cancer deaths, whereas lung cancer is the leading cause of cancer in males, accounting for 17 % of total the total cancer cases and 23 % of the cancer deaths.[1]

These statistics are certainly alarming, which is why an interest among scientists is on the rise to develop new drugs for earlier detection and treatment of the disease.

Radiopharmaceuticals are medical formulations containing radioactive nuclides (radioisotopes) which are safe for humans and can be used in nuclear medicine applications for the diagnosis or therapy of various diseases. More than 80 % of current radiopharmaceuticals are used for diagnosis. The radioactive nuclides used for diagnosis are photon emitters – gamma (γ) and positron particles (β^+) while therapeutic radionuclides are alpha (α) or beta (β^-) emitters.[2]

Diagnostic and therapeutic pharmaceuticals are mostly small organic and inorganic compounds with definite composition, but they can also be marcomolecules such as monoclonal antibodies and antibody fragments that are labelled with a radioactive nuclide. Radiopharmaceuticals can be divided into two classes: those whose chemical and physical

[1] Jemal, A., Bray, F., Center, M. M., Ferlay, J., Ward, E., Forman, D., CA. Cancer J. Clin., **61**, 69-90, 2011.
[2] Zuckman, S. A., Freeman, G. M., Trouter, D. E., Volkert, W. A., Holmes, R. A., Van Derveer, D. G., Barefield, E. K., *Inorg. Chem.*, **20**, 2386, 1981.

properties determine their biodistribution and those whose biodistribution are determined by their biological interactions or receptor binding.[3]

1.2 History of Radiopharmaceuticals and Nuclear Medicine

Many scientists in different disciplines contributed to the history of nuclear medicine and because of the multidisciplinary nature of Nuclear Medicine it is difficult to determine the exact date of discovery.

Artificial radionuclides were first discovered by Frederic Joliot-Curie and Irene Joliot-Curie in 1934 and were considered to be the most significant milestone in nuclear medicine. The first clinical trial with artificial radioisotopes was done in 1937 for the treatment of leukemia at the University of California. George de Hevesy was the first to use radioactive tracers, while studying transport systems from roots to leaves in plants and he was also involved in the first administration of radioactive compounds (Na_3PO_4) to humans in 1937 where he investigated the excretory route of phosphorous. The first successful treatment with ^{32}P was in 1939 for a disease called polycythemia vera, where an excess of red blood cells and sometimes white blood cells are produced due to an abnormality in the bone marrow.[2]

In 1946, it was discovered that ^{131}I can be used for the treatment of thyroid cancer and its use later expanded to include imaging of the thyroid gland, quantification of the thyroid function and therapy for hyperthyroidism.[2] In the 1950's the development of the gamma camera revolutionized the nuclear medicine field, nuclear reactors, cyclotrons and accelerators to be used for the production of medical radioactive isotopes. Widespread clinical use of nuclear medicine started to grow rapidly in the 1950's as the knowledge grew about radionuclides, detection of radioactivity, using certain radionuclides to trace biochemical processes.[2] The Society of Nuclear Medicine began the publication of the Journal of Nuclear medicine in 1960.

In the 1970's most organs of the human body could be imaged using Nuclear Medicine procedures[2] and in 1971, American Medical Assosiation officially recognized nuclear medicine as a medical specialty. By the 1980's, the equipment was sophisticated enough to

[3] Shuang, L., Edwards, D. S., *Chem. Rev.*, **99**, 2235, 1999.

diagnose heart conditions and today there are more than 100 different procedures that use radioisotopes for diagnosis and treatment of different conditions in the human body.

1.3 Metals used in Radiopharmaceuticals

The use of radiometals in nuclear medicine imaging and therapy is a relatively new area and the majority of radiopharmaceuticals (95 %) are used for diagnostic purposes (imaging). These involve the determination of the organ function, shape, or position of the radioactivity distribution within an organ or region in the body from an image.[4] Two main modalities used in nuclear medicine for imaging are SPECT (single photon emission computed tomography) and PET (positron emission tomography).[5]

In the late 1950's David E. Kuhi and Roy Edwards introduced SPECT which involve an imaging technique that uses gamma rays and is able to provide a 3D image of a patient's functional information. The technique requires a radiopharmaceutical (radionuclide attached to a pharmaceutical). The radioisotope is of interest only for its radioactive properties and the pharmaceutical is of interest for its chemical binding properties to certain types of tissues. The injected radiopharmaceutical will concentrate in the area of interest after which it can be detected by a gamma camera. The gamma detectors used today are designed for detection of lower energy single photon emitting radioisotopes, like 140 keV for ^{99m}Tc and about 72 keV for X-rays ^{201}Tl.[6] The ^{99}Mo/^{99m}Tc generator system was developed in 1959 by the Brookhaven National Laboratory[4,7] and the most used isotope in nuclear medicine is the daughter isotope ^{99m}Tc with half life of 6 hours and emits at 140 keV γ-ray with 89 % abundance which is nearly optimal for imaging with commercial gamma cameras.[5]

Michel Ter-Pogossen developed Positron Emission Tomography (PET) in the 1970's which involves a short-lived radioactive substance which is injected into the human body and after a period produces 3D images of the organ or tissue of interest with the imaging scanner. When the positron-emitting radionuclide decays, a positron is emitted from the nucleus and travels in the tissue for a short distance during which time it loses kinetic energy, until it decelerates

[4] McCarthy, T. J., Scharz S. W. and Welch, M. J., *J. Chem. Ed.*, **71**, 830.
[5] Bartholoma, M. D., Loie, A. S., Valliant, J. F. and Zubieta, J., *Chem. Rev.*, **110**, 2903-2920, 2010.
[6] Anderson, C. J. and Welch, M. J., *Chem. Rev.*, **99**, 2219, 1999.
[7] Harper, P. V., Beck, R., Charleston, D., Lathrop, K. A., *Nucleonics*, **22**, 50, 1964.

to a point where it can interact with an electron producing a pair of annihilation (gamma) photons moving in approximately opposite directions.[4,8]

Radioisotopes such as ^{15}O ($t_{1/2}$ =2 min), ^{13}N ($t_{1/2}$ =10 min), ^{11}C ($t_{1/2}$ = 20 min) and ^{18}F ($t_{1/2}$ = 110 min) are generally used for PET imaging because of their short half lives. These radioisotopes are incorporated in molecules (water, glucose and ammonia) normally used by the human body. Therefore, their distribution can be traced. The development of PET as a clinically imaging modality has its origin due to the synthesis of fluorine-18 fluorodeoxyglucose (FDG), a glucose analogue where the oxygen atom is replaced by ^{18}F (Figure 1.1).[4] FDG is the most widely used ^{18}F radiotracer for PET.

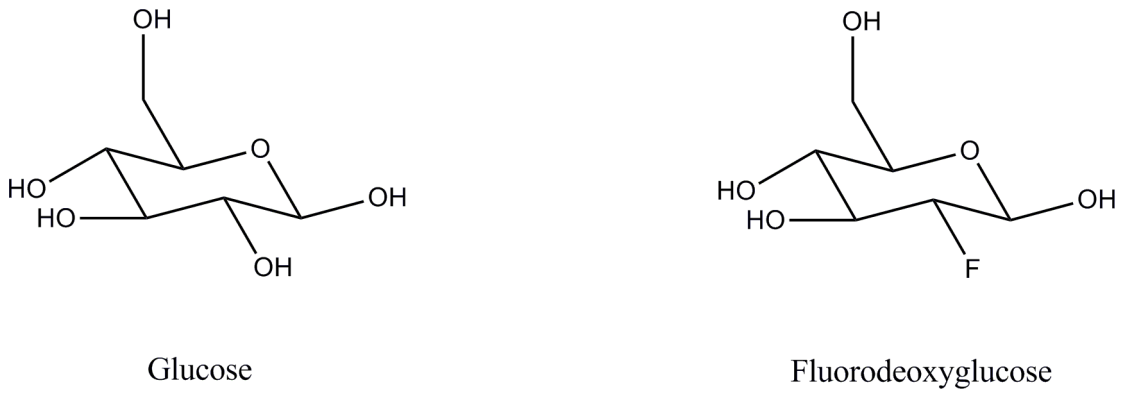

Figure 1.1 Molecule structures of glucose and Fluorodeoxyglucose[4]

The FDG molecule is taken up as glucose and serves as a substrate for hexokinase, but due to the structural differences from the original molecule, glucose, the FDG is trapped in the cell because phosphorylation cannot continue (Figure 1.2).[4] Today, FDG is used in 90 % of PET scans.[9]

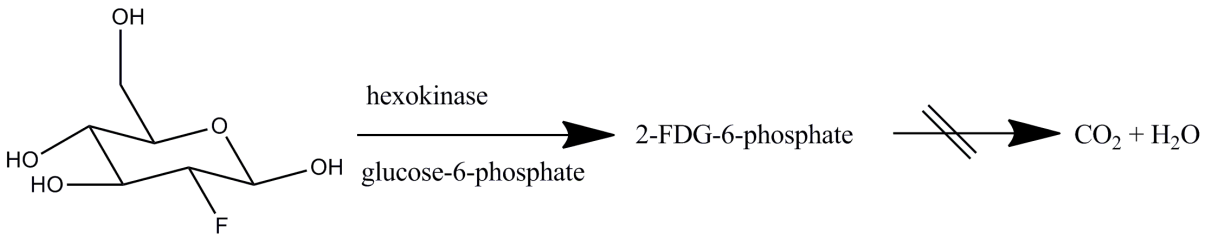

Figure 1.2 Illustration of the reaction when fluorodeoxyglucose enters the tissue then converted into fluoroglucose-6-phosphate, which cannot be metabolized further thus is trapped in the tissue[4]

[8] Cook, G. J. R., Maisey, M. N., *Clinical Radiology*, **51**, 603, 1996.
[9] Reivich, M., *Positron Emission Tomography*, 131, 1985.

1.4 Aim of this Study

^{99m}Tc is the isotope of choice for nuclear imaging, but other alternatives need to be explored. One of the obvious alternatives is the isotopes of gallium which include ^{67}Ga (used for SPECT) and ^{68}Ga (used for PET), because the radiopharmaceutical coordinating chemistry of Tc and Ga are similar. These radionuclides have gamma decay properties which are suitable for either SPECT or PET imaging. The nuclide, ^{67}Ga ($t_{1/2}$ = 78.3 h) is cyclotron produced by the ^{68}Zn (p, 2n) - ^{67}Ga reaction and the nuclide was first produced for human use in 1953.[6] ^{68}Ga ($t_{1/2}$ = 68 min) is produced from a ^{68}Ge/^{68}Ga generator and its parent isotope ^{68}Ge ($t_{1/2}$ = 280 days) has a sufficiently long enough half-life for the manufacturing of long-lived generator systems which is suitable for radiopharmaceutical applications.[5]

Ga(III) is a possible therapeutic agent and this can be illustrated in the fact that simple salts like gallium nitrate has antitumor effects and interferes with cellular iron metabolism.[10,11,12] The tendency of gallium salts towards hydrolysis and formation of non-soluble gallium oxides is a big drawback in membrane penetration and absorption and that is why the chelating *O,O'*- *N,O*- and *N,N'*- donor ligands linked to gallium salts can assist in stabilizing gallium against hydrolysis which also leads to an increase in anticancer stability.[13,14]

Radioisotopes of gold, such as $^{177\text{-}183}$Au, are alpha emitters and has relatively short half-lives. $^{185\text{-}196}$Au decay by gamma emission, electron capture and in something even positron emissions. The only long-lived isotope with a half-life of 183 days is ^{195}Au. ^{198}Au is widely used for tracer studies, in medical diagnosis and in radiotherapy.

^{199}Au has suitable nuclear properties[15], it has not been extensively investigated for radiotherapy applications because Au(III) coordination chemistry is relatively scarce in the literature. Gold(III) is very difficult to work with because it is unstable to reduction. It readily undergoes hydrolysis reactions and Au(III) complexes often tents to precipitate as

[10] Kaluderovic, M. R., Gomez-Ruiz, S., Gallego, B., Hey-Hawkins, E., Paschke, R., Kaluderovic, G. N., *Euro. J. Med. Chem.*, **45**, 519, 2010.
[11] Bernstein, L. R., Prarmacol. Rev., 50, 665-682, 1998.
[12] Arion, V. B., Jakupec, M. A., Galanski, M., Unfried, P., Keppler, B. K., *J. Inorg. Biochem.*, **91**, 298-305, 2002.
[13] Harpstrite, S. E., Prior, J. L., Rath, N. P., Sharma, V., *J. Inorg. Biochem.*, **101**, 1347-1353, 2007.
[14] Rudnev, A. V., Forteeva, L. S., Kowol, C., Berger, R., Jakupec, M. A., Arion, V. B. Timberbaey A. R., Keppler, B. K., *J. Inorg. Biochem.*, **100**, 1819-1826, 2006.
[15] Volkert, W.A., Goeckeler, W.F., Ehrhardt, G.J., Ketring, A.R., *J. Nucl. Med.*, **32**, 174, 1991.

$AuCl_4^-$, $AuCl_2^-$ or mixed $AuCl_4^-/AuCl_2^-$ salts with poor solubility. Gold(III) complexes are considered to be kinetically inert compared to that of gold(I).

The main aims of the study can be briefly summarized as follows:

1. To synthesize a range of carboxamide ligands (*N*,*N'*-tetradentate ligands) which can be coordinated to metals like gallium(III) and gold(III).
2. To characterize the carboxamide ligands and the metal complexes using techniques such as X-ray crystallography and Nuclear Magnetic Resonance Spectroscopy (NMR) and Ultraviolet/Visible spectroscopy (UV/Vis).
3. To determine the intimate mechanism of the substitution reactions of a gallium(III) complex with 4-methylpyridine by means of a kinetic study and isolation and characterisation of the final products formed.
4. To perform cell studies on the all of the compounds that were successfully synthesized.

2 Literature Study

2.1 Radiopharmaceuticals

2.1.1 Introduction

Radiopharmaceuticals are drugs which contain a radionuclide and are used in nuclear medicine departments for the diagnosis or therapy of various diseases. They are usually small inorganic or organic molecules with definite composition, but can also be macromolecules such as monoclonal antibodies. Radiopharmaceuticals can be divided into two classes: those whose biodistribution is determined by their physical and chemical properties and those whose distribution is determined by their receptor binding or other biological interactions.[1]

Molecular imaging provides images to visualize specific moleculear changes in various diseases. Molecular imaging requires specific modalities such as computed tomography, ultrasound, magnetic resonance imaging, optical imaging and scintigraphy. The main tools for scintigraphy are positron emission tomography (PET) and single photon emission computed tomography (SPECT), where both PET and SPECT require a radionuclide or a radiolabeled pharmaceutical. Almost all the radiopharmaceuticals currently in use for nuclear medicine imaging are used for molecular imaging because of the concept of a 'radiotracer', which includes a specific radiolabeled molecule that can trace the *in vivo* behaviour of molecules and provides information about a specific biological process.[2]

[1] Liu, S., Edwards, D.S., *Chem. Rev.*, **99**, 2235, 1999.
[2] Lee, Y-S., *J. Nucl. Med.*, **2**, 178, 2010.

2.1.2 General considerations when designing Radio-pharmaceuticals

To develop a new radiopharmaceutical for a specific biological target or disease the following factors must be considered: the choice of the radionuclide because of the different diseases; the different half-life of each radionuclide and the *in vivo* behaviour of the potential imaging agents.[2]

The diagnostic radionuclide need to emit γ-rays or photons (X-rays or annihilation photons from positron emissions). PET scanners detect the two annihilation photons emitted when the positron interacts with an electron while SPECT scanners detect the γ-rays emitted. More than 80 % of all the diagnostic scans in the hospitals are done with ^{99m}Tc radiopharmaceuticals.[3,4] ^{99m}Tc emits a single γ-ray of 140 keV which is suitable for imaging with SPECT while isotopes such as ^{11}C, ^{15}O, ^{18}F and ^{82}Rb emit two 511 keV annihilation photons when the positron interacts with an electron which are detected by the PET scanners and are used for PET scanning.

The *in vivo* behaviour of the imaging agents can be predicted by looking at the following properties: the specificity of the target, including the size and charge of the molecule, the specific activity, the affinity, the stability, lipophilicity, stereochemistry and the metabolism of the radiolabeled compounds. For instance, positively charged complexes goes to the hart while negatively charged complexes to the kidneys and neutral complexes can cross the blood-brain barrier. If the complex is lipohilic it can accumulate in fatty tissues and it usually goes to the liver, gall, bladder or bile ducts. Another indicator of the *in vivo* behaviour is the kinetic stability, as predicted by Anders and co-workers.[5] Radiopharmaceuticals such as Ga(III) and In(III) complexes have a high thermodynamic stability and are kinetically inert to *in vivo* exchange with transferrin. For Cu(II) complexes to be stable *in vivo*, the kinetic inertness is more important than the thermodynamic stability. The understanding of the relationship between the *in vivo* stability and kinetic inertness, specifically for Cu(II) complexes is still researched by Anderson and co-workers for predicting the *in vivo* stability.[5]

[3] Parker, D., Roy, P.S., *Inorg. Chem.*, **27**, 4127, 1988.
[4] Zuckman, S.A., Freeman, G.M, Trouter, D.E., Volkert, W.A., Holmes, R.A., Van Derveer, D.G., Barefield, E.K., *Inorg. Chem.*, **20**, 2386, 1981.
[5] Anderson, C.J., Welch, M.J., *Chem. Rev.*, **99**, 2219, 1999.

The term pharmacokinetics is conventionally used to refer to the movement of the drug in the body which includes the absorption, distribution, metabolism and elimination, but in terms of radiopharmaceuticals it refers to the distribution and elimination of the radionuclide after the radiopharmaceutical has been administered. The radiolabeled compound should have a high target uptake with a useful signal-to-noise ratio in a short period of time. Therefore, new radiopharmaceuticals should have a short blood residence time to minimize the radiation to non-target tissue.

To modify the pharmacokinetics of a radiopharmaceutical, chemical modification is necessary of the targeting molecule, the metal chelate, linker or ligands. The chemical modification can be achieved by introducing various hydrophilic or lipophilic groups onto the side chains of amino acids.

Chelating agents with different charge and hydrophilicity can also be introduced by using a single hydrocarbon chain as a linker that will improve lipophilicity while an amino acid sequence will increase hydrophilicity and renal clearance.

2.1.3 Choice of Radionuclide

When choosing an effective and appropriate radionuclide for radiopharmaceuticals a complex process and a few characteristics/properties[6,7] need to be looked at: type of radionuclide, specific decay characteristics, physical half-life, chemical properties, production method, *in vivo* pharmacokinetics of the radiopharmaceutical, cost and availability, stability of the daughter nuclides (if any has formed) and the ratio of penetrating to non-penetrating radiation.

The specific decay mode and the physical half-life are independent of any physicochemical condition and cannot be changed with any other method, such as a physicochemical modification. Therefore, one must select which radionuclide is adequate for the target molecule which is visualized, measured or characterized.[2]

[6] Volkert, W.A., Goeckeler, W.F., Ehrhardt, G.J., Ketring, A.R., *J. Nucl. Med.*, **32**, 174, 1991.
[7] Ehrhardt, G.J., Ketring, A.R., Ayers, L.M., *Appl. Radiat. Isot.*, **49**, 295, 1998.

2.1.3.1 Half-life

The physical half-life of the radionuclide is very important when designing radiopharmaceuticals. The physical half-life of any given radionuclide should approach the biological half-life of the radiopharmaceutical at the tumor site. It must be compatible with the rates of biolocalization in target tissue along with clearance of radioactivity from normal tissue.[6] The half-life of the radionuclide should be sufficiently long enough to: allow the manufacturing of the radiopharmaceutical, the transportation to the hospital, the administration to the patient, maximum accumulation in the target tissue and optimally cleared from the non-target organs.

The half-life should also be as short as possible to minimize the radiation dose to the patient, without changing the goals above. Radionuclides with shorter half-lives (from a few hours to a few days) are more effective for targeting of disseminated cells, where as longer-lived radionuclides (from one to a few weeks) are more desired for tumors especially if high uptakes is needed.[8] Useful radionuclides for molecular imaging are given in Table 2.1 and the physical characteristics of potential therapeutic radionuclides are given in Table 2.2.

Table 2.1 Useful radionuclides for molecular imaging[2]

Radioisotopes	Physical half-lives	Decay Mode (%)	γ-Ray Energy (KeV)	Production
^{11}C	20.4 min	β^+ (100)	511	Cyclotron
^{13}N	9.96 min	β^+ (100)	511	Cyclotron
^{15}O	2.03 min	β^+ (100)	511	Cyclotron
^{18}F	109.8 min	β^+ (97)	511	Cyclotron
^{62}Cu	9.76 min	β^+ (97), EC (3)	511	Cyclotron
^{64}Cu	12.8 hours	β^+ or β^-, EC	511	Cyclotron
^{67}Ga	3.3 days	EC (100)	93, 184, 300	Cyclotron
^{68}Ga	68 min	β^+ (89), EC (11)	511	Generator
^{82}Rb	75 sec	β^+ (95), EC (5)	511	Generator
^{94m}Tc	52 min	β^+ (72), EC (28)	511	Cyclotron
^{99m}Tc	6.0 hours	IT (100)	140	Generator
^{111}In	2.8 days	EC (100)	171, 245	Cyclotron
^{123}I	13.2 hours	EC (100)	159	Cyclotron
^{124}I	4.2 days	β^+ (23), EC (77)	511	Cyclotron
^{125}I	60 days	EC (100)	35	Reactor

[8] Carisson, J., Aronsson, E.F., Hietala, S., Stigbrand, T., Tennvall, J., *Radiotherapy & Oncology*, **66**, 107, 2003.

Table 2.2 Physical characteristics of potential therapeutic radionuclides[9,10,11]

Radionuclides	Physical half-lives	Radiation type (MeV)	Source	Particle max. range
^{32}P	14.3 days	β (1.71)	Nuclear reactor	8.7 mm
^{67}Cu	2.58 days	β (0.54), γ (0.185)	^{68}Zn (p,2p) ^{67}Cu	1.8 mm
^{67}Ga	3.26 days	Auger, γ (0.09)	^{68}Zn (p,2p) ^{67}Ga	10 nm
^{77}As	1.62 days	β (0.68), γ (0.239)		2.5 mm
^{80m}Br	4.42 hours	Auger, γ (0.037)		< 10 nm
^{89}Sr	50.5 days	β (1.49)	Nuclear reactor	8.0 mm
^{90}Y	2.67 days	β (2.28)	^{90}Sr/^{90}Y Generator	12.0 mm
^{105}Rh	1.48 days	β (0.57), γ (0.320)	Nuclear reactor	1.9 mm
^{111}Ag	7.47 days	β (1.05), γ (0.34)	^{110}Pd (n,γ) ^{111}Pd (β^-) - ^{111m}Ag (γ) ^{111}Ag	4.8 mm
^{125}I	60.0 days	Auger, γ (0.027)	^{124}Xe (n,γ) ^{125}Xe/ ^{125}I	10 nm
^{127}Te	9.4 hours	β (0.7)		2.6 mm
^{131}I	8.0 days	β (0.6), γ (0.364)	^{131}Te (n,γ) ^{131}I	2.0 mm
^{142}Pr	19.1 hours	β (2.16), γ (1.6)		11.3 mm
^{149}Pm	2.21 days	β (1.07), γ (0.289)	Nuclear reactor	5.0 mm
^{153}Sm	1.95 days	β (0.8), γ (0.103)	^{152}Sm (n,γ) ^{153}Sm	3.0 mm
^{161}Tb	6.91 days	β (0.51), γ (0.025)		1.7 mm
^{169}Er	9.5 days	β (0.34)		1.0 mm
^{177}Lu	6.7 days	β (0.497), γ (0.208)	^{176}Lu (n,γ) ^{177}Lu	1.5 mm
^{186}Re	3.77 days	β (1.08), γ (0.131)	^{186}Re (n,γ) ^{186}Re	5.0 mm
^{188}Re	16.95 hours	β (2.13), γ (0.155)	^{188}W/^{188}Re Generator	11.0 mm
^{198}Au	2.7 days	β (0.97), γ (0.411)	^{197}Au (n,γ) ^{198}Au	4.4 mm
^{211}At	7.2 hours	α (6.8)		65 μm
^{212}Bi	1.0 hours	α (7.8), γ (0.72)		70 μm

2.1.3.2 Chemical and Biochemical Properties

The biochemical nature of a radionuclide needs to be considered because of the redistribution of radioactivity upon metabolism of the carrier molecule. An important fact is the clearance and localization characteristics of the radionuclides agents in non-target tissues since production of radiotoxic side-effects in these types of tissues will limit the activity that can be administered to the patients.[12,13] Naruki *et al*. have shown that the rate at which the

[9] Schubiger, P.A., Smith, A., *Pharmaceutica Acta Helvetiae*, **70**, 203-217, 1995.
[10] Brown, E., Dairiki, J., Doebler, R.E., Shibab-Elden, A.A., Jardine, L.J., Tuli, J.K., Byurn, A.B., *Table of Isotopes*, 7th Edition, 1978.
[11] Firestone, R.B., Shirley, V.S., Baglin, S.B., Chu, S.Y.F., Zipkin, J., *Table of isotopes*, 1996.
[12] Motta-Hennessy, C., Sharkey, R.M., Goldenberg, D.M., *J. Nucl. Med.*, **31**, 1510-1519, 1990.
[13] Bucheggar, F., Pelgrin, A., Delaoya, B., Bischof-Delaloye, A., *J. Nucl. Med.*, **31**, 1035-1044, 1990.

radionuclide is released can vary significantly when the radiolabeled compound is internalized.[14] Other studies have also shown that the nature of the bifunctional chelator can also have an effect on the rate at which the radionuclide is cleared.[15,16] Increasing clearance of activity from normal tissues can reduce radiation doses to these normal tissues as long as the catabolised form of the radionuclide does not redistribute to other radiosensitive non-target tissues.[17]

2.1.3.3 Reliability

The radionuclide which was chosen and produced must be of good quality and need to be reproducible within a narrow range of reliability because impurities can have an effect on the labelling and yields thereof. Radiometals are produced from generators, cyclotrons, nuclear reactors and accelerators. The use of cyclotrons, nuclear reactors and accelerators are more expensive and it produces only one isotope at a time. Therefore, the most economical choice to produce radiometals is to use generators. The short-lived daughter radionuclide and the long-lived parent isotope can easily be separated by using ion exchange chromography or solvent extraction.

2.1.3.4 Particle Emission Properties, Energy and Range

Tumor cells are most successfully killed by radiometals which emits high linear energy transfer radiations. There are a wide variety of vehicles that can be used to transfer radionuclides to the desired site. Therefore, the optimal range of the linear energy transfer emissions within the tissue will vary for all the different radiopharmaceuticals because the vehicle and receptor site varies.

In Table 2.3 some radionuclide distribution patterns of radiation doses to the cell nucleus are given, as calculated by Wernli in 1986.

[14] Nakuri, Y., Carrasquillo, J.A., Reynolds, J.C. et al., *Nucl. Med. Biol. Int. J. Radiat. Appl. Inst*, **17**, 201-207, 1990.
[15] Yokoyama, K., Carrasquillo, J.A. Chang, A.E., et al. J. Nucl. Med., **30**, 320-327, 1989.
[16] Roselli, M., Schlom, J., Gansow, O.A., et al., J. Nucl. Med., **30**, 672-682, 1989.
[17] Schunberg, D.A., Strand, M., *Cancer Res.*, **43**, 265-272, 1983.

Table 2.3 Different radionuclide distribution patterns[18]

Nuclide distribution	**Auger**		**β^-**		**α**
	^{67}Ga (< 10 keV)	**^{131}I (180 keV)**	**^{111}Ag (350 keV)**	**^{90}Y (930 keV)**	**^{211}At (≥ 5900 keV)**
Homogeneous	1	1	1	1	1
Cell nucleus	~ 20	~ 1	~ 1	~ 1	~ 1
Cytoplasm	< 0.2	~ 1	~ 1	~ 1	~ 1
Cell surface (20 µm)	0	~ 1	~ 1	~ 1	~ 0.9
Capillary (50 µm)	0	~ 0.9	~ 1	~ 1	~ 0.8
Capillary (200 µm)	0	~ 0.8	~ 0.9	~ 1	0
Capillary (1000 µm)	0	~ 0.3	~ 0.7	~ 0.9	0

Auger electron emitters are very potent cell killing agents, but only if they can penetrate the cell membrane and come into close contact with the nucleus. α-Emitters are also very potent within a restricted range of 50 µm in the tissue. For these two radionuclides to be effective, the dose distribution must be highly homogeneous with respect to the tumor volume in order to irradiate all the tumor cells. β-Emitters shows a homogenous dose distribution even with heterogeneously distribution of nuclides in the target tissue.

The energy and range of particles which are emitted from the radiopharmaceutical must be compatible with the microdistribution of the radionuclide with respect to the target and normal tissue. A radiopharmaceutical that has an inhomogeneous distribution of the carrier molecule and also absorbs low energy particles will cause incomplete irradiation of the target tissue, thus to ensure uniform irradiation the distribution of the radionuclides must be homogeneous. A too long range with respect to a small target will resulted in an increase of the dose to the non-target tissue and a decrease of the dose to the specific target.

α-Particles are high energy helium nuclei. They have high ionisation densities which they deposit via linear tracks over short distances, usually 40 – 80 µm, therefore limiting the cell's ability to repair damage to DNA. α-Emitters are used for tumors within a short range and for treatment of small tumor nests or single disseminated tumor cells. High therapeutic ratios

[18] Baidoo, K.E, Zhan, Y-G., Lin, K-S., Scheffel, U., Waggner, H.N., *J. Nucl. Med.*, **39**, 7P, 1998.

can result while sparing the normal tissue surrounding the tumor. There are many α-emitters which exist, but only two radionuclides are suitable for radiotherapeutic application, astatine (^{211}At) and bismuth (^{212}Bi).

β-emitting radionuclides are exclusively used in clinical radiotherapeutic application. They produce low ionisation densities, therefore low LET radiation. β-Particles are high-energy, high-speed electrons or positrons emitted by certain types of radioactive nuclei. The range of these particles is much higher than alpha particles. These high energy particles are not effective with small tumors or disseminated cells. Only a small amount of the energy will be deposited in the target cells while most of the energy will be emitted by the non-target tissue causing unnecessary irriadiation. β-Particles can be heterogeneously distributed in large tumor areas, but due to irradiation, it still gives a uniform/homogeneously dose distribution.

Radionuclide imaging of the tracer biodistribution is possible with γ-ray energy. There are several advantages and disadvantages of using radionulides where γ-ray emission accompanies particulate emission during radioactive decay. γ-Rays will increase the radiation dose to the whole body but do not contribute significantly to the tumor dose. Nuclides with a low abundance of γ-radiation and energy (75 – 250 keV) are ideal to be used for γ-ray emitters and this will provide optimal properties for scintigraphy, biodistribution studies, measurements and dosimetric calculations.[6]

Auger-electron emitters such as ^{67}Ga, ^{99m}Tc, ^{111}In and ^{123}I can also be used for tumor targeting, as already stated, but only if they can penetrate the cell membrane and come into close proximity of the nucleus. Because of its short range, the radionuclides must be carried directly into the nucleus of every cell within the tumor.

2.1.4 Labelling Techniques of Radiopharmaceuticals

There are several labelling techniques of biomolecules. The choice of which labelling technique used depends on the type of biomolecule to be labelled and the purpose of the study. The two strategies that are most often used for the design of receptor-specific targeting molecules are the integrated approach or bifunctional approach.

2.1.4.1 Integrated Approach

The integrated approach[19] involves the replacement of part of a known high affinity receptor ligand with the requisite radionuclide chelate, which means the radionuclide is directly incorporated into the targeting moiety (Figure 2.1). This is achieved by making the minimum changes in size, conformation and receptor binding affinity. This helps to improve the stability of the radiopharmaceutical as well as the tumor uptake and retention. The disadvantages of the integrated approach are a decrease in receptor binding affinity and that a more challenging target molecule needs to be synthesized.[20]

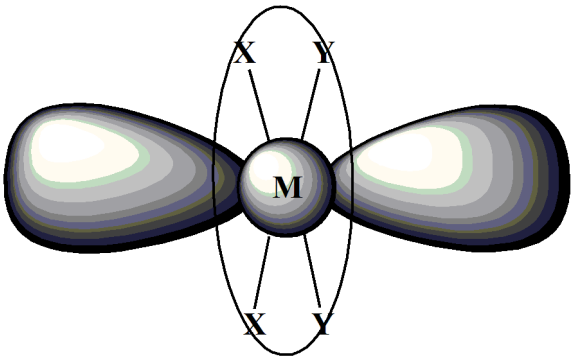

Figure 2.1 Schematic representation of an integrated approach in a radiopharmaceutical design

2.1.4.2 Bifunctional Chelate Approach

The bifunctional chelate approach (BFCA) consists of a ligand system which is connected to a radiometal and contains a functional group suitable for linking the complex to a targeting molecule. A linker (pharmacokinetic modifier) is used to bind the radiometal complex to the targeting biomolecule (Figure 2.2). The best possible reaction conditions for conjugation involves mild aqueous conditions close to physiological pH, short reaction times and minimum purification.[21] The metal chelate is often far apart from the receptor binding mortif to minimize the possible interference of the receptor binding by the metal chelate.[1] The functionalities used to bind the metal to the biomolecule are usually a carboxylate or an amine group which can be activated. The properties of a chelating agent should be strong enough to coordinate to the metal at low concentrations, yield only one product at high

[19] Engelbrecht, H.P., Otto, S., Roodt, A., *Acta Crystallogr. Sect. C*, 199, C55, 1648.
[20] Hom, R.K., Katzenellenbogen, J.A., *Nucl. Med. Biol.*, **24**, 485, 1997.
[21] Bartholoma, M.D., Louie, A.S., Valliant, J.F., Zubieta, J., *Chem. Rev.*, **110**, 2903-2920, 2010.

percentage, form a kinetically and thermodynamic stable complex with the radioactive metal under *in vivo* conditions and not influence the biological properties of the conjugate.

Figure 2.2 Schematic representation of Bifunctional Approach in a radiopharmaceutical design

2.1.4.3 Receptor Imaging in the BFCA Approach

A receptor-based, target-specific radiopharmaceutical using the bifunctional approach can be divided into four parts: a targeting molecule, a linker, a bifunctional chelating agent (BFCA) and a radionuclide. The targeting molecule serves as the vehicle, which carries the radionuclide to the receptor site at the tumor. The targeting molecules are usually antibodies or small biomolecules, peptides, peptidomimetrics and non peptide receptor ligands. The targeting biomolecule is determined by the disease target. The radionuclide is the radiation source and between the targeting biomolecule and the radionuclide is the BFCA. It is connected to the nuclide and convalently attached to the targeting molecule either directly or through a linker. The choice of the bifunctional chelating agent is determined by nature and oxidation state of the nuclide. The linker is usually a hydrocarbon chain or a long poly(ethylene glycol), which is often used to modify the pharmacokinetics. For example a metabolizable linker is sometimes used to increase the blood clearance and to reduce the background activity, thus improving the target-to-backgroung ratio.[18]

The term ‘receptor’ was defined by biochemists as entities that can recognize a receptor ligand with high affinity and selectivity. A receptor is usually proteins embedded in lipid molecules and are characterized by means of its biological properties, specificity, saturability, high ligand affinity and distribution in relation to physiological response.[22] These properties are determined experimently and is made possible because of the use of a high specific activity radiotracers such as ^{125}I-fibrinogen.[1] Receptor imaging is more advantageous over scintigraphic imaging because of the high specificity of receptor binding, therefore results in selective uptake and distribution of the receptor at the tumor site. A ligand can be referred to

[22] Eckelman, W. C., *Nucl. Med. Biol.*, **21**, 759, 1994.

be agonists, thus means the receptor ligand binds to the receptor site with the complete 'native ligand' attach to it and then causes a cascade of biochemical effects. If a complex is called an antogonits, indicates that it will binds to the receptor site with high affinity. Receptor ligands should have a very high receptor binding affinity and high specificity to be a useful targeting molecule.

Receptors can be either intracellular or extracellular, which will determine the design of the radiopharmaceutical, the selected chelating agent, the radionuclide and the degree of tolerance of the receptor ligand toward chemical modifications. Intracellular receptors ligands are usually too small to cross the cell membrane to reach the receptor site and its chemical constitution is not easily altered.[20] In the case of an extracellular receptor ligand the ligand does not have to cross the cell membrane to interact with the receptor, but the metal chelate needs to be neutral if no intracellular vehicle is present. The receptor system must be chosen in such a way that both clinical and chemical properties were taken into consideration. First, the clinical need of the new radiopharmaceutical must be identified to diagnose a tumor and the relationship between the tumor and the receptors. Secondly, the receptor concentration must be very high and finally the receptor must be able to recognize to the targeting biomolecule with high specificity and affinity.

2.2 Gallium as Coordination Metal

2.2.1 A Brief History of Gallium

Gallium was discovered and isolated spectroscopically in France (1875) by Paul Emile Lecoq de Boisbaudran (an investigator in the field of spectroscopy) by its characteristic spectrum (two violet lines 4172 Å and 4033 Å respectively).[23] Even though it was noted by him in 1863 that the spectral lines of the boron-aluminum family form patterns of the same type with regular variations from one element to the next where he discovered that one element was missing between aluminium and indium. He started to search for it and found success twelve years later. He isolated hydrated gallium oxide from zinc by chemical methods and obtained the free metal from electrolysis in a solution of its hydroxide in potassium hydroxide. Gallium was the first element to be discovered spectroscopically and was also the first to be discovered as the three "eka" elements which were told by Mendeleev in 1870.

[23] Weeks, M. E., "Discovery of the Elements", *J. Chem. Educ.*, Press, Easton, Pa., 1948.

2.2.2 Properties of Gallium

Gallium, with an atomic number of 31 and molecular weight of 69.72 g/mol does not occur free in nature but as gallium(III) salt with trace amounts of zinc and bauxite ores. This can be obtained by smelting. It is silvery in colour and when solidified the metal expands by 3.1 %. That's why it not stored in metal or glass containers. Generally gallium has the same chemical properties as aluminum but differ in some respects. Gallium is soluble in HNO_3, HCl, H_2SO_4, NaOH and *aqua regia*. The metal, gallium has a low melting point of 29.75 °C and a high boiling point of 1983-2070 °C.[24] There are only two other elements with a lower melting point, cesium (28.5 °C) and mercury (~30 °C). The density of gallium is 5.904 g/ml (solid) at 29.6 °C and 6.095 g/ml (liquid) at 29.8 °C.

2.2.3 Applications of Gallium

The oldest application for gallium was introduced by Boisbaudran to use gallium as a filler for high-temperature thermometers. However high-temperature thermometers could not be made until quarts capillary tubes were available, which enables the temperature range to increase from 700 °C to 1200 °C. The first successful high-temperature thermometer was made by Boyer in 1925.[25] The metal, gallium is used in gold alloys for dental restoration work and the low melting alloys of gallium are also used in fusible parts of fire alarms and fuses. It is also used as an excitant in phosphors for luminous paints and fluorescent lights[26] and also acts as a heat-exchange medium for high-temperature applications, because of its low vapor pressure, high thermal conductivity and thermal stability.[27] Gallium has a rich ultraviolet spectrum and that is why it is used as a constituent of vapor lamps. Gallium salts have been used on an experimental basis but possibly the most interesting development is the application of the radioactive isotopes of gallium which involves ^{67}Ga and ^{72}Ga, where ^{67}Ga is used for inflammation and tumor imaging and ^{72}Ga is used for the treatment and diagnosis of bone cancer.[28]

[24] *Liquid-Metals Handbook*, Atomic Energy Commission, U.S. Government Printing Office, Washington, D.C., June 1, 31, 1950.
[25] Boyer, S., *Ind. Eng. Chem.*, **17**, 1252, 1925.
[26] Dement and Dake, *Rare Metals*, Chemical Publishing Co., Brooklyn, N. Y., 28, 1946.
[27] *Minerals Yearbook*, U.S. Bureau of Mines, 1310-1311, 1949.
[28] Dudley, H. C., *Naval Med. Research Inst., Rept*. NM-011-013, 1949.

2.3 Gallium as Radiopharmaceutical

2.3.1 Introduction

The purpose of medical imaging by using radiotracers and molecular probes is to obtain rapid, noninvasive evaluation of the organ function, pathology and/or physiology. The advantage of using molecular imaging is that it ensures early detection of a disease.

Nuclear medicine relies on two imaging modalities, positron emission tomography (PET) and single photon emission computed tomography (SPECT). Positron emission tomography (PET) offers a higher sensitivity and resolution, while single photon emission computed tomography (SPECT) offers a more readily available, longer lived radioisotope with a lower direct cost.[29,30,31,32] SPECT radiotracers have a molecular weight of < 2000 and are labeled with a gamma-emitting isotope such as ^{67}Ga, ^{99m}Tc, ^{111}In and ^{123}I for diagnosis. ^{99m}Tc is the workhorse of all the radioisotopes currently in used for the diagnosis of nuclear medicine and ^{99m}Tc radiopharmaceuticals reflects the ideal nuclear properties for commercial properties.[33,34] It emits a gamma-ray of 140 keV with an 89% abundance which is almost most favourable for the imaging of gamma cameras and has a half life of 6 hours, which allows central preparation of the radiopharmaceuticals, distribution to hospitals, administration, accumulation in target tissue and collection of the image, while still ensuring that the patient is radiated with a minimal dose. The importance of ^{99m}Tc is clearly observed in 2007 in the United States for diagnostic imaging when ^{99m}Tc is used in almost 19 million radiopharmaceutical injections (which represent 85 % of the total radiopharmaceutical injections in that particular year) for bone, kidney, gall bladder, lung, liver and cardiac scans.

^{99m}Tc is the medical isotope of choice for nuclear imaging but there are continuous supply problems because two nuclear reactors which provided a large fraction to the world were shut down for repairs and maintenance. The National Research Universal (NRU) Reactor in Chalk River, Canada (build in 1975), which provided 45 % of ^{99}Mo (parent isotope of ^{99m}Tc) to the world supply, will end production between 2010 and 2020. The same goes for the

[29] Hruska, C. B., Philips, S. W., Whaley, D.H., Rhodes, D. J., O'Connor, M. K, *Am. J. Roentgenol*, **191**, 1805, 2008.
[30] Berman, C. G., *Cancer Control*, **14**, 338, 2007.
[31] Garcia, E. V., Faber, T. L., *Cardiol Clin*. **27**, 227, 2009.
[32] Slomka, P. J., Patton, J. A., Berman, D. S., Germano, G., *J. Nucl Cardiol.*, **16**, 255, 2009.
[33] Jurisson, S. S., Lydon, J. D., *Chem. Rev.*, **99**, 2205, 1999.
[34] Dilworth, J. R., Parrott, S., *J. Chem. Soc. Rev.*, **27**, 43, 1998.

High Flux Reactor (HFR) in Petten, Nederland (built in 1961) which supplies 30 % of the Mo demand underwent six months of maintenance in 2010.[21]

There are a number of alternatives proposed but the most obvious alternative to ^{99m}Tc is the radioisotopes of gallium which involves ^{68}Ga for PET and ^{67}Ga for SPECT. The general question is whether gallium chemistry provides complexes which offer equivalent *in vivo* stability, a range of biodistributions and ease of radioconjugate formation with the same characteristics of ^{99m}Tc agents. The only way to solve this question is by comparing and contrasting the coordination chemistry, production of radioisotopes, availability and ease of use in nuclear medicine clinics of the two radiometals. Now by considering these aspects a hypothesis can be concluded that the knowledge obtained over the past 20 years for Tc radiopharmaceutical development could be used for the development of Gallium-based probes.[21]

2.3.2 Properties and Production of Gallium

There are currently 30 different known isotopes of gallium including ^{69}Ga with a natural abundance of 60.11 % and ^{70}Ga with a natural abundance of 39.89 %. ^{69}Ga and ^{70}Ga are the most stable and nonradioactive isotopes of them all. The radioactive isotopes of gallium does not occur freely in nature and out of all the radioactive isotopes (which already exits) only ^{68}Ga, ^{67}Ga and ^{66}Ga has radionuclides properties and availabilities that can be used for PET and SPECT studies.[35,36]

2.3.2.1 Gallium-67

^{67}Ga is produced from ^{68}Zn as shown in Figure 2.3. A thin layer of ^{68}Zn is electrochemically plated on a target metal like zinc or copper. After irradiation, acid for example HCl is used to dissolve the gallium from the target metal. Separation and concentration is achieved by solvent/solvent extraction, extraction chromatography or ion exchange chromatography.[37,38]

[35] Audi, G., Bersillon, O., Blachot, J. A., Wapstra, A. H., *Nucl. Phys*., **A729**, 3, 2003.
[36] *Health Physics & Radiological Health Handbook*, 3rd edition, Williams & Wikins: Baltimore, MD., 6-53, 1998.
[37] El-Azony, K. M., Ferieg, K. H., Saleh, Z. A., *Appl. Radiat. Isot.*, **59**, 329, 2003.
[38] Hupf, H. B., Beaver, J. E., *Int. J. Appl. Radiat. Isot.*, **21**, 75, 1970.

^{67}Ga has a reasonable price of ca. $19/mCi with a half-life of 78.3 hours which allows shipment of the radioisotopes over long distances and centralized preparation of the radiopharmaceuticals in a radiopharmacy.

Citric acid are sometimes added which acts as a solubilizer followed by neutralization and sterilization of the aqueous solution during clinical applications.[39] ^{67}Ga is a pure gamma-ray source and emits gamma photons of different energies at 93 keV (36 %), 185 kev (20 %), 300 keV (16 %) and 394 keV (5 %). ^{67}Ga is mostly used for tumor and inflammation imaging.[40]

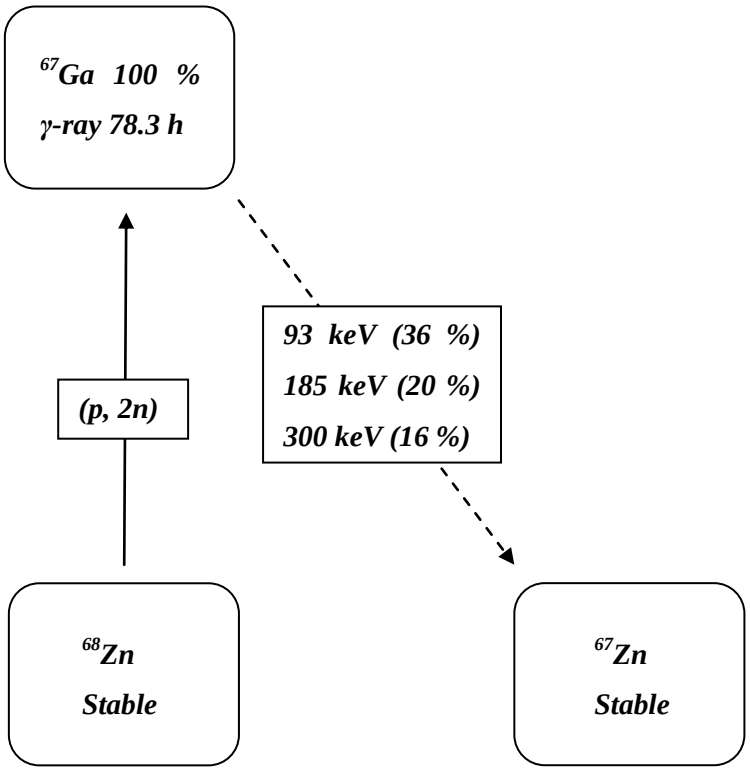

Figure 2.3 Schematic representation of the production and decay of ^{67}Ga

[39] Ruth, T. J., Pate, B. D., Robertson, R., Porter, J. K., *Nucl. Med. Biol.*, **16**, 323, 1989.
[40] Green, M. A., Welch, M. J., *Nucl. Med. Biol.*, **16**, 435, 1989.

2.3.2.2 Gallium-68

^{68}Ga is produced from Ga^{69} (illustrated in Figure 2.4), has a half-life of 68 minutes, an electron capture of 11 %, positron emission of 89 % and the positron energy per disintegration maximum is 1899 keV (Table 2.4).[41,42]

Table 2.4 Gallium radionuclides[21]

	^{67}Ga	^{68}Ga	
Imaging modality	SPECT	PET	
Decay mode	e^- -capture	e^+ -emission	
	0.091 MeV (2.9 %)	β^+ Energies	Emitted γ
	0.093 MeV (35.7 %)	**1899 keV (88 %)**	**0.51 MeV (176 %)**
	0.185 MeV (19.7 %)	822 keV (1 %)	0.80 MeV (0.4 %)
	0.209 MeV (2.2 %)		1.08 MeV (3.5 %)
	0.300 MeV (16.0 %)		1.24 MeV (0.14 %)
	0.394 MeV (4.5 %)		1.87 MeV (0.15 %)
	0.888 MeV (0.1 %)		
Physical half-life	3.26 days	1.13 hours	
Specific activity	5.67 x 10^4 Ci/g, 2.210 TBq/g	4.10 x 10^7 Ci/g, 1.51 x 10^{18} Bq/g	
Preparation	^{68}Zn (p,2n) - ^{67}Ga cyclotron	^{68}Ge/^{68}Ga generator	

The half-life of ^{68}Ga allows purification and preparation of the molecular probes and imaging so long as the pharmacokinetics of the agent are sufficiently rapid, high resolution and high sensitivity into picomolar, however it does not allow shipment of the isotope over long distances.[43]

^{68}Ge is the parent isotope of ^{68}Ga and has half-life of 270.8 days. This half-life is sufficiently long enough to allow manufacturing of long-lived generator systems which is operational for 1-2 years and suitable for radiopharmaceutical uses.[44] ^{68}Ga/^{68}Ge parent/daughter generator is a potential source of PET in the absence of a nearby cyclotron facility.[45] The disadvantages

[41] Bandoli, G., Dolmella, A., Tisato, F., Porchia, M., Refosco, F., *Coord. Chem. Rev.*, **253**, 56-77, 2009.
[42] Wadas, T. J., Wong, E. H., Weisman, G. R., Anderson, C. J., *Chem. Rev.*, **110**, 2858-2902, 2010.
[43] Chaves, S., Mendonca, A. C, Marques, S. M., Prata, M. I., Santos, A. C., Martins, A. F., Geraldes, C. F. G. C., Santos, M. A., *J. Inorg. Biochem.*, **105**, 31, 2011.
[44] Asti, M., De Pietri, G., Fraternali, A., Grassi, E., Sghedoni, R., Fioroni, F., Roesch, F., Versari, A., Salvo, D., *Nucl. Med, Biol.*, **35**, 721, 2008.
[45] Hsiao, Y-M., Mathias, C. J., Wey, S-P., Fanwick, P. E., Green, M. A., *Nucl. Meb. Biol.*, **36**, 39, 2009.

of these gallium generators is that it produces a low concentration ^{68}Ga, thus additional concentration of the radioactive solution is necessary to obtain high yields of the radiolabeled compounds. The importance of myocardial imaging for the detection of coronary artery disease has motivated the development of ^{68}Ga labeled agents to substitute the cardiac agents ^{99m}Tc-tetrofosmin (Myoview) and ^{99m}Tc-sestamibi (cardiolite), but suitable lipophilic ^{68}Ga radiopharmaceuticals is found to be exclusive because of the fact that high and complete first pass extraction from the blood into the tissue is required to ensure distribution of tracer regional tissue perfusion.[45]

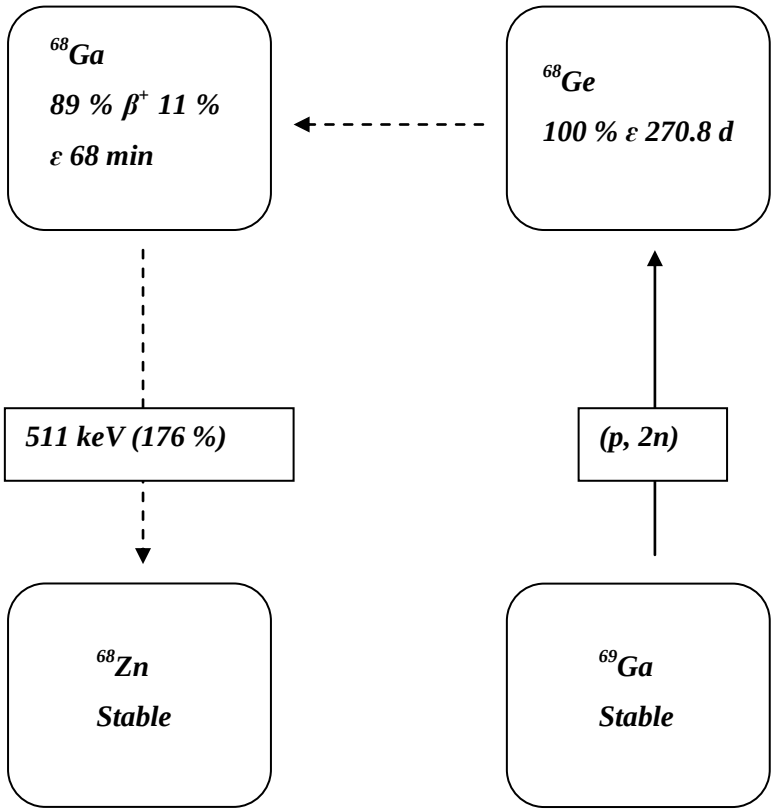

Figure 2.4 Schematic representation of the production and decay of ^{68}Ge and ^{68}Ga

2.3.3 Properties and Coordination Chemistry of Gallium

Gallium is observed in group 13 of the periodic table and is known to be a non-physiological metal, because of its low redox potential. Ga(III) ions have similar biochemical pathways than that of Fe(III), however gallium in the oxidation state +2, is energetically unfavourable and gallium in oxidation state +1, physiological conditions, is almost impossible, that's why redox chemistry of Ga(III) is not possible in biological mediums. This phenomenon utilizes

Ga(III) to be a possible therapeutic agent and is confirmed when simple salts like Gallium nitrate has antitumor effects and interferes with cellular iron metabolism.[46,47,48] The tendency of gallium salts towards hydrolysis and formation of non-soluble gallium oxides is a major impediment in membrane penetration and absorption and that is why chelating *O,O'*- *N,O'*- and *N,N'*- donor ligands are linked to Gallium salts because these types of ligands stabilizes gallium against hydrolysis which leads to a increase in anticancer stability.[49,50] Possible *N,N'*- donor ligands that can be linked to the gallium salts are shown in Figure 2.5[51] and Figure 2.6.[51]

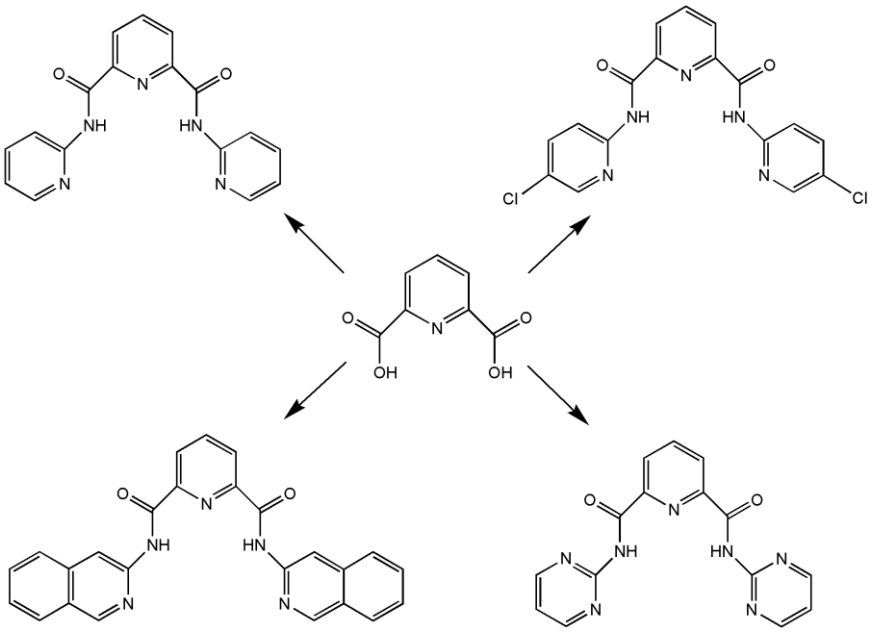

Figure 2.5 Schematic representation of possible *N,N'*-tetradentate ligands[51]

[46] Kaluderovic, M. R., Gomez-Ruiz, S., Gallego, B., Hey-Hawkins, E., Paschke, R., Kaluderovic, G. N., *Euro. J. Med. Chem.*, **45**, 519, 2010.
[47] Bernstein, L. R., Prarmacol. Rev., 50, 665-682, 1998.
[48] Arion, V. B., Jakupec, M. A., Galanski, M., Unfried, P., Keppler, B. K., *J. Inorg. Biochem.*, **91**, 298-305, 2002.
[49] Harpstrite, S. E., Prior, J. L., Rath, N. P., Sharma, V., *J. Inorg. Biochem.*, **101**, 1347-1353, 2007.
[50] Rudnev, A. V., Forteeva, L. S., Kowol, C., Berger, R., Jakupec, M. A., Arion, V. B. Timberbaey A. R., Keppler, B. K., *J. Inorg. Biochem.*, **100**, 1819-1826, 2006.
[51] Jain, S. L., Bhattacharyya, P., Milton, H. L., Slawin, A. M. Z., Crayston, J. A. and Woollins, J. D., *Dalton Trans.*, pp. 862-871, 2004.

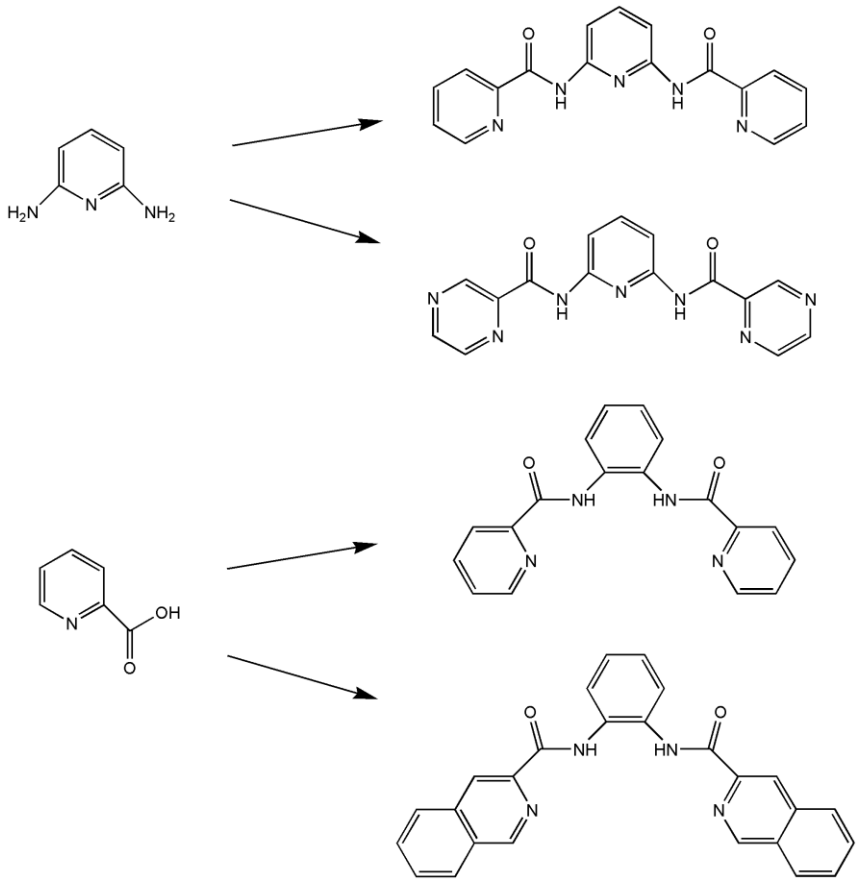

Figure 2.6 Schematic representation of possible *N,N'*-tetradentate ligands[51]

2.3.4 Gallium Chelators

The purpose of a chelator for radiopharmaceutical studies is that it should form complexes with high thermodynamics and/or kinetic inertness to prevent any hydrolysis or ligand-exchange *in vivo* and to insure rapid and efficient chelation of the metal at a specific pH that will not degrade biovectors. The similarity of the coordination chemistry of trivalent iron and gallium should be taken into consideration when designing or selecting gallium chelates and imaging agents. By using an abundant plasma protein (transferrin) that has two iron binding sites with high affinity to Ga(III), ligand exchange is made possible. The formation constants of blood serum at bicarbonate concentrations are log β_1 = 22.8 and log β_2 = 44.3 for Fe(III) and log β_1 = 20.3 and log β_2 = 39.6 for Ga(III).[52,53]

[52] Green, M. A., Welch, M. J., *Nucl. Med. Biol.*, **16**, 435, 1989.
[53] Harris, W. R., Pecoraro, V. L., *Biochem.*, **22**, 292, 1983.

The nature of the bifunctional chelate plays a crucial role in the biodistribution of the radiopharmaceutical. Various different chelates have already been suggested for *in vivo* use with high stability and selectivity for linkage to Ga(III).

Table 2.5 Formation constants of Ga(III) with different Ligands

Ligand	**K_1**
DOTA	21.33
EDTA	21.7
DTPA	23.32
NOTA	30.98
oxalic acid	6.45
citric acid	10.02
transferrin	20.3

It's already known that four and five coordinate gallium complexes are of sufficient stability for *in vivo* use, but polydentate ligands with hard donor groups remains the optimal choice for gallium labeled biomolecules. The most prominant multidentate ligands are TAME Hex, DTPA, NOTA and DOTA and their molecular structures are shown in Figure 2.7.[54,55,56] These types of ligands are able to encapsulate Ga(III) with high specificity, and the anionic complexes of this nature are more sensitive than the uncharged complexes towards proton-catalyzed dissociation.

[54] Fani, M., Andre, J. P., Maecke, H. R., *Contrast Media Mol. Imaging*, **3**, 53, 2008.
[55] Bandoli, G., Domella, A., Tisato., F., Porcia, M., Refosco, F., *Coord. Chem. Rev.*, **253**, 56, 2009.
[56] Yang, D. J., Azhdarinia, A., Kim, E. E., *Curr. Med. Imaging Rev.*, **1**, 25, 2005.

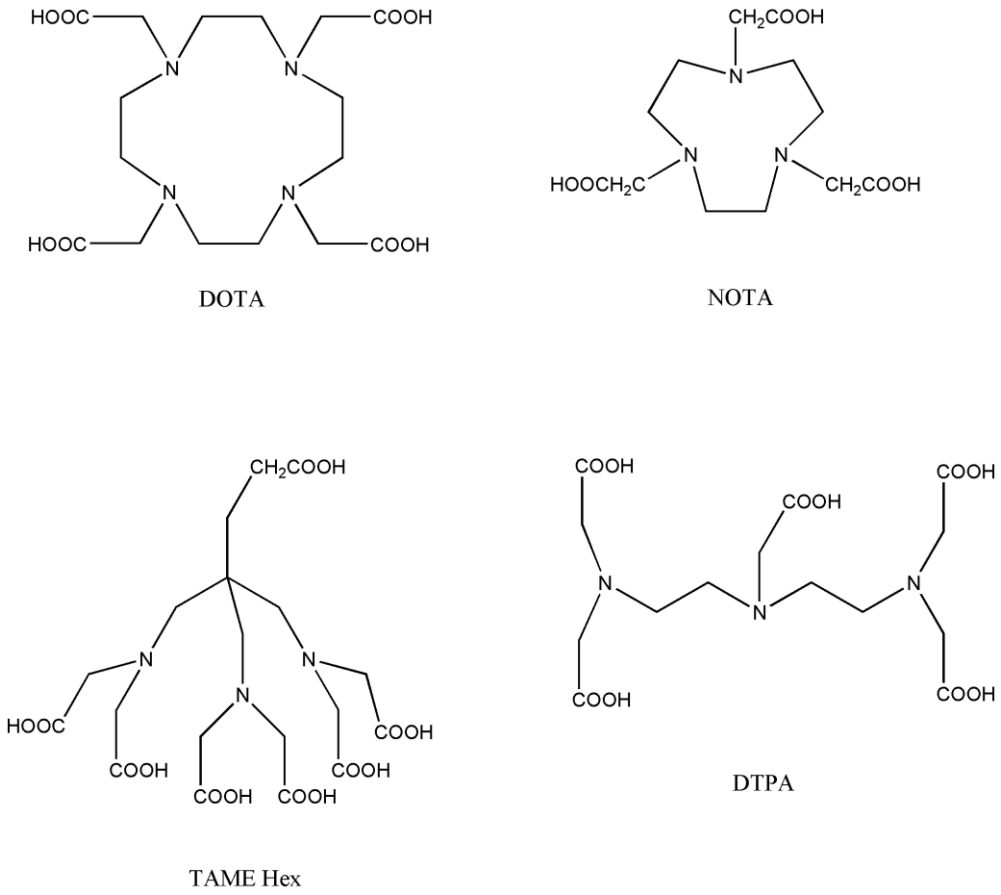

Figure 2.7 Schematic representation of the ligands DOTA, NOTA, TAME Hex and DTPA

2.3.5 Conjugation Strategies for ^{68}Ga

The conjugation strategies of Gallium-based agents are similar to that of the conjugation strategies of ^{99m}Tc. DOTA forms very stable metal-chelate complexes and has been linked to many different biomolecules (Table 2.6). The linkage occur either through an amide or thiourea linkage. By changing one of the carboxylic acids on DOTA a NHS-ester was generated and this chelate was then used to bind many different vectors, including peptides and botin.[57] *p*-Isothiocyanatobenzyl DOTA (Figure 2.8) is a derivative of DOTA and was used with antibodies and proteins.[58] DOTA-tris(*tert*-butyl ester) (Figure 2.8) is a ligand that is used to link DOTA to a peptide on a solid support. But this ligand can only be used to derivatize the N-terminus of the peptide chain which is attached to the lysine side chain or the

[57] Blom, E., Langstrom, B., Velikyan, I., *Bioconjugate Chem.*, **20**, 1146, 2009.
[58] Kruper, W. J., Rudolf, P. R., Janghoff, C. A., *J. Org. Chem.*, **58**, 3869, 1993.

solid support.[59] The problem with this system is the time required for deprotection to cleave the *tert*-butyl esters (it takes too long).

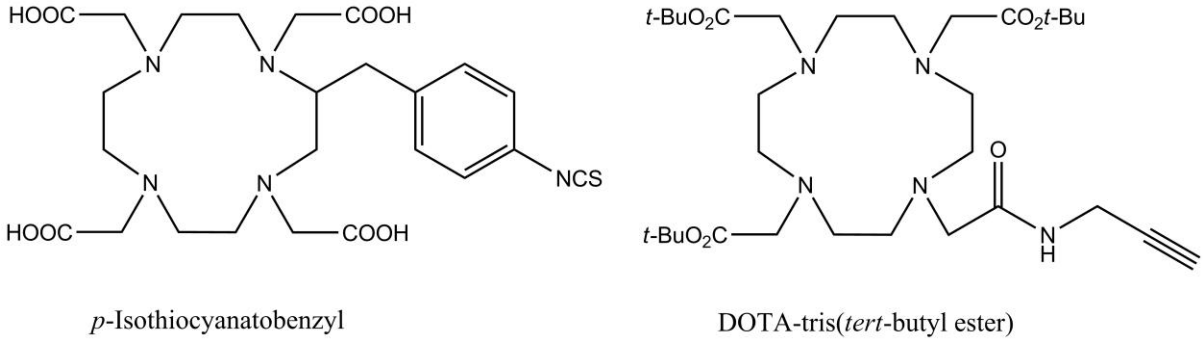

Figure 2.8 Schematic representation of *p*-Isothiocyanatobenzyl DOTA and DOTA-tris(*tert*-butyl ester)

The biomolecule, human epidermal growth factor (hEGF) was prepared by binding the N-sulfosuccinimide ester of DOTA (Figure 2.8) to hEGF. (Figure 2.9). Binding data of this complex showed high affinity in glioma U343 cells and carcinoma A431 cells. Biodistribution studies confirmed uptake of radioactivity in the EGFR-expression organs and in xenografts, indicating that it can be used for imaging EGFR overexpressed in tumors.[60]

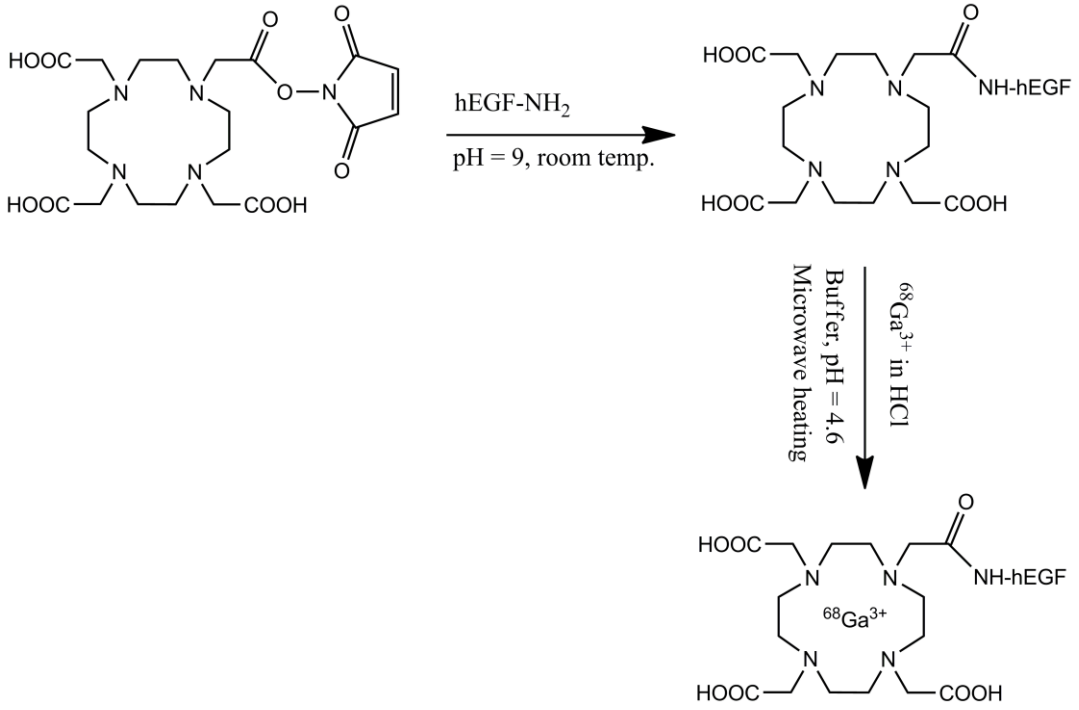

Figure 2.9 Reaction scheme for the preparation of ^{68}Ga-DOTA-hEGF

[59] De Leon-Rodriquez, L. M., Kovacs, Z., *Bioconjugate Chem.*, **19**, 391, 2008.
[60] Velikyan, I., Sunberg, A. L., Lindhe, O., Hoeglund, A. U., Eriksson, O. W., Werner, E., Carlsson, J., Bergstrom, M., Laangstrom, B, Tolmachev, V., *J. Nucl. Med.*, **46**, 1881, 2005.

^{68}GaDOTA-(Tyr^3)octreotate complex (Figure 2.10) was develop for the imaging of somatostatin receptor-positve tumors. This complex showed better preclinical, pharmacological performance when it was compared to the ^{111}In labeled complex and the Gallium complex derivative showed nearly 2.5 times greater tumor uptake in a mouse and lower kidney uptake than that of the ^{111}In complex derivative.[54]

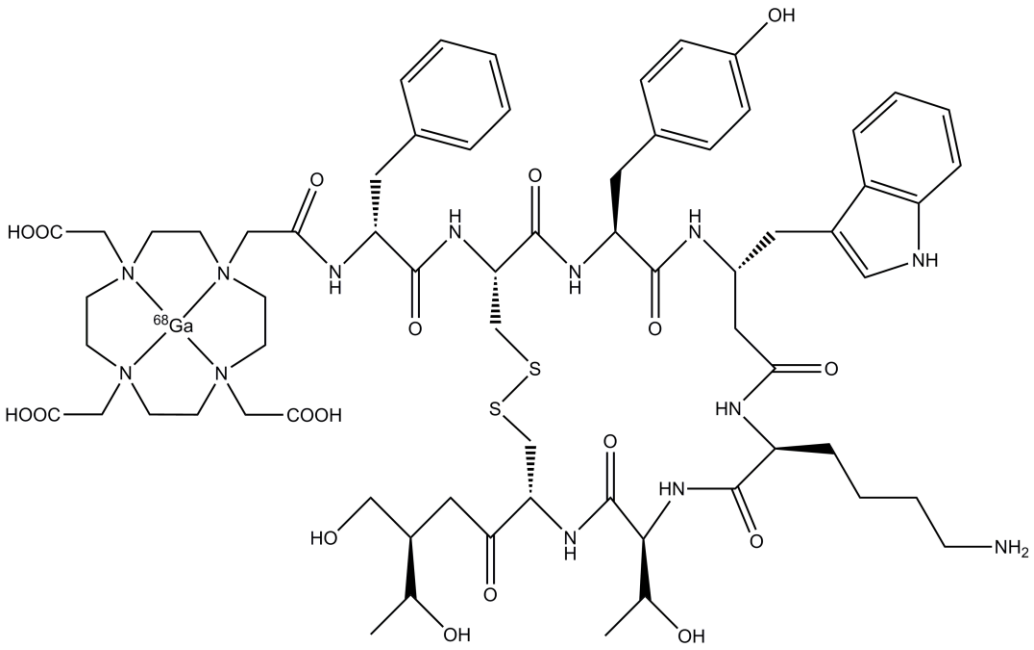

Figure 2.10 Schematic representation of ^{68}GaDOTA-(Tyr^3)octreotate

(Tyr^3)octreotate (TATE) can be prepared within 10 min at room temperature and it was found that the complex was stable in the reaction mixture of phosphate buffer and in human plasma after it is incubated into a human.[61] Some conjugation strategies and chelate systems for targeted gallium radiopharmaceuticals are given in Table 2.6.

[61] Velikyan, L., Maecke, H., Langstrom, B., *Bioconjugate Chem.*, **19**, 569, 2008.

Table 2.6 Some conjugation strategies and chelate systems for targeted gallium radiopharmaceuticals

Conjugation Strategy	Chelate	Biomolecule
amide formation	DOTA	biotin peptide MMP-2 octreotate Human epidermal growth factor (h EGF) bombesin somatostatin
thiourea formation	DOTA	protein and antibody
amide formation	NOTA	Peptides (TATE) [Tyr^3]-octreotide
thiourea formation	NOTA	cRGDyK RGD peptide [Tyr^3]-octreotide

The availability of these different bifunctional chelates, particularly the NOTA and DOTA derivatives will help support the development of new gallium agents.

2.3.6 Medical Applications of Gallium Complexes

2.3.6.1 Radioactive Gallium Complexes as Tumor Imaging Agents

Many studies have demonstrated that radioactive ^{67}Gallium citrate which is injected into tumor-bearing animals is observed in the malignant cells[62] and because of this the development of ^{67}Ga scan for the detection of malignant tumor in patients were investigated.[63] ^{67}Ga scanning was normally used for patients with Hodgkin's and non-Hodgkin's lymphomas to detect the residual disease or the disease that has relapsed following treatment with radiotherapy or chemotherapy.[64] The intensity of ^{67}Ga uptake by malignancies such as lymphoma reflects the metabolic activity of the tumor. Therefore, a ^{67}Ga scan after the treatment of lymphoma indicates the presence of malignancy and the

[62] Edwards, C. L., hayes, R. L., *J. Nucl. Med.*, **10**, 103-105, 1969.
[63] Johnston, G. S., *Int. J. Nucl. Med. Biol.*, **8**, 249-255, 1981.
[64] King, S. C., Reiman, R. J., Prosnitz, L. R., *J. Clin. Oncol.*, **12**, 306-311, 1994.

aggressiveness of a tumor.[65] The radioactive gallium can also be used to be taken up by macrophages which may show the areas of inflammation after a positive ^{67}Ga scan. However, tumor imaging with ^{18}F-fluorodeoxyglucose PET has its limitations. Tumors overexpressing somatosin centers like hepatocellular carcinoma, neuroendocrine tumors and indolent (slow growing) lymphomas may not take up FDG. To overcome these limitations ^{68}Ga-labeled radiopharmaceuticals for tumor imaging were developed. ^{68}Ga labelled-DOTA coupled to bombesin PET has been used to diagnose prostate cancer and ^{67}Ga- and ^{68}Ga-deferoxamine (DFO)-folate has been used to image tumors that shows high levels of cell surface folate receptors in a tumor xenograft model.[66]

2.3.6.2 Antineoplastic Activity of Gallium Nitrate in Cancer Treatment

The antineoplasitc activities of different metals such as aluminium, gallium, indium and thallium were investigated at the National Cancer Institute (NCI) and out of these metal complexes, gallium nitrate proved to be both highly effective in suppressing the growth of implanted tumors and also the least toxic. As a result of this, clinical studies on gallium nitrate were admistered by two different schedules: a short intravenous infusion (15 – 30 minutes) or continuous intravenous infusions over 24 hours for a week to assess the antitumor effectively and toxicity in different malignancies. It was discovered that this drug displayed its strongest antineoplastic activity in the treatment of bladder cancer and non-Hodkin's lymphoma. Studies have shown 30 % of patients with relapsed lymphomas and 17 – 63 % of patients with bladder cancer responded well to treatment with gallium nitrate.

2.3.6.3 Application of Gallium Complexes as Immunosupressive and Anti-inflammatory Agents

Many studies using *in vitro* and *in vivo* animal systems have shown that gallium complexes have immunosuppressive activity in animal models of autoimmune disease. Gallium nitrate has shown to suppress autoimmune encephalomyelitis and prevent inflammatory arthritis through suppression of macrophage function and T-cells in rats.[67] This complex can also

[65] van Amsterdam, J. A., Kluin-Nelemans, J. C., van Eck-Smit, B. L., Pauwels, E. K., *Ann. Hematol.*, **72**, 202-207, 1996.
[66] Mathias, C. J., Wang, S., Lee, R. J., Waters, D. J., Low., P. S., Green, M. A., *J. Nucl. Med.*, **37**, 1003-1008, 1996.
[67] Whitacre, C., Apseloff, G., Cox, K., Matkovic, V., Jewell, S., Gerber, N., *J. Neuroimmunol*, **39**, 175-181, 1992.

suppress lupus and prevent cardiac allograft rejection in murine models. Gallium nitrate and transferrin-gallium have also shown to prevent mixed lymphocyte culture response and lengthen the survival rate of mice with severe graft-versus-host disease in a murine bone marrow transplant model. Further investigations are on-going to establish whether the results of these animal studies are applicable to patients with autoimmune or inflammatory diseases.

2.3.7 Some Future Development of Gallium Complexes in Medicine

2.3.7.1 New Gallium Complexes with Antitumor Activity

Gallium nitrate can be considered to be one of the first generation of gallium complexes, but other novel gallium agents and gallium-based metallodrugs are in development and given in Table 2.7. Gallium moltolate prevent hepatocellular carcinoma cell growth and induces apoptosis through action on the mitochondrial pathway in lymphoma cell lines.[68] G4544 is discovered to be active for an antineoplastic agents but it is also studied in clinical trials for bone metastases and metabolic bone diseases. KP46 (Tris(8-Quinolonato)Ga(III) is examined clinically and has shown to induce apoptosis in a panel of malignant cell lines.

Table 2.7 Gallium compounds in preclinical and clinical development

Gallium complexes	**Tumors or diseases that were/being investigated**
Gallium nitrate	Hypercalcemia, metabolic bone disease Bladder cancer, lymphoma, other cancers Microbial infections
Gallium moltolate	Hepatome, lymphoma, microbial infections
G4544	Metabolic bone disease, osteoporosis, skeletal metastases
KP46 (Tris(8-Quinolonato)Ga(III)	Lung cancer, melanoma, other cancers
Orgnometallic gallium complexes	Various malignant cell lines

The lymphoma cell lines that are resistant to gallium nitrate–induced to apoptosis gives the opportunity to examine whether the newer gallium complexes developed are also cross-resistaned to gallium nitrate or whether they be more effective as therapeutic agents.

[68] Chitambar, C. R., Purpi, D. P., Woodliff, J., Yang, M., Wereley, J. P., *J. Pharmacol. Exp. Ther.*, **322**, 1228-1236, 2007.

2.3.7.2 New Gallium Complexes as Antimicrobial Agents

The ability of gallium to interfere with the utilization of iron by certain microorganisms inspired people to explore the potential of gallium as an antimicrobial drug. Gallium complexes such as transferrin-gallium and gallium nitrate were shown to block the iron-depended growth of *Mycobacterium tuberculosis* and *M. avium* complex extrallulary and also within human marcophages. Gallium interfered with iron acquisition by *Mycobacterium tuberculosis* within the macrophage phagosome which resulted in a bactericidal action if excess iron was not prevented.[69] It was discovered in some studies that gallium nitrate could inhibit *Pseudomonas aeuginosa* growth and kill biofilm bacteria *in vitro* through mechanisms that included interference with iron uptake. In this particular study, thermal injured mice were injected with *Pseudomonas aeuginosa* and gallium maltolate produced a 100 % survival rate with mice that were treated compared to 100 % mortality rate with mice that were not treated with gallium.[70]

2.4 Kinetic studies on Gallium(III) complexes

2.4.1 Introduction

Positron emission tomography (PET) plays an imperative role in medical diagnosis and for medical use the isotope has to fulfill certain requirements such as the specific activity obtained after irradiation of a target, particle range in the tissue and optimal particle energy, decay mode and the half-life. The most studied PET isotopes are ^{11}C and ^{18}F, however suitable metal isotopes also gain a lot of interests because they can be easier produced. One major drawback of metal isotopes is their toxicity when applied as a free aqua ion and that is why metal radioisotopes must be used in a stable format to avoid deposition and to suppress their toxicity. For *in vivo* application of the radioactive metal complexes, both their kinetic inertness and thermodynamic stability play a very important role. Among many metal-based PET agents, the radioactive gallium isotope (^{68}Ga with a half-life of 67.6 min) attracted much attention due to its exceptional properties.[71]

[69] Olakanmi, O., Britigan, B. E., Schlesinger, L. S., *Infect. Immun.*, **68**, 5619-5627, 2000.
[70] DeLeon, K., Balldin, F., Watters, C., Hamood, A., Griswold, J., Sreedharan, S., Rumbaugh, K. P., *Antimicrob. Agents Chemother*, **53**, 1331-1337, 2009.
[71] Kubicek, V., Havlickova, J., Kotek, J., Tircso, G., Hermann, P., Toth, E. & Lukes, I., *Inorg. Chem.*, **49**, 10960-10969, 2010.

Many of the interpretations of the kinetic behaviour of octahedral metal complex formation are based on a proposal by Eigen[72] that a 'dissociative-interchange' mechanism is obeyed, however recent kinetic studies of the gallium(III) complex formation showed an 'associative-interchange' mechanism is operative at least as far as the unhydrolyzed form of the cation.

Corigli *et.al.*[73] studied the kinetics and equilibria involved with the reaction between gallium(III) and salicylic acid (H_2SAL), 5-chlorosalicylic acid (H_2ClSAL), 5-nitrosalicylic acid (H_2NSAL) and 3,5-dinitrosalicylic acid (H_2DNSAL) in aqueous solution within a range of 0.0075 M to 0.2 M at temperatures ranging from 15.0 – 45.0 °C. They found that two complexes, GaL^+ and $GaHL^+$, were obtained with H_2SAL, H_2ClSAL and H_2NSAL whereas for the H_2DNSAL only the GaL^+ complex was obtained. The determined equilibrium constant, K_1, and forward and reverse rate constants for the Gallium(III)-3,5-Dinitrosalicylate ion at different temperatures are given in Table 2.9. The activation parameters of Gallium(III)-3,5-Dinitrosalicylate ion is given in Table 2.10.

Table 2.9 Values of the equilibrium constant K_1 and the forward and reverse rate constants for gallium(III)-3,5-Dinitrosalicylate ion

	15.0 °C	**25.0 °C**	**35.0 °C**	**45.0 °C**
K_1	18.7 ± 2.2	25.7 ± 1.6	34.6 ± 1.0	42.1 ± 3.5
k_1 ($M^{-1}s^{-1}$)	3.55 ± 0.15	8.01 ± 0.41	16.3 ± 1.0	32.9 ± 2.7
$10k_2$ (s^{-1})	0.87 ± 0.19	3.49 ± 0.51	14.4 ± 1.4	49.7 ± 3.5
$10k_{-1}$ ($M^{-1}s^{-1}$)	1.87 ± 0.08	3.14 ± 0.16	4.87 ± 0.31	7.62 ± 0.62
10^5k_{-2} (s^{-1})	0.46 ± 0.10	1.37 ± 0.20	4.29 ± 0.41	11.5 ± 0.8

Table 2.10 Activation parameters for the gallium(III)-3,5-Dinitrosalicylate ion

path	$10^{-3}(\Delta H^{\neq})/JM^{-1}$	$\Delta S^{\neq}/M^{-1}K^{-1}$	**path**	$10^{-3}(\Delta H^{\neq})/JM^{-1}$	$\Delta S^{\neq}/M^{-1}K^{-1}$
k_1	54.0 ± 2.0	-47 ± 7	k_{-1}	33.1 ± 2.0	-144 ±7
k_2	100.9 ± 4.5	85 ± 15	k_{-2}	80.0 ± 4.5	-12 ± 15

It was concluded that the negative $\Delta S^{\neq}$ obtained for k_1 agrees well with an 'associative-interchange' mechanism. They also concluded that both the rate constants increase with the basicity of the ligand and this behaviour is often a proof for an associative mechanism.

[72] Eigen, M. Z., Tamm, K., *Elektrochem.*, **64**, 115, 1960.
[73] Corigli, R., Secco, F. & Venturini, M., Inorg. Chem., **21**, 2992-2998, 1982.

Kubicek *et al.*[71] studied the complex formation of Ga(III) with 1,4,7,10-tetraazacyclododecane-1,4,7,10-teraacetic acid ($DOTA^{4-}$) and its derivative mono(n-butylamide), $DO3AM^{Bu})^{3-}$. The thermodynamic stability constants, log K(GaDOTA) = 26.05 and log K($GaDO3AM^{Bu}$) = 24.64, were determined by potentiometric titrations. The kinetics and dissociation of the complex formation of ^{71}Ga under both acidic and basic conditions were also followed and showed that the GaDOTA complex is more kinetically inert ($t_{1/2}$ = 12.2 d at pH = 0 and $t_{1/2}$ = 6.2 h at pH = 10) than that of $GaDO3AM^{Bu}$ ($t_{1/2}$ = 2.7 d at pH = 0 and $t_{1/2}$ = 0.7 h at pH = 10).

It was also established that Ga(III) forms highly stable hydroxocomplexes and that Ga(III) hydroxide precipitates already at pH ~3.5 and dissolves back at pH ~8 forming the tetraogallate anion and that $GaDO3AM^{Bu}$ was the only complex that formed a mixed hydroxocomplex. A significant decrease in stability was observed when a nitrogen atom of the cyclen skeleton was substituted with oxygen or a pyridine ring and that Ga(III) forms less thermodynamically stable complexes with DOTA-like ligands than that of NOTA-like ligands which is a much lower basicity ligand.[74]

Macdonald *et al.*[75] studied the equilibrium and kinetics of the formation of Ga(III) with 4-nitrocatachol in aqueous solutions. The reaction between $Ga(ClO_4)_3$ and 4-nitrocatachol were investigated at λ = 420 nm over a pH range of 2-3. The measured spectrophotometrically determined equilibrium constant, K = 0.034 ± 0.003 M, is in good agreement with the determined kinetic value of 0.034 ± 0.001 M at 25.0 °C. The complexation increased with pH and at very high acidities (pH < 0.5) no complex formation was observed.

Furthermore, over the pH range studied, the complex formation reactions between the monohydroxo $(H_2O)_5Ga(OH)^{2+}$ and the 4-nitrocatechol rate constants for the forward reaction at 25.0 °C is 7.4 x 10^{-3} $M^{-1}s^{-1}$ and for the reverse (decomposition) reaction at 25.0 °C is 65 ± 3 JK^{-1}. The activation parameters for the reverse reaction was determined as $\Delta H^{\neq}$ = 65 ± 3 $kJmol^{-1}$ and $\Delta S^{\neq}$ = -1 ± 5 $JK^{-1}mol^{-1}$ showing evidence of a 'dissociative-interchange' mechanism.

[74] Clarke, E. T. & Martell, A. E., *Inorg. Chem., Acta*, **181**, 273-280, 1991.
[75] Macdonald, C. J., *Inorg. Chim. Acta*, **311**, 33-39, 2000.

Campisi *et al.*[76] studied the kinetics and equilibrium reactions of the formation between Ga(III) and thiocaynate $(NCS)^-$ in aqueous solutions, where they measured the reaction over a wide acidic pH range and various temperatures. The entire study was focused primarily on the hydrolysis of the complex to form the desired product. They observed that the hydrolysis formation occurs in three steps where the forward rate constants at 25.0 °C are $k_1 = 57 \pm 4\ M^{-1}s^{-1}$, $k_2 = 1.08 \pm 0.01 \times 10^5\ M^{-1}s^{-1}$ and $k_3 = 3 \times 10^{-6}\ M^{-1}s^{-1}$, respectively. The equilibrium constant was determined *via* a spectrophotometric titration as $20.8 \pm 0.3\ M^{-1}$ at 25.0 °C at ionic strength of 0.5 M. The activation parameters at 25.0 °C for paths, k_1, k_2, and k_{-1} were determined as $\Delta H_1^{\neq} = 70 \pm 8\ kJmol^{-1}$, $\Delta S_1^{\neq} = 24 \pm 20\ JK^{-1}mol^{-1}$, $\Delta H_2^{\neq} = 43 \pm 7\ kJmol^{-1}$, $\Delta S_2^{\neq} = -7 \pm 24\ JK^{-1}mol^{-1}$ and $\Delta H_{-1}^{\neq} = 77 \pm 8\ kJmol^{-1}$, $\Delta S_1^{\neq} = 23 \pm 20\ JK^{-1}mol^{-1}$.

2.4.2 Discussion

All the kinetic studies mentioned above involving the formation of Ga(III) complexes were done in aqueous solutions were hydrolysis play a significant role[71,73,74,75,76]. It is clear from literature that most of the kinetic studies in literature involve the formation of gallium(III) complexes with different ligands where the focus is primarily on the pH dependence of these reactions[71,73,74,75,76] There is still to date very little reactivity studies that have been done on the aqua or methanol substitution of gallium(III) complexes with different ligands.

2.5 Gold as Coordination Metal

2.5.1 A Brief History of Gold

Gold was the first metal to be discovered by civilizations as shining yellow nuggets. The symbol of Gold is 'Au' and it was derived from the Latin word 'aurum', which is related to the goddess of dawn, Aurora. People almost instantly attribute a high value to gold, where they associated it with power, beauty and cultural elite.

Archeological digs suggest that gold was first used in the Middle East and experts in the study of fossils have observed pieces of gold in Spanish caves used by Paleolithic Man in about 40000 BC. The first pieces of gold, which dated from the third millennium BC, were discovered in the tombs of Queen Zer of Egypt and Queen Pu-abi of Ur in Sumeria. The largest collection of gold, jewellery and a gold coffin in the world was dated from the second

[76] Campisi, A. & Tregloan, P. A., *Inorg. Chim. Acta*, **100**, 251-259, 1985.

millennium BC. The Persian Empire (now Iran) made frequent use of gold in their artwork as part of their religion of Zoroastrianism. These artwork mainly depicted animals, which were modified after the Arabs conquered the area in the seventh century AD. Gold was first used as money in around 700 BC by Lydian merchants (Western Turkey).

2.5.2 Physical and Chemical properties of Gold

Gold is a transitional metal and is found in nature as a free metal. This metal is obtained from its ore by smelting and has an atomic number of 79 and a molecular weight of 196.97 g/mol. Gold is bright yellow in colour and is a soft, ductile and the most malleable of any element. This metal is a good conducter of electricity and heat and reflects radiation. Gold is soluble in *aqua regia* and solutions of azoimide and is unaffected by air, nitric, hydrochloric and sulphuric acids. It has a melting point of 1064.76 °C and a boiling point of 2700 °C, with a density of 19.3 g/ml.

2.5.3 Applications of Gold

Gold is mainly used for coinage, ornaments, jewellery and gliding. This metal is also used in the textile industry and the isotopes of gold are used for radiotherapy.

2.6 Gold as Radiopharmaceutical

2.6.1 Introduction

There are thirty-six gold isotopes that have been discovered so far ($^{170\text{-}205}$Au). These include one stable (^{197}Au), 27 proton-rich and 8 neutron-rich isotopes.[77] The different radioactive isotopes were produced by methods such as: fusion evaporation (FE), light-particle (LP), deep-inelastic (DI), neutron capture (NC), photo-nuclear (PN) and spallation (SP) reactions.

2.6.2 Production of Gold Isotopes and Radioactive Isotopes

The only stable gold isotope is ^{197}Au which contains 79 protons and 118 neutrons. Neutron-deficient isotopes are produced by bombarding the lighter atoms with positively charged

[77] Schuh, A., Fritsch, A., Ginepro, J. Q., Heim, M., Shore, A., Thoennessen, M., Atomic Data and Nuclear Data Tables, 96, 307-314, 2010.

particles in a linear accelerator or in a cyclotron. All the known isotopes of gold are given in Table 2.8.

Table 2.8 Gold radionuclides with their respected half-life's and decay's

Atomic number	Physical half-lives	Decay mode
177	1.35 sec	A
178	2.65 sec	A
179	7.25 sec	A
181	11.55 sec	α, EC
183	45.5 sec	A
185	4.3 min	α, EC
186	12 min	EC, γ
187	8 min	α, EC
188	8 min	EC, γ
189	29.7 min	EC, γ
189m	4.7 min	EC, γ
190	39 min	EC, γ
191	3.2 hours	EC, γ
192	5.0 hours	EC, β^+, γ
193	17.5 hours	EC, γ
193m	3.9 sec	Γ
194	39.5 hours	EC, β, γ
195	183 days	EC, γ
195m	31.0 sec	β^+, γ
196	6.2 days	EC, β, γ
196m	9.7 hours	Γ
197	Stable	
197m	7.5 sec	Γ
198	2.70 days	β, γ
199	3.15 days	β, γ
200	48.4 min	β, γ
201	26 min	β, γ
202	30 sec	β, γ
203	55 sec	β, γ
204	4.05 sec	β, γ

The isotopes with an atomic weight from 177 to 183 are all alpha emitters and have relative short half-lives (less than a minute). The isotopes with mass numbers from 185 to 196 decay by gamma emission, electron capture and in some cases also positron emissions. Of these

isotopes the only long-lived isotope with a half-life of 183 days is ^{195}Au. This isotope is produced by the following reaction:

$$^{195}_{78}Pt + ^{1}_{1}p \rightarrow ^{195}_{79}Au + ^{1}_{1}n$$

Platinum with an atomic mass of 195 is bombarded with 22 MeV protons in a cyclotron to produce the ^{195}Au isotope. This is a very expensive process and ^{195}Au is not very widely used.

Neutron-heavy isotopes are prepared by neutron capture reactions and all of them decay by beta emissions and gamma radiation. The most important isotope in this group is ^{198}Au and it is prepared by the following reaction:

$$^{197}_{79}Au + ^{1}_{0}n \rightarrow ^{198}_{79}Au$$

^{198}Au is widely used for tracer studies, in medical diagnosis and in radiotherapy.

^{199}Au is a reactor-produced radionuclide which is considered to be one of the potential radioisotopes for the use in therapeutic nuclear medicine. It emits β^- particle emissions (E_{max} = 0.46 MeV) with a half-life of 3.15 days and also emits γ-radiation (E_γ = 158.208 MeV), which makes it suitable for external detection by single-photon imaging instrumentation used in nuclear medicine departments. More importantly ^{199}Au is potentially available in high specific activity, which makes it amenable for targeting limited numbers of receptors on tumor cells. For this isotope to be used in radiotherapy, a complex of gold must be kinetically stable to substitution and reduction under biological conditions, such as, 37 °C and blood pH of 7.4.[78,79]

2.6.3 Properties and Coordination Chemistry of Gold

In complexes with only one gold atom attached to a specific ligand, the oxidation states of +1, +2, +3 and +4 are well investigated and gold can also form many complexes with metal-metal bonds in which it is very difficult to establish the oxidation states of the metal atom. The oxidation state of gold(III) is very important but rare for silver and copper. All known gold(III) complexes are diamagnetic with the low-spin $5d^8$ electron configuration and most of

[78] Barnholtz, S. L., Lydon, J. D., Huang, G., Venkatesh, M., Barnes, C. L., Ketring, A. R. and Jurisson, S. S., *Inorg. Chem.*, **40**, 972-976, 2001.
[79] Bottenus, B. N., Kan, P., Ballard, B., Rold, T. L., Barnes, C., Cutler, C., Hoffman, T. J., Green, M. A., Jurisson, S. S., *Nuclear Medicine and Biology*, **37**, 41-49, 2010.

these complexes have a four co-ordinate, square-planar stereochemistry. Examples of these complex ions are $[AuCl_4]^-$ and $[Au(NH_3)_4]^{3+}$.

Gold(I) chemistry is dominated by complexes with soft bases such as oxygen donor ligands and tertiary phosphines with fluorides. This is less prominent in the case of gold(III) chemistry, thus an extensive chemistry of gold(III) with soft ligands like tertiary phosphines and thiols and also harder ligands like fluoride and nitrogen- donor ligands are still extensively investigated.

Gold(III) complexes with the low-spin $5d^8$ electron configuration are considered to be kinetically inert compared to the d^{10} of gold(I)

Although ^{199}Au has suitable nuclear properties, it has not been extensively investigated for radiotherapy applications because Au(III) coordination chemistry is relatively scarce in literature and gold(III) is very difficult to work with, due to the fact that it is unstable to reduction. It readily undergoes hydrolysis reactions and Au(III) complexes often tends to precipitate to form $AuCl_4^-$, $AuCl_2^-$ or mixed $AuCl_4^-/AuCl_2^-$ salts that exhibit poor solubility. The literature of gold(III) complexes showed to be predominantly square planar in geometry with ligands such as amine, imine, Schiff base and amide ligands that is coordinated to the metal center to form the gold(III) complexes.[78,79]

2.6.4 Medical Applications of Gold-based Therapeutic Agents

2.6.4.1 Introduction

Gold was used as a medicinal character throughout the ancient history in the form of amulets and medallions, where it was used to ward off evil spirits and diseases. Potions (in the form of gold powders) were also used to treat ill patients. But after chemists discovered that gold could be dissolved in *aqua regia*, gold complexes and elemental gold were more frequently used in medical applications.

2.6.4.2 Applications

The first application of gold complexes was against pulmonary tuberculosis but it was not very effective. Jacque Forestier discovered that the use of gold compounds to treat rheumatoid arthritis was more effective but not to all the patients that were treated. Many gold thiolates were used for this purpose but only four gold complexes are still used

clinically: gold sodium thiomalate and gold thioglucose (In the United States) as well as sodium bis(thiosulfato)gold(I) and sodium thiopropanolsulfonate-S-gold(I) (In Europe). The only new gold complex that was introduced into clinical use was auranofin. Most of the molecular structures of these complexes mentioned above, are shown in Figure 2.11.

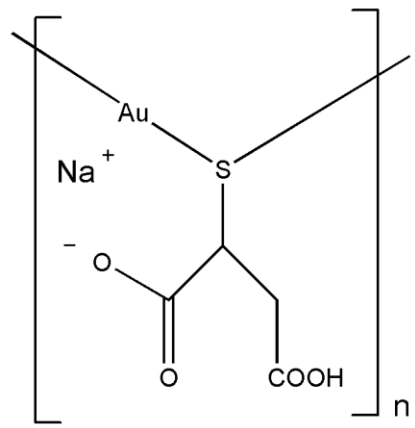

gold sodium thiomalate

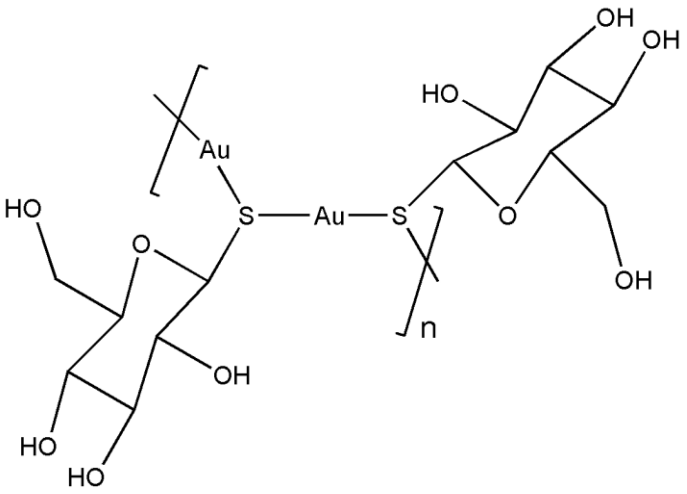

gold thioglucose

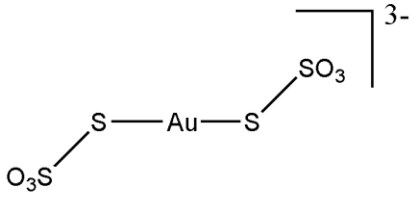

bis(thiosulfato)gold(I)

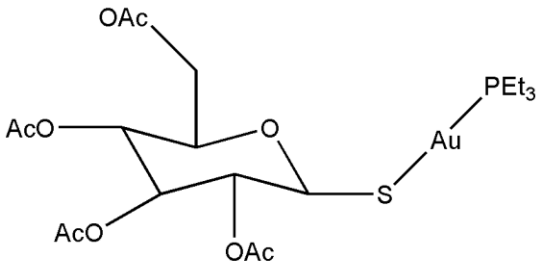

auranofin

Figure 2.11 Schematic representation of gold sodium thiomalate, gold thioglucose, bis(thiosulfato)gold(I) and anranofin

Gold complexes can also be used for the treatment of arthritis, an autoimmune disease of the skin, asthma and pemphigus. In addition, gold complexes could also be used for the treatment of cancer, HIV and malaria.[80]

[80] Shaw III, C. F., *Chem. Rev.*, **99**, 2589-2600, 1999.

3 Basic Theory of IR, UV-Vis, ^{1}H NMR, Chemical Kinetics and X- Ray Diffraction

3.1 Introduction

A brief overview of the characterisation techniques employed in this study will be discussed here. These include infrared spectroscopy, ultraviolet-visible spectroscopy (UV-Vis), nuclear magnetic resonance (NMR) and single crystal X-Ray diffractometry (XRD). The structures of different ligands and complexes were fully characterized and discussed by UV-Vis spectroscopy in Chapter 4 and by X-ray diffractometry in Chapter 5.

These characteristic techniques play a major role in the determination of starting materials, possible intermediates and finals products of reaction mixtures. It is especially important in chemical kinetics where these techniques play a major role in determining the intimate mechanism of reactions.

3.2 Spectroscopic Techniques

3.2.1 Infrared Spectroscopy

Infrared spectrophotometry is an analytical technique which can be used for the identification of organic and inorganic compounds. All chemical compounds, except for some homonuclear compounds such as O_2, N_2 and Cl_2, absorb infrared radiation.[1] Each molecular species, with the exception of chiral molecules in the crystalline state, has a unique infrared spectrum.

[1] D.A. Skoog, D.M. West, F.J. Holler, S.R. Crouch, *Fundamentals of Analytical Chemistry*, 8th Edition, California, Thomson Brooks/Cole, 2004.

Infrared spectroscopy is not as effective as Ultraviolet-Visible spectroscopy for quantitative analysis because of lower sensitivity and frequency deviations from Beer's law, which makes the absorption measurements less precise.[1]

This technique is based on the absorption measurement of different IR frequencies of a compound placed in the path of an IR beam. The frequency, *v*, is defined as the number of wave cycles that pass through a point in one second and wavelength, λ, which is the length of one complete wave cycle. The relation between frequency, *v*, and wavelength, λ, is given by Eq. 3.1.

$$v = \frac{c}{\lambda} \qquad \text{... Eq. 3.1}$$

where c is the speed of light with a constant value of $3x10^{10}$ cm/sec. To calculate the energy Eq. 3.2 can be used:

$$E = hv = \frac{hc}{\lambda} \qquad \text{... Eq. 3.2}$$

where h is Plank's constant with a value of $6.600x10^{-34}$ J.s

The energy of infrared radiation can excite vibrational and rotational transitions, but it is unable to excite electronic transitions. For liquid and solid samples, changes in rotational energy can give rise to a series of peaks for each vibrational state. This rotation is often hindered or prevented, so the effects of these small energy differences are not detected. Therefore, an IR spectrum is produced from transitions between two vibrational levels of the molecule in the ground state and is observed as absorption spectra.

During the absorption of infrared radiation, molecules are excited into a higher-energy state. Molecules can only absorb infrared radiation if it corresponds to the national stretching and bending vibrational frequencies of the molecule. The energy that is absorbed increases the amplitude of the vibrational motions of the bonds in the molecule.[2] Each type of bond has a different natural frequency of vibration and although two compounds that may have the same type of bonds; the bonds will experience two slightly different environments, and therefore cannot give the same radiation absorption pattern, and thus an infrared spectrum of each different molecule is unique and can be used to identify different molecules.

[2] K. Nakomato, *Infrared Spectra of Inorganic and Coordination Compounds*, 2nd Edition, New York, Wiley & Sons, Ltd., 1970.

Triple bonds, like a carbonyl group, have higher stretching frequencies than double bonds and the latter have higher stretching frequencies than single bonds. For example $[Re(C_{14}H_{17}N_3O)(CO)_3]Br \cdot CH_4O$, the carbonyl group is often used for complex characterisation because the carbonyl stretching produces a distinct absorption peak (the stretching and bending frequency of a metal carbonyl complex (M - CO) ranges from 1700 – 2200 cm^{-1}).[3] The carbonyl group is permanently polarised, which means that any vibrational stretching of this bond will affect the dipole moment. The carbonyl group (CO) is a very good π-acceptor ligand and for this reason makes it an excellent ligand for stabilizing an electron-rich low-valent metal centre. The ability of the ligands to donate electron density to the metal plays a role on the actual amount of electron density on the metal. If the electron density on the metal centre increases the π-backbonding to the carbonyl group will also increase. Ligands positioned *trans* to the CO group have a big effect on the CO π-backbonding to the metal and if this ligand is a σ-donating ligand, the metal carbonyl bond will get stronger because of metal to CO π-backbonding (Figure 3.1).

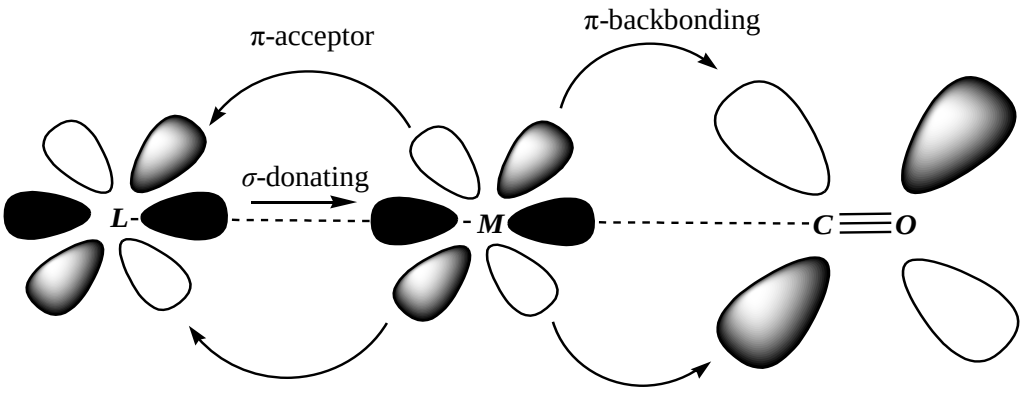

Figure 3.1 A σ-donating ligand will increase the M-CO bond strength because of CO π-backbonding

3.2.2 Ultraviolet- Visible Spectroscopy

Ultraviolet- Visible spectroscopy is a widely used analytical technique to identify functional groups and to determine the content of a specie. The UV-Vis spectroscopy technique is based on the absorption of radiation of atoms or molecules, which occur in different electronic absorption bands, from the lowest energy state (ground state) to the highest electronic energy level state (excited state).[1] The total electromagnetic radiation absorbed

[3] B. Stuart, Modern Infrared Spectroscopy, Editor. D. J. Ando, England: John Wiley & Sons, Ltd., 1996.

consists of energy, which is equal to the energy difference between the excited energy state (highest energy level) and the ground state (lowest energy level) (Figure 3.2).[4]

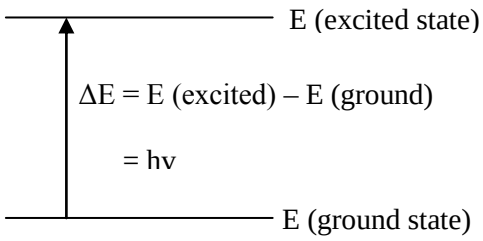

Figure 3.2 The excitation process is where electrons are exited from the ground state to the exited state when radiation energy is absorbed

In UV-Vis spectroscopy the absorption of electromagnetic radiation causes transitions between the electronic energy levels. As the electrons absorb ultraviolet or visible light, these electrons are excited from the ground state (highest occupied molecular orbital – HOMO) to the excited state (lowest unoccupied molecular orbital – LUMO). Transitions are usually smaller than 200 nm. Single bonds like carbon/carbon and carbon/hydrogen possess good orbital overlaps. The energy difference for $\sigma \rightarrow \sigma^*$ is relatively large and the excitation of π electrons require less energy $(\pi \rightarrow \pi^*)$. Nonbonding electrons can also be excited into higher-energy states: $n \rightarrow \sigma^*$ and $n \rightarrow \pi^*$ (Figure 3.3).

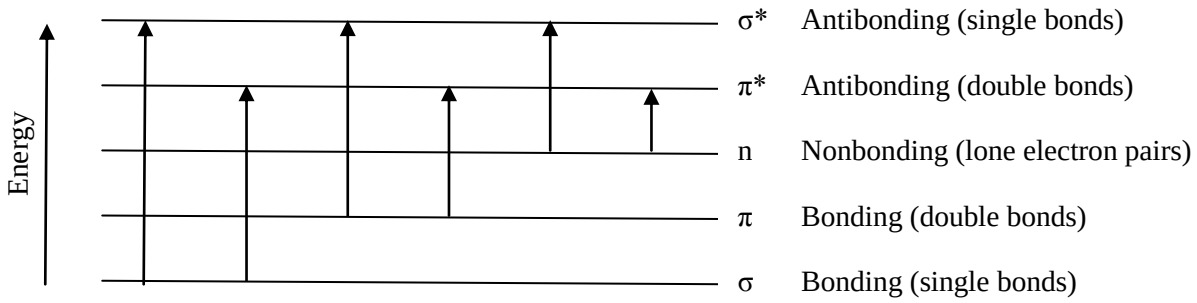

Figure 3.3 Energy levels of orbitals and the transitions between the respective orbitals

The absorption of radiation energy by molecules in the UV-Vis region (180-780 nm) results from interaction between photons and electrons that either participated directly in bond formation or are localized about atoms such as Nitrogen, Sulphur, Oxygen and the halogens. The wavelength at which molecules absorb in the electromagnetic region depends on how

[4] D.L. Pavia, G.M. Lampman and G.S. Kriz, *Introduction to Spectroscopy*, 3 rd Edition, USA: Thomson Learning, Inc., 2001.

tightly the electrons are bonded. The shared electrons in carbon/hydrogen or carbon/carbon are so strongly held that their excitation requires energies corresponding to wavelengths below 180 nm. Electrons involved in double and triple bonds of molecules are not strongly held thus the excitation by radiation can occur much easier and therefore, exhibit useful absorption peaks. Unsaturated organic functional groups that absorb in the UV-Vis region are called chromophores. Saturated compounds containing Nitrogen, Sulphur, Oxygen and the halogens have non-bonding electrons that can be excited by radiation in 170-250 nm regions.

In general, ions and complexes of elements in the first two transition series absorb broad bands of visible radiation in at least one of their oxidation states. Absorption involves transitions between unfilled and filled *d*-orbitals with energies that are depended on the ligands bonded to the metal ions, and the energy difference between these *d*-orbitals are depended on the position of the element in the periodic table, the nature of the ligand bonded to it and its oxidation state.[1]

Ultraviolet- Visible spectroscopy is used for qualitative and quantitative analysis, but it does not provide sufficient structure data for the identification of a molecule. Therefore, other analytical techniques, such as nuclear magnetic resonance (NMR) and X-ray diffractometry must be used to support the results obtained from Ultraviolet- Visible spectroscopy for the identification of a molecule.

3.2.3 Nuclear Magnetic Resonance Spectroscopy

Nuclear magnetic resonance (NMR) spectroscopy was developed in 1924 by W. Pauli and this analytical technique is based on the measurement of absorption of electromagnetic radiation in the radio-frequency region 4 – 900 MHz. Nuclear magnetic resonance (NMR) is a very powerful tool that chemists and biochemists can use to determine a detailed chemical structure of a compound. It is a non-destructive method and a very small amount of compound (less than one milligram) can be used to obtain good data. NMR gives a spectrum that provides information about the atoms that are magnetically distinct.

This analytical technique is based on the fact that the nucleus of an atom has magnetic properties and rotates around its own axis, thus also have the property of spin. A nucleus that has spin has angular momentum. According to quantum mechanics the maximum values for angular momentum is its spin quantum number, I. Nuclei with a spin of I have $(2I + 1)$

possible orientations and the component of angular momentum for these orientations in any direction can have one of the following values, I, $I - 1$, $I - 2$, ... $- I$. The orientations will have an equal energy if no magnetic field is applied.

In order to obtain a complete NMR spectrum, the nucleus with a spin quantum number I must not have a zero value. The most common nuclei that chemists and biochemists used are ^{1}H, ^{13}C, ^{19}F and ^{31}P with a spin quantum number of, $I = 1/2$. Nuclei with spin quantum numbers greater than 1/2 generally gives broad NMR lines.[5] A nucleus with spin 1/2 can have two orientations. +1/2 which is parallel to the applied magnetic field and -1/2 which is anti parallel to the applied magnetic field. When an external field is applied a split of energy levels will occur (as shown in Figure 3.4) and each energy level has a quantum number m, a spinning charge nucleus generates a magnetic field and the resulting spin-magnet has magnetic moment u, which is proportional to the angular momentum p of a spinning nucleus.

$$u = \gamma p = \frac{\gamma h}{2\pi} \qquad \text{... Eq. 3.3}$$

where h = Planck's constant and γ = magnetogyric ratio. The two orientations are separated by an energy difference, ΔE, which is dependent on the strength of the applied field and size of the nucleus angular moment (Figure 3.4).[6]

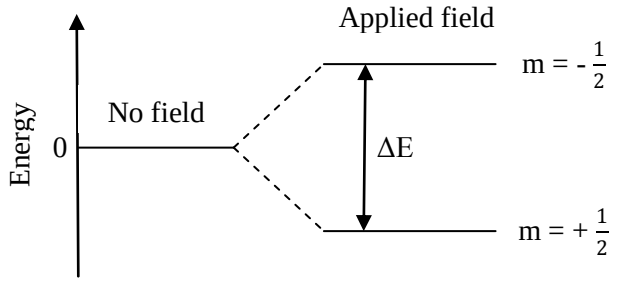

Figure 3.4 Energy levels of a nucleus with a spin quantum number of 1/2

In general, if a magnet is spinning around its north and south axis, because of the gyroscopic effect, the force that is applied by the field to the axis causes rotation but not in the plane that the force is applied but perpendicular to this plane; thus the axis of this rotating particle,

[5] P.J. Hore, *Nuclear Magnetic Resonance*, New York: Oxford University Press, Inc., 1995.
[6] D.A. Skoog, F.J. Holler, S.R. Crouch, *Principle of Instrumental Analysis*, 6th Edition, Thomson Brooks/Cole, 2007.

therefore, moves in a circular motion. This motion is also applicable to a magnetically active nucleus and is demonstrated in Figure 3.5.

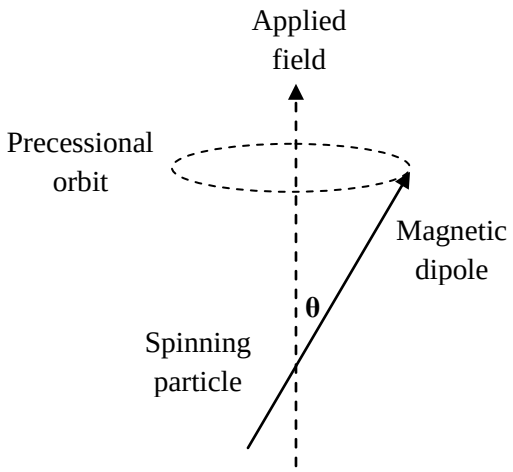

Figure 3.5 Precession of a rotating particle in an electromagnetic field

The angular velocity of this motion is calculated in radians per second and is given by Eq. 3.4.

$$\omega_0 = \gamma B_0 \qquad \text{... Eq. 3.4}$$

where B_0 is the applied field. The angular velocity can be converted to the *Larmor frequency* by using Eq. 3.5.

$$\nu_0 = \frac{\gamma B_0}{2\pi} \qquad \text{... Eq. 3.5}$$

If the rotational frequency of the magnetic vector of radiation is the same as the precessional frequency of a nucleus, absorption takes place. Flipping of the magnetic dipole can then occur.[6]

A NMR spectrum is produced from the protons within a molecule. The protons differ from one another because they have different chemical and electronic environments, which result in distinctive frequency absorptions. The protons are shielded by the surrounding valence electrons with varied hydrogen atoms, which cause a magnetic field. These unique absorption frequencies result in different signals, which are called chemical shifts, δ. Different factors such as polar functionality group, geometry, stereochemistry and hydrogen bonding can affect the shielding of the proton and alter the chemical shift.

A proton can be affected by the magnetic field of a neighbouring proton, which produces magnetic interactions between nuclei. This effect is known as *spin-spin coupling*, whereby the resonance frequency of one proton is split by the presence of another proton. The difference between the split frequencies (observed as peaks) is known as the *coupling constant, J*, which indicates the degree of interaction between neighbouring nuclei.[4] There are three rules that can be applied to interpret the splitting patterns:

- A proton with a number of N equivalent neighbouring protons are split in (N + 1) peaks.
- A proton with N non-equivalent neighbouring protons is split in 2^N peaks.
- Equivalent protons undergoes no *spin-spin coupling* with each other, they only cause splitting to the neighbouring protons.

3.3 Chemical Kinetics

3.3.1 Introduction

The purpose of kinetic investigations is to gain insight about the intimate mechanism by which chemical changes occur. Ultraviolet- Visible spectrophotometry is a technique, which is often used to make kinetic measurements. This method is usually used for slow reactions, and it is based on the fact that each molecule has its own absorption spectrum.

The kinetics of almost every known reaction can be studied by using some sort of technique.[7] From the Beer-Lambert law, the relationship between the concentration, c of single absorbing specie, and intensity of the incident monochromatic light, I_0 and the transmitted intensity, I_{trs} can be found:[8]

$$\log_{10} \frac{I_0}{I_{trs}} = \varepsilon cl = A \qquad \text{... Eq. 3.6}$$

where l is the path length, ε is the extinction coefficient and A is the absorbance of a solution. The total absorbance is the sum of all the individual absorbances of each species:

$$A = \sum_1 \varepsilon C.l \qquad \text{... Eq. 3.7}$$

[7] S.W. Banson, *The Foundations of Chemical Kinetics*, McGraw-Hill, New York, 1960.
[8] P.W. Atkins, Physical Chemistry, Oxford University Press, 1994.

Factors such as concentration, pressure, temperature, homogeneity and sensitivity to light and air can affect the rate constant and rate mechanism of a chemical reaction. If the temperature, pressure and volume of a system are kept constant, the rate constant is simply the rate of change in time of any reactants or products.

3.3.2 Reaction Rate and Rate Laws

For a general reaction the rate is defined as the changes in the concentration of a reactant or product per unit time:

$$aA + bB \xrightarrow{k} mM \quad \text{... Eq. 3.8}$$

and for a closed system, thus at constant volume, the rate can be described as:

$$Rate = -\frac{d[A]}{dt} = -\frac{d[B]}{dt} = \frac{d[M]}{dt} \quad \text{... Eq. 3.9}$$

where t is the time and $[x]$ is the concentration of each compound. The general rate of consumption or formation is in the form:

$$Rate = k[A]^y [B]^z \quad \text{... Eq. 3.10}$$

where *k* is the rate constant, y and z are the partial orders respectively to the concentration of A and B. The order of a reaction is defined as the variation of rate because of changes in concentration from one or both the reactants. It is very difficult to determine these types of values experimentally. A way to overcome this problem is to make use of *pseudo*-first order conditions, where one of the concentrations is kept constant while the other one is changed. For example, [B] >> [A], and this will give rise to Eq. 3.11.

$$Rate = k_{obs}[A]^y \text{ and } Rate = k_{obs}[B]^z \quad \text{... Eq. 3.11}$$

k_{obs} is the *pseudo*-first order rate constant, and by varying the concentration of B, the rate constant can be determined.

The second order rate law (where y and z = 1) of a simple reaction can be as follows:

$$a[A] + b[B] \underset{k_2}{\overset{k_1}{\rightleftharpoons}} m[M]$$

$$Rate = k_1[A][B] + k_2[A] \quad \text{... Eq. 3.12}$$

and for *pseudo*-first order conditions, k_{obs} can be described as:

$$k_{obs} = k_1[B] + k_2 \quad \text{... Eq. 3.13}$$

The equilibrium constant of a closed system where the temperature and pressure are kept constant can be given as:

$$K_{eq} = \frac{k_1}{k_2} = \frac{[M]^m}{[A]^a[B]^b} \quad \text{... Eq. 3.14}$$

The half-life, $t_{1/2}$, of a first order reaction can be defined as the time required for the concentration to fall one half (50 %) of its initial value and is given by Eq. 3.15.

$$t_{1/2} = \frac{\ln 2}{k} = \frac{0.693}{k} \quad \text{... Eq. 3.15}$$

By integrating Eq. 3.15 the following is obtained when t = 0:

$$\ln \frac{[M]_t}{[M]_0} = k_{obs} \text{ or } [M]_t = [M]_0 e^{k_{obs}t} \quad \text{... Eq. 3.16}$$

$[M]_t$ and $[M]_0$ is the concentration change of the reactant at time = 0 and t respectively.

By using Eq. 3.17:

$$\ln \frac{k}{T} = -\frac{\Delta \overline{H}^{0^*}}{RT} + \frac{\Delta \overline{S}^{0^*}}{R} + \ln \frac{R}{Nh} \quad \text{... Eq. 3.17}$$

a graph of $\ln \frac{k}{T}$ and $\frac{1}{T}$ can be drawn to calculate the activation parameters of a first order reaction.

The activation parameters like ΔS, give inside information about the pathway that the reaction will follow. For example, a negative ΔS value will follow the associative pathway, which indicates an increase in order in the system and a positive ΔS value will follow a dissociative pathway.

3.4 Theoretical Aspects of X-Ray Crystallography

3.4.1 Introduction

Mineralogy is the study of naturally-occurring chemical compounds, which gave birth to the scientific field of crystallography. Crystals fascinated people from the ancient times, because of their regularity and symmetry. The word crystals originated from the Greek term '*krystallos'* which means ice. The term was applied to quartz, because it was believed that the mineral was water that had been crystallized at high pressure deep inside the earth over the years.[9]

3.4.2 X-Ray Diffraction

X-Rays was discovered by C.W. Röntgen in 1895 and the diffraction of X-rays by crystals was discovered by Max von Laue in 1912. This discovery from Max von Laue allowed the determination of previously unknown chemical compounds. The general procedure of determining[10] a crystal structure of a chemical compound is as follows:

- Select a crystal which a suitable for XRD analysis and then mount it
- Obtain the unit cell geometry and preliminary symmetry information
- Measure the intensity data
- Data reduction
- Solve the structure by using the Patterson function, direct method and other methods
- Complete the structure and find all the atoms: Fourier and difference Fourier synthesis
- Refine the crystal structure and determine a least squares model fit
- Lastly, interpret the obtained results

IR and NMR spectroscopy are analytical techniques that give information regarding the structure of a compound, in the manner of which it emits or absorbs radiation. X-ray crystallography measures the scattering of monochromatic radiation and these scattering waves can either add constructively or deconstructively, depending on the direction of the

[9] H.R. Wenk and A. Bulakh, Minerals: *Their Constitution and Origin*, UK: Cambridge University Press, 2004.
[10] W.Clegg, *Crystal Structure Determination*, New York: Oxford University Press, Inc., 1998.

diffracted beam and the atomic positions.[11] Diffraction or interference effects cause these intensity variations, which results in the creation of a complex scattering pattern and measurements of this pattern can now be used to determine the positions of the atoms in a compound.[10]

X-ray crystallography is mostly focused on the crystal. A *crystal* can be defined as a solid, three-dimensional structure and a *crystal structure* is the geometric arrangement of the atoms within a crystal. The *lattice* of a structure is the array of identical points, which are points with exactly the same environments. A *unit cell* is defined as a small portion of the crystal, which is repeated indefinitely to reproduce a whole part of the crystal.[12] A unit cell consists of three lengths (a, b, c) and three angles (α, β, γ) and the positions of the atoms in a unit cell can be listed as their Cartesian coordinates. There are 230 space groups, which describe the symmetry of a unit cell and all of these different space groups are fully described in the *International Tables of* Crystallography.[13] The Miller indices, hkl, are used to describe the directions and planes within a crystal lattice.

By rotating the crystal in the X-ray beam, X-rays are scattered by each atom in the crystal which then results in the formation of a complete scattering pattern. The diffraction pattern consists of three properties, which correspond to three properties of the crystal structure. The three properties are:

- The geometry of the pattern is related to the geometry of the unit cell and the lattice of the crystal structure.
- The symmetry of the pattern is related to the symmetry of the unit cell of the crystal structure.
- The pattern consists of a varied intensities, which give information about the position of the atoms in the unit cell.[10]

[11] M.F.C. Ladd and R.A. Palmer, *Structure Determination by X-ray Crystallography*, New York: Plenum Press, 1977.
[12] D.W.A. Sharpe, *The Penguin Dictionary of Chemistry*, 3rd Edition, London: Penguin Books Ltd., 2003.
[13] *International Tables for Crystallography*, Volume A, 5th Edition, The Netherlands: Kluwer Academic Publishers, 2002.

3.4.3 Bragg's Law

William Lawrence Bragg proposed in 1912 that when X-rays are diffracted by crystals, which act as though reflected by 'atomic mirror planes' within the crystal. However, parts of the X-ray beam may not have been reflected but penetrate deeper into the crystal and undergo the same process at the deeper level. All the X-rays that are reflected from a given plane remain in the phase after reflection. The two X-rays that are reflected from neighbouring planes are thus out of phase after reflection because of the different path lengths taken. To compensate for this difference in phases, Bragg's law can be used.[11]

Bragg's law are defined in Eq. 3.18.

$$n\lambda = 2d_{hkl}\sin\theta \qquad \text{... Eq. 3.18}$$

where n is the integer, λ is the wavelength of incident wave, d_{hkl} is the distance between parallel planes in the atomic lattice and θ is the angle between incidence of the X-ray beam and lattice planes (Figure 3.6).

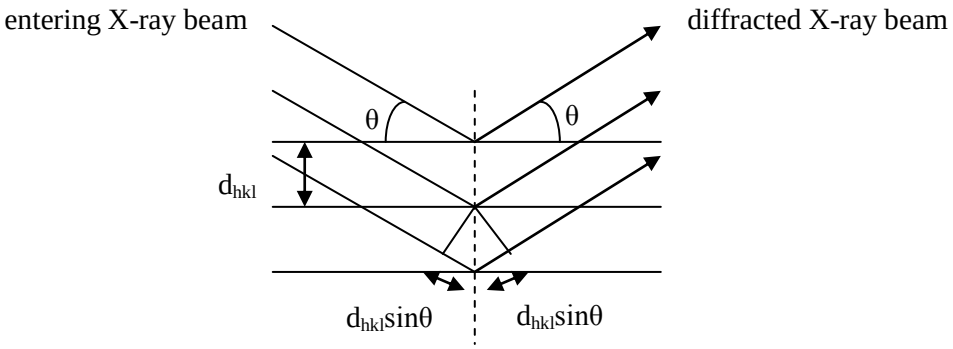

Figure 3.6 The diffraction of X-rays proposed by Bragg

Each of the hkl values represents a point in the reciprocal space relative to the set of hkl planes in real space. If the reciprocal lattice that is created from the diffracted X-rays is indexed, hkl values can be assigned to each diffraction spot. First, the Laue class is assigned from the relation of the intensity weighed reciprocal lattice to a crystal and then the space group are assigned, by using the systematic extinctions in the reciprocal space. The systematic extinctions originate from the specific symmetry in the crystal and are determined from the structure factors in a particular space group. If the correct space group is chosen, then the chances are fairly high that the structure can be solved.

3.4.4 Structure Factor

The position of atoms in a unit cell is expressed in terms of fractional coordinates (h, k, l) with each a number between 0 and 1. The cell edges are defined by vectors a, b and c, thus the position of an atom in a unit cell can be expressed as:

$$r = hx + ky + lz \quad \text{... Eq. 3.19}$$

The structure factors, F_{hkl}, of a known structure can be calculated by using the resultant of N waves scattered in the reflection (hkl) direction.

The resultant wave for the unit cell is therefore:[11]

$$F_{hkl} = \sum_{d=1}^{N} f_d e^{2\pi i(hx_d + ky_d + lz_d)} \quad \text{... Eq. 3.20}$$

The f_d values represent the scattering factors of N atoms and $2\pi i(hx_d + ky_d + lz_d)$ represent the length of each scattered wavelength. The structure can also be expressed as in terms of the electron density *p* within the unit cell:

$$F_{hkl} = \int p(x, y, z) e^{2\pi i(hx_d + ky_d + lz_d)} dV \quad \text{... Eq. 3.21}$$

F_{hkl} is the Fourier transform of p(x, y, z) and the electron density at coordinates (x, y, z) can be calculated by using the following equation where V is the unit cell volume.[14]

$$p(x, y, z) = \frac{1}{V} \sum_h \sum_k \sum_l F_{hkl} e^{-2\pi i(hx+ky+lz)} \quad \text{... Eq. 3.22}$$

The transform is the sum of discrete values obtained from the structure factors of all the hkl reflections. In X-ray diffraction, it is expressed in terms of the scattered wave from the unit, I_{hkl}, where I_{hkl} (also known as the ideal intensity) is proportional to the magnitude squared of the structure factor F_{hkl}:

$$I_{hkl} \propto \left|F_{hkl}\right|^2 \quad \text{... Eq. 3.23}$$

[14] G.H. Stout, L.H. Jensen, X-ray Structure Determination: A practical Guide, Londen: the Macmillan Company, 1968.

Eq. 3.23 forms the basis of X-ray studies because it allows the experimental values of I_{hkl} to be directly related to the structure through F_{hkl}.

3.4.5 The 'Phase' Problem

The structure of a chemical compound cannot be determined directly from the obtained intensity data. The modulus $|F_{hkl}|$ can be obtained from the intensity data (Eq. 3.9). The phase, ϕ_{hkl}, corresponding to F_{hkl} cannot be directly measured. However, to determine the crystal structure both the amplitude and phase must be known. The problem with structure determination by X-ray diffraction is the inability to determine the complete vectorial structure factors. This inability to determine the phase, ϕ_{hkl}, is known as the 'Phase Problem', but it can be overcome by two methods, the Patterson function method and the Direct method.

3.4.5.1 Direct Method

The Direct method is based on the determination of the approximate reflection phases from measured X-ray intensities using mathematical formulae. The direct method is used in compounds where only light atoms are present and the Patterson function is used with compounds, which contain a single atom or a small number of heavier atoms.[11]

3.4.5.2 The Patterson Function

Patterson suggested in 1934 to use this function (Eq. 3.24) to help determine the crystal structure of a chemical compound:

$$p(u,v,w) = \frac{1}{V}\sum_{h}\sum_{k}\sum_{l}|F_{hkl}|^2 e^{-2\pi(h_u + k_v + l_w)} \quad \text{... Eq. 3.24}$$

The Patterson function looks like an electron density map with peaks of positive electron density in various positions, and these are not the positions of the atoms in the crystal structure. For each peak seen in the map, there are two atoms in the crystal structure whose x coordinates differ with u, the y coordinates differ with v and the z coordinates differ w. The peaks observed show the positions of the atoms relative to each other and not to the unit cell origin. The Patterson peaks are also proportional to the size of the atoms involved.[10]

3.4.6 Least-Squares Refinement

Once the correct crystal structure is believed to be obtained, then the structure can be refined by a least squares treatment. The least squares refinement compares the calculated structure factor $|F_c|$ to the experimental data $|F_o|$. This comparison is described in terms of the residual index of R-value which is defined by Eq. 3.25.

$$R = \frac{\sum \| F_o | - | F_c \|}{\sum |F_o|} \quad \text{... Eq. 3.25}$$

A crystal structure resulting in an R-value of < 0.10 is acceptable and R-values between 0.02 – 0.07 is considered to be very good measured experimental data.

4 Synthesis of Carboxamide Ligands and their Gallium(III)- and Gold(III) Complexes

4.1 Introduction

The carboxamide [-C(O)NH-] group is an important ligand construction unit for coordination chemists. Pyridine carboxamides are prepared from condensation reactions between pyridyl-bearing amine or carboxylic acid precursors, promoted by a coupling reagent such as triphenylphosphite. These type of carboxamides ligands have found many uses such as molecular receptors[1], asymmetric catalysis[2], dendrimer synthesis[3] and platinum(II) complexes with antitumor properties.[4] Gallium(III) complexes with *N,N'*- donor ligands can assist in stabilizing gallium against hydrolysis which can lead to an increase in anticancer stability.[5]

Jain *et al.*[6] synthesized a range of these types of carboxamide ligands. These ligands are coordinated to a variety of different transition metals however, very little amount of synthetic work has been done on the coordination modes of these types of ligands on gallium and gold. Therefore, the aim of this study is to synthesize new carboxamide ligands which can be coordinated to Ga(III) and Au(III) and then to explore the reactivity towards aqua substitution of the gallium(III) complex with a monodentate ligand such as 4-methylpyridine, as entering ligand.

---

[1] Collinson, S. R., Gelbrick, T., Hursthouse, M. B., & Tucker, J. H. R., *Chem. Commun.*, 555, 2001.
[2] Trost, B. M. & Hachiya, *J. Am. Chem. Soc.*, **120**, 1104, 1998.
[3] Epperson, J. D., Ming, L. J., Baker, G. R. & Newkome, G. R., *J. Am. Chem. Soc.*, **123**, 8583, 2001.
[4] Zhang, J., Liu, Q., Duan, C., Shao, Y., Ding, J., Miao, Z., You, X. & Guo, Z., *J. Chem. Soc., Dalton Trans.*, 591, 2002.
[5] Harpstrite, S. E., Prior, J. L., Rath, N. P., Sharma, V., *J. Inorg. Biochem.*, **101**, 1347-1353, 2007.
[6] Jain, S. L., Bhattacharyya, P., Milton, H. L., Slawin., A. M. Z., Crayston, J. A. & Woollins, J. D., *Dalton Trans.*, pp. 862-871, 2004.

Here we describe the synthesis and characterisation of new *N,N'*-tetradentate ligands prepared from o-phenyldiamine and picolinic acid, 4,5-dimethyl-1,2-phenylendiamine and picolinic acid and also the gallium(III) and gold(III) complexes prepared from the ligands. The synthesis and characterisation of the gallium(III) methanol solvento complex is also described in this Chapter.

4.2 Chemicals and Instrumentation

All the reagents used for the synthesis and characterization of compounds were of analytical grade and purchased from Sigma-Aldrich, South Africa. All the organic solvents were dried and distilled before used. Triphenylphosphite was used as a promoting coupling reagent for the synthesis of the carboxamide ligands and sodium acetate for deprotonation of the ligand.

The infrared spectra were recorded on a Bruker Tensor 27 Standard System spectrophotometer with a laser range of 4000 – 370 cm^{-1}. All the samples were analyzed as solid state species *via* ATR infrared spectrophotometry at room temperature. The UV/Vis spectra were collected on a Varian Cary 50 Conc UV/Visible Spectrophotometer, equipped with a Julabo F12-mV temperature cell regulator (accurate within 0.1 °C) in a 1.000 cm quartz cuvette. All the ^{1}H NMR spectra were obtained in either $(CD_3)_2SO$ or $(CCD_3)_2NCOD$ on a Bruker 300 nuclear magnetic spectrometer. ^{1}H chemical shifts are reported relative to tetramethylsilane (TMS) using the $(CD_3)_2SO$ (2.50 ppm) and $(CCD_3)_2NCOD$ (2.75 ppm, 2.95 ppm, 8.03 ppm) peaks. All the ^{13}C NMR spectra were obtained in either $(CD_3)_2SO$ or $(CCD_3)_2NCOD$ on a Bruker 600 nuclear magnetic spectrometer. ^{13}C chemical shifts are reported relative to TMS using the $(CD_3)_2SO$ (39.52 ppm) and $(CCD_3)_2NCOD$ (29.76 ppm, 34.89 ppm, 163.15 ppm) peaks. All the chemical shifts were reported in parts per million (ppm) and coupling constants in hertz (Hz). Elemental analysis was also done on all of the compounds that were synthesized.

4.3 Synthetic Procedures

The synthesis of all the carboxamide ligands, gallium- and gold complexes were performed under aerobic conditions.

4.3.1 Synthesis of Carboxamide Ligands

4.3.1.1 Synthesis of *N,N'*-(1,2-phenylene)bis(pyridine-2-carboxamide) (bpb)

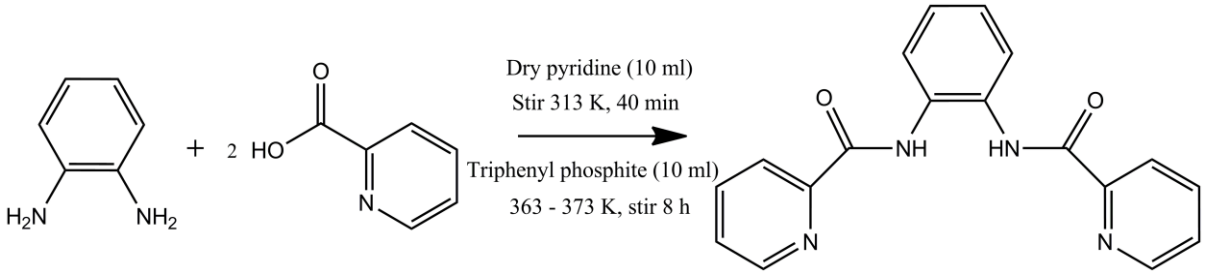

Scheme 1 Reaction scheme of the formation of bpb

Picolinic acid (2.4010 g, 19.503 mmol) was added as a solid in one portion to a suspension of o-phenyldiamine (1.0003 g, 9.251 mmol) in dry pyridine (10 ml) and the mixture was stirred at 40 °C for 40 min. Triphenylphosphite (10 ml) was added dropwise over 10 min, after which time the temperature was increased to 90 – 100 °C and stirred for a further 24 hours. On cooling the white precipitate was filtered off, washed with H_2O (50 ml) and then MeOH (50 ml). (Yield: 0.5021 g, 17 %). **IR (cm^{-1}):** *ν*(C=O) = 1666.17 and *ν*(N-H) = 3315.02. **UV/Vis:** λ_{max} = 270.0 nm, ε = 4560 $cm^{-1}.M^{-1}$. **^{1}H NMR (DMSO-*d*$_6$):** δ_H = 10.75 (s, 2H), 8.65 (d, 2H, J = 4.4 Hz), 8.18 (d, 2H, J = 7.8 Hz) 8.06 (td, 2H, J = 7.7 Hz, 1.5 Hz), 7.78 (dd, 2H, J = 5.9 Hz, 3.6 Hz), 7.66 (m, 2H), 7.31 (dd, 2H, J = 6.0 Hz, 3.6 Hz). **^{13}C NMR (DMSO-*d*$_6$):** δ = 122.90, 125.81, 126.15, 127.54, 131.47, 138.60, 148.98, 149.91, 163.25. **Elemental analysis:** calculated: C = 67.91 %, H = 4.43 %, N = 17.60 %, O = 10.05 %; found: C = 67.95 %, H = 4.41 %, N = 16.80 %, O = 10.84 %.

4.3.1.2 Synthesis of *N,N'*-(4,5-Dimethyl-1,2-phenylene)bis(pyridine-2-carboxamide) (di-Mebpb)

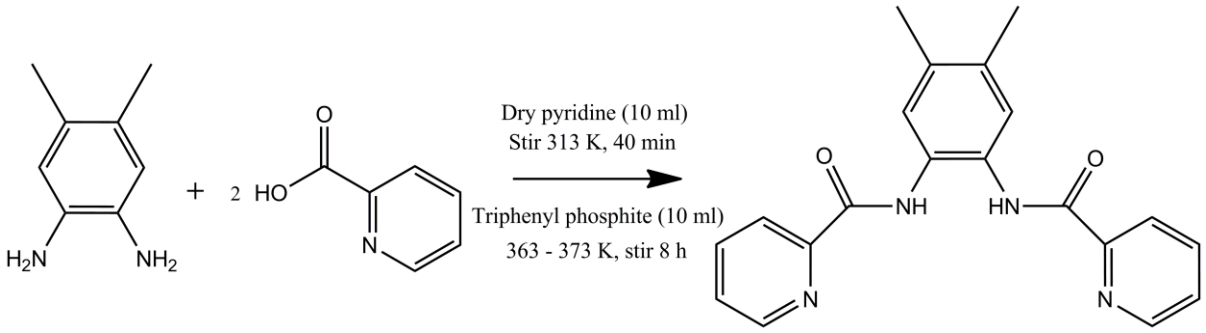

Scheme 2 Reaction scheme of the formation of di-Mebpb

Picolinic acid (0.9542 g, 7.751 mmol) was added as a solid in one portion to a suspension of 4,5-dimethyl-1,2-phenylenediamine (0.4996 g, 3.668 mmol) in dry pyridine (10 ml) and the mixture was stirred at 40 °C for 40 min. Triphenylphosphite (10 ml) was added dropwise over 10 min, after which time the temperature was increased to 90 – 100 °C and stirred for a further 24 hours. On cooling the white precipitate was filtered off, washed with H_2O (50 ml) and then MeOH (50 ml). (Yield: 0.4077 g, 32 %). **IR (cm^{-1}):** ν(C=O) = 1663.53 and ν(N-H) = 3328.24. **UV/Vis:** λ_{max} = 268.0 nm, ε = 4430 $cm^{-1}.M^{-1}$. **^{1}H NMR (DMSO-d_6):** δ_H = 10.61 (s, 2H), 8.63 (d, 2H, J = 4.3 Hz), 8.16 (d, 2H, J = 7.8 Hz) 8.04 (td, 2H, J = 7.7 Hz, 1.5 Hz), 7.63 (m, 2H), 7.53 (s, 2H), 2.24 (s, 6H). **^{13}C NMR (DMSO-d_6):** δ = 19.54, 122.79, 126.44, 127.41, 128.96, 134.13, 138.54, 148.94, 150.04, 163.11. **Elemental analysis:** calculated: C = 69.35 %, H = 5.24 %, N = 16.17 %, O = 9.21 %; found: C = 68.46 %, H = 5.61 %, N = 16.02 %, O = 9.91 %.

4.3.2 Synthesis of Gallium(III) Complexes

4.3.2.1 Synthesis of $[Ga(bpb)(H_2O)_2]NO_3 \cdot CH_3OH$

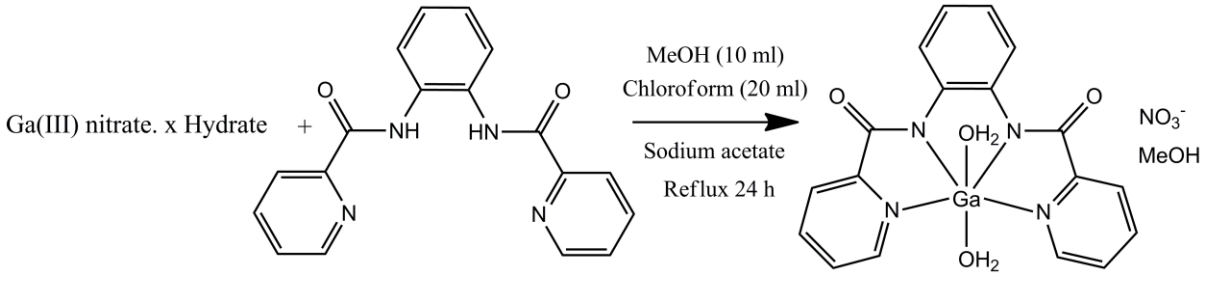

Scheme 3 Reaction scheme of the formation of $[Ga(bpb)(H_2O)_2]NO_3 \cdot CH_3OH$

Bpb (0.1266 g, 0.398 mmol) in chloroform (20 ml) was slowly added to a solution of gallium(III)nitrate hydrate (0.1006 g, 0.393 mmol) in MeOH (10 ml), followed by $Na(OAc)_2$ (0.0385 g, 0.469 mmol) in MeOH (10 ml). The reaction mixture was stirred at 70 °C for 24 hours. After cooling the yellow precipitate was filtered off, washed with chloroform and recrystallised in MeOH. (Yield: 0.0586 g, 32 %). **IR (cm^{-1}):** *ν*(C=O) = 1622.01. **UV/Vis:** λ_{max} = 362.0 nm, ε = 6500 $cm^{-1}.M^{-1}$. **^{1}H NMR (DMSO-*d*$_6$):** δ_H = 9.25 (d, 2H, J = 5.2 Hz), 8.67 (dt, 2H, J = 7.0 Hz, 3.5 Hz), 8.54 (d, 4H, J = 4.3 Hz) 8.08 (m, 2H), 7.06 (m, 2H). **^{13}C NMR (DMSO-*d*$_6$):** δ = 119.25, 123.41, 124.17, 128.65, 134.70, 143.70, 145.58, 149.55, 158.45. **Elemental analysis:** calculated: Ga = 13.15 %, C = 44.22 %, H = 3.91 %, N = 13.57 %, O = 24.80 %; found: Ga = 13.25 %, C = 45.10 %, H = 3.58 %, N = 14.40 %, O = 23.67 %.

4.3.2.2 Synthesis of $[Ga(di\text{-}Mebpb)(H_2O)_2]NO_3$

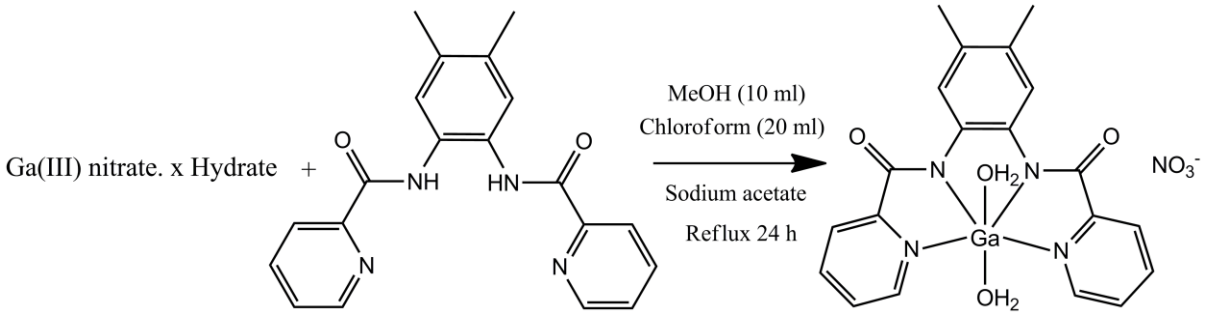

Scheme 4 Reaction scheme of the formation of $[Ga(di\text{-}Mebpb)(H_2O)_2]NO_3$

Di-Mebpb (0.1369 g, 0.3951 mmol) in chloroform (20 ml) was slowly added to a solution of gallium(III)nitrate hydrate (0.1000 g, 0.3910 mmol) in MeOH (10 ml), followed by $Na(OAc)_2$ (0.0385 g, 0.464 mmol) in MeOH (10 ml). The reaction mixture was stirred at 70 °C for 24 hours. After cooling the yellow precipitate was filtered off and washed with chloroform. (Yield: 0.0406 g, 19 %). **IR (cm^{-1}):** *ν*(C=O) = 1655.66. **UV/Vis:** λ_{max} = 382 nm, ε = 7000 $cm^{-1}.M^{-1}$. **^{1}H NMR (DMSO-*d*$_6$):** δ_H = 9.23 (d, 2H, J = 5.2 Hz), 8.68 (d, 2H, J = 7.8 Hz), 8.58 (m, 2H), 8.51 (s, 2H), 8.11 (t, 2H, J = 6.3 Hz), 2.32 (s, 6H). **^{13}C NMR (DMSO-*d*$_6$):** δ = 20.22, 120.45, 124.08, 128.48, 130.76, 132.50, 143.92, 146.42, 149.68, 157.91. **Elemental analysis:** calculated: Ga = 13.61 %, C = 46.91 %, H = 3.94 %, N = 13.68 %, O = 21.87 %; found: Ga = 13.30 %, C = 46.68 %, H = 4.23 %, N = 13.98 %, O = 21.81 %.

4.3.2.3 Synthesis of *trans*-[Ga(bpb)(CH$_3$OH)$_2$]NO$_3$

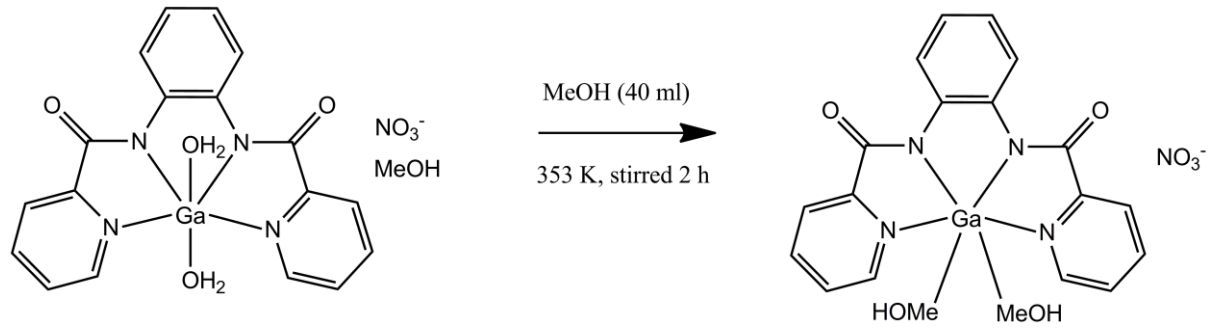

Scheme 5 Reaction scheme for the formation of *trans*-[Ga(bpb)(CH$_3$OH)$_2$]NO$_3$

[Ga(bpb)(H$_2$O)$_2$]NO$_3$·CH$_3$OH (0.1000 g, 0.194 mmol) was dissolved in dry MeOH (30 ml). The reaction mixture was stirred at 80 °C for 2 hours. After cooling the yellow precipitate was filtered off and washed with chloroform. (Yield: 0.1552 g, 64 %). **IR (cm^{-1}):** *ν*(C=O) = 1647.40. **UV/Vis:** λ_{max} = 369.62 nm, ε = 7360 cm^{-1}.M^{-1}. **^{1}H NMR (DMF-*d*$_6$):** δ_H = 9.68(d, 2H, J = 4.9 Hz), 8.92(dd, 2H, J = 5.8, 3.6 Hz), 8.76 (d, 4H, 3.8 Hz), 8.12 (dd, 2H, J = 5.8, 3.6 Hz), 7.23 (m, 2H), 3.96 (s, 6H). **^{13}C NMR (DMF-*d*$_6$):** δ = 158.30, 150.33, 149.78, 148.76, 143.11, 138.16, 131.36, 125.73, 125.27, 122.42, 118.98. **Elemental analysis:** calculated: Ga = 15.58 %, C = 48.25 %, H = 2.70 %, N = 15.63 %, O = 17.85 %; found: Ga = 12.79 %, C = 45.43 %, H = 4.75 %, N = 13.86 %, O = 23.17 %.

4.3.3 Synthesis of Gold(III) Complexes

4.3.3.1 Synthesis of [Au(bpb)]Cl

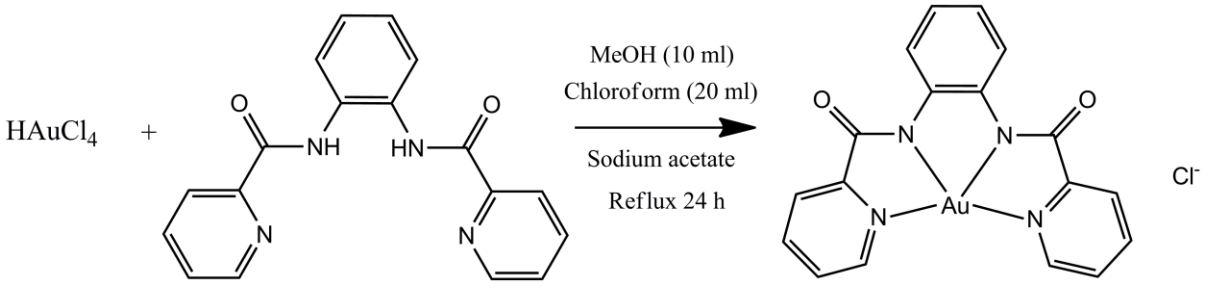

Scheme 6 Reaction scheme of the formation of [Au(bpb)]Cl

Bpb (0.0845 g, 0.265 mmol) in chloroform (20 ml) was slowly added to a solution of gold(III)chloride (0.0893 g, 0.263 mmol) in MeOH (10 ml), followed by Na(OAc)$_2$ (0.0457 g, 0.551 mmol) in MeOH (10 ml). The reaction mixture was stirred at 70 °C for 24 hours.

After cooling the yellow precipitate was filtered off and washed with chloroform. (Yield: 0.0769 g, 53 %). **IR (cm^{-1}):** ν(C=O) = 1652.85. **UV/Vis:** λ_{max} = 368 nm, ε = 6210 $cm^{-1}.M^{-1}$. **^{1}H NMR (DMSO-*d*$_6$):** δ_H = 9.27 (d, 2H, J = 5.5 Hz), 8.66 (t, 2H, J = 7.7 Hz), 8.26 (dd, 2H, J = 6.1 Hz, 3.4 Hz) 8.20 (t, 4H, J = 7.1 Hz), 7.14 (dd, 2H, J = 6.1 Hz, 3.4 Hz). **^{13}C NMR (DMSO-*d*$_6$):** δ = 121.43, 121.58, 126.92, 129.41, 130.72, 141.90, 146.05, 148.34, 163.75. **Elemental analysis:** calculated: Au = 35.89 %, C = 39.40 %, H = 2.20 %, N = 10.21 %, Cl = 6.46 %, O = 24.80 %; found: Au = 37.28 %, C = 37.43 %, H = 2.54 %, N = 10.56 %, Cl = 6.79 %, O = 5.40 %.

4.3.3.2 Synthesis of [Au(di-Mebpb)]Cl

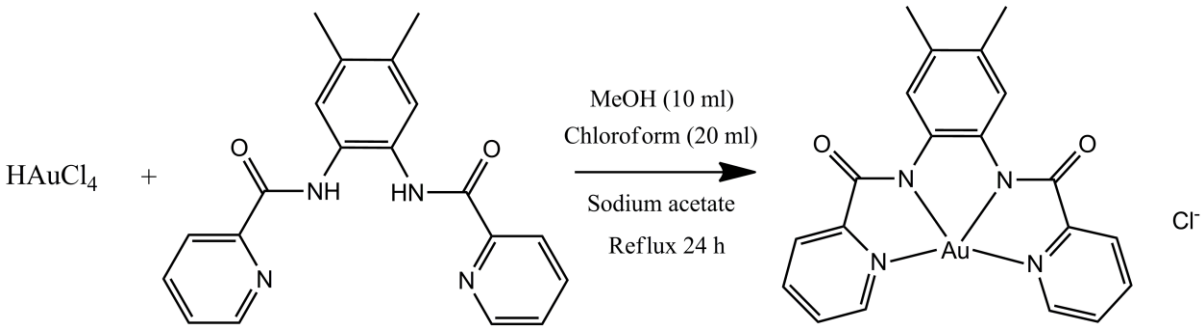

Scheme 7 Reaction scheme of the formation of [Au(di-Mebpb)]Cl

Di-Mebpb (0.0810 g, 0.234 mmol) in chloroform (20 ml) was slowly added to a solution of gold(III)chloride (0.0786 g, 0.231 mmol) in MeOH (10 ml), followed by $Na(OAc)_2$ (0.0403 g, 0.485 mmol) in MeOH (10 ml). The reaction mixture was stirred at 70 °C for 24 hours. After cooling the yellow precipitate was filtered off and washed with chloroform. (Yield: 0.0846 g, 63 %). **IR (cm^{-1}):** ν(C=O) = 1666.78. **UV/Vis:** λ_{max} = 389 nm, ε = 6805 $cm^{-1}.M^{-1}$. **^{1}H NMR (DMSO-*d*$_6$):** δ_H = 9.20 (d, 2H, J = 5.3 Hz), 8.65 (t, 2H, J = 7.6 Hz), 8.18 (t, 4H, J = 7.4 Hz) 7.97 (s, 2H), 2.19 (s, 6H). **^{13}C NMR (DMSO-*d*$_6$):** δ = 19.55, 121.22, 129.01, 130.25, 134.59, 139.34, 145.69, 147.66, 153.65, 162.78. **Elemental analysis:** calculated: Au = 34.15 %, C = 41.65 %, H = 2.80 %, N = 9.71 %, Cl = 6.15 %, O = 5.55 %; found: Au = 32.54 %, C = 42.85 %, H = 2.71 %, N = 9.46 %, Cl = 7.30 %, O = 5.14 %.

4.4 Discussion

The synthesis of the two ligands and the five metal complexes were fairly straight forward. Relatively low yields were obtained for both the ligands as well as their respective complexes. The low yields obtained might be due to the repeated washing of the product with respective solvents to get rid of impurities. All the synthesized crystals were quite stable when exposed to air or temperatures higher than 0 °C which makes it very easy for the crystals to be collected for analysis on the X-Ray diffractometer. Only two of the synthetic procedures namely, $[Ga(di\text{-}Mebpb)(H_2O)_2]NO_3$ and [Au(di-Mebpb)]Cl, did not form crystals suitable for analysis on the X-Ray diffractometer. Several attempts were made to recrystallize the products in different solvents, but to no avail.

All the IR spectroscopic data for the ligands and the complexes is summarised in Table 4.1.

Table 4.1 Summary of IR spectroscopic data for all the compounds synthesized

	IR frequencies	
Compound	***v*(N-H) (cm^{-1})**	***v*(C=O) (cm^{-1})**
bpb	3315.02	1666.17
di-Mebpb	3328.24	1663.53
$[Ga(bpb)(H_2O)_2]NO_3 \cdot CH_3OH$	Not observed	1622.01
$[Ga(di\text{-}Mebpb)(H_2O)_2]NO_3 \cdot CH_3OH$	Not observed	1655.66
trans-$[Ga(bpb)(CH_3OH)_2]NO_3$	Not observed	1647.40
[Au(bpb)]Cl	Not observed	1652.85
[Au(di-Mebpb)]Cl	Not observed	1666.78

It is clear from Table 4.1 that slight changes in *v*(C=O) is observed when the ligands are coordinated to the two metals, but that this technique on its own is not sufficient to evaluate metal coordination.

The ^{1}H NMR and ^{13}C NMR spectra provide further confirmation of the structures of all the compounds as well as metal coordination. Selected ^{1}H NMR and ^{13}C NMR spectroscopic data for the ligands and the complexes is summarised in Table 4.2.

Table 4.2 Summary of selected ^{1}H NMR and ^{13}C NMR spectroscopic data for all the compounds synthesized

Compound	^{1}H NMR δ(N-H) (ppm)	^{13}C NMR δ(C=O) (ppm)
bpb	10.75	163.25
di-Mebpb	10.61	163.11
$[Ga(bpb)(H_2O)_2]NO_3 \cdot CH_3OH$	Not observed	158.45
$[Ga(di\text{-}Mebpb)(H_2O)_2]NO_3$	Not observed	157.91
trans-$[Ga(bpb)(CH_3OH)_2]NO_3$	Not observed	158.30
[Au(bpb)]Cl	Not observed	163.75
[Au(di-Mebpb)]Cl	Not observed	162.78

All the ^{1}H NMR signals for all the compounds were fully and correctly integrated to confirm that the correct compounds were successfully synthesized. By comparing the respective ^{1}H NMR spectra of the tetradentate ligand with the respective ^{1}H NMR spectra of the metal complex a definite chemical shift is observed. This change in chemical shift for the respective ligand with complex in the ^{13}C NMR spectra is also observed. Table 4.2 shows the chemical shift for the selected spectroscopic data where the signal of the amide disappears and the shift of carbonyl group after addition of the metals indicating coordination to the metal.

4.5 Conclusion

Two pyridine carboxamide ligands, (bpb) and (di-Mebpb), as well as their gallium(III) and gold(III) complexes, $[Ga(bpb)(H_2O)_2]NO_3 \cdot CH_3OH$, $[Ga(di\text{-}Mebpb)(H_2O)_2]NO_3$, [Au(bpb)]Cl and [Au(di-Mebpb)]Cl, were successfully synthesized and characterized with IR, ^{1}H NMR, ^{13}C NMR spectroscopy and elemental analysis. The gallium(III) methanol solvento complex, *trans*-$[Ga(bpb)(CH_3OH)_2]NO_3$, was also successfully synthesized and characterized by means of IR, ^{1}H NMR, ^{13}C NMR spectroscopy and elemental analysis.

The characterization with X-ray crystallography for the two carboxamide ligands and the two metal complexes, $[Ga(bpb)(H_2O)_2]NO_3 \cdot CH_3OH$ and [Au(bpb)]Cl, was successfully completed and is discussed in detail in Chapter 5.

5 Crystallographic Study of Carboxamide Ligands, Gallium(III)- and Gold(III) Complexes

5.1 Introduction

In this chapter the structures of two ligands namely, *N*,*N'*-(4,5-Dimethyl-1,2-phenylene)bis(pyridine-2-carboxamide)[1] (di-Mebpb) and *N*,*N'*-(1,2-phenylene)bis(pyridine-2-carboxamide)[2] (bpb) and two metal complexes, $[Ga(bpb)(H_2O)_2]NO_3 \cdot CH_3OH$ and [Au(bpb)]Cl were investigated and characterised by means of X-ray crystallography. All the instruments and procedures involved are described below.

5.2 Experimental

The reflection data were colleted on a Bruker X8 Apexll 4K diffractometer, equipped with a graphite monochromated Mo Kα radiation and with ω- and φ- scans at -173 °C. The cell refinements were performed with Bruker SAINT-Plus[3] and data reduction with Bruker SAINT-Plus and XPREP[3] software packages, respectively. Data was corrected for absorption effects using the multi-scan technique SADABS.[4] The data for the [Au(bpb)]Cl complex were collected on a Oxford Diffraction Xcalibar 3 Crysalis system[5] using a Mo Kα radiation and with ω scans at -120 °C. The intensity data were extracted and integrated using

[1] Van der Berg, P. C. W., Visser, H. G., Roodt, A. & Muller, T. J., *Acta Cryst*., **E68**, o2739, 2012.
[2] Lin, J., Zhang, J-Y., Xu, Y., Ke, X-K. & Guo, Z., *Acta Cryst.*, **C57**, 192-194, 2001.
[3] Bruker, *SAINT-Plus* and *XPREP*, Bruker AXS Inc., Madison, Wisconsin, USA, 2008.
[4] Bruker, *SADABS*, Bruker AXS Inc., Madison, Wisconsin, USA, 2008.
[5] Crysalis CCD. Oxford Diffraction Ltd., Abingdon, Oxfordshire, U.K., 2005.

Crysalis RED.[6] All the crystal structures were solved by direct methods package, SIR97[7], and refined with software packages, WinGX[8] and SHELXL-97[9]. The program, DIAMOND[10], was used for the molecular graphics and representations of the crystal structures. The amides, aromatic and methyl hydrogen atoms were positioned geometrically and allowed to ride on their parent atoms, N-H =0.86 Å and $U_{iso}(H) = 1.2\ U_{eq}$, C-H (aromatic C) = 0.95 Å and $U_{iso}(H) = 1.2\ U_{eq}$ and C-H (methyl C) = 0.98 Å and $U_{iso}(H) = 1.5\ U_{eq}$ respectively. The methyl groups were allowed to rotate, giving six half-H sites for the di-Mebpb ligand.[1]

[6] Crysalis RED. Oxford Diffraction Ltd., Abingdon, Oxfordshire, U.K., 2005.
[7] Altomare, A., Burla, M. C., Camalli, M., Cascarano, G. L., Giacovazzo, C., Guagliardi, A., Moliterni, A. G. G., Polidori, G., Spagna, R., *J. Appl. Cryst.*, **37**, 837, 1999.
[8] Farrugia, L. J., *J. Appl. Cryst.*, **32**, 837-838, 1999.
[9] Sheldrick, G. M., *Acta Cryst.*, **A64**, 112-122, 2008.
[10] Brandenburg, K. & Putz, H., *DIAMOND*, Crystal Impact GbR, Bonn, Germany.

Table 5.1 Crystallographic data of di-Mebpb and bpb

Crystallographic data	**di-Mebpb**	**bpb**
Empirical formula	$C_{20}H_{18}N_4O_2$	$C_{18}H_{14}N_4O_2$
Formula weight (g mol^{-1})	346.38	318.33
Crystal system	Monoclinic	Monoclinic
Space group	*Cc*	$P2_1/c$
a (Å)	12.1299(8)	12.0328(11)
b (Å)	18.9418(8)	5.5257(4)
c (Å)	7.7549(4)	22.492(2)
α (°)	90.000	90.000
β (°)	100.375(4)	95.587(5)
γ (°)	90.000	90.000
Volume ($Å^3$)	1752.65(16)	1488.4(2)
Z	4	4
ρ_{calc} (gcm^{-3})	1.313 Mg/m^3	1.421 Mg/m^3
Crystal colour	Colourless	Colourless
Crystal morphology	needle	Needle
Crystal size (mm)	0.778 x 0.078 x 0.74	0.637 x 0.094 x 0.029
μ (mm^{-1})	0.088	0.097
F (000)	728.0	664
θ range (°)	3.09 – 28.00	1.82 – 27.99
Index ranges	$-16 < h < 16$	$-15 \leq h \leq 15$
	$-24 < k < 24$	$-17 \leq k \leq 5$
	$-10 < l < 10$	$-29 \leq l \leq 29$
Reflections collected	15674	20622
Unique reflections	3860	3587
R_{int}	0.0309	0.0503
Completeness	28.00, 99.9 %	27.99, 99.9 %
Data/restraints/parameters	3860 / 2 / 237	3555 / 0 / 233
GooF	1.035	1.033
R [$I > 2\sigma(I)$]	$R_1 = 0.0363$	$R_1 = 0.0441$
	$wR_2 = 0.0864$	$wR_2 = 0.0955$
R (all data)	$R_1 = 0.0415$	$R_1 = 0.0683$
	$wR_2 = 0.0898$	$wR_2 = 0.1063$

Table 5.2 Crystallographic data of $[Ga(bpb)(H_2O)_2]NO_3 \cdot CH_3OH$ and [Au(bpb)]Cl

Crystallographic data	**$[Ga(bpb)(H_2O)_2]NO_3 \cdot CH_3OH$**	**[Au(bpb)]Cl**
Emperical formula	$C_{19}H_{20}GaN_5O_8$	$C_{18}H_{12}AuClN_4O_2$
Formula weight (g mol^{-1})	516.12	548.74
Crystal system	Orthorhombic	Triclinic
Space group	*Pbca*	$P\bar{1}$
a (Å)	15.572(4)	8.521(2)
b (Å)	13.401(5)	8.812(5)
c (Å)	19.422(6)	11.422(3)
α (°)	90.00	78.451(2)
β (°)	90.00	74.698(2)
γ (°)	90.00	89.243(19)
Volume ($Å^3$)	4053(2)	809.8(5)
Z	8	2
ρ_{calc} (gcm^{-3})	1.419	2.250
Crystal colour	Yellow	Yellow
Crystal morphology	Needle	Cuboid
Crystal size (mm)	0.722 x 0.055 x 0.053	0.24 x 0.2 x 0.17
μ (mm^{-1})	1.419	9.270
F (000)	2112	520
θ range (°)	2.26 - 28.36	2.48 - 28.00
Index ranges	$-20 \leq h \leq 20$	$-11 \leq h \leq 5$
	$-17 \leq k \leq 17$	$-11 \leq k \leq 11$
	$-25 \leq l \leq 25$	$-15 \leq l \leq 14$
Reflections collected	49244	6720
Unique reflections	5048	3907
R_{int}	0.0587	0.0279
Completeness	28.36, 99.7 %	28.00, 97.1 %
Data/restraints/parameters	5048 / 0 / 316	3794 / 0 / 235
GooF	1.023	1.100
R [$I > 2\sigma(I)$]	$R_1 = 0.0291$	$R_1 = 0.0438$
	$wR_2 = 0.0652$	$wR_2 = 0.1057$
R (all data)	$R_1 = 0.0467$	$R_1 = 0.0465$
	$wR_2 = 0.0730$	$wR_2 = 0.1094$

5.3 Crystal structure of *N,N'*-(4,5-Dimethyl-1,2-phenylene)bis(pyridine-2-carboxamide)

5.3.1 Introduction

Colourless crystals of the title compound were synthesized as reported in Paragraph 4.3.1. The general crystal data is given in Table 5.1, while the numbering scheme of di-Mebpb is shown in Figure 5.1. The most important bond distances, bond angles and torsion angles are reported in Table 5.3, Table 5.4 and Table 5.5, respectively. All the positional and thermal parameters are given in the Appendix in Table A.1 and A.2 while all the bond distances and bond angles are given in Table A.3 and A.4.

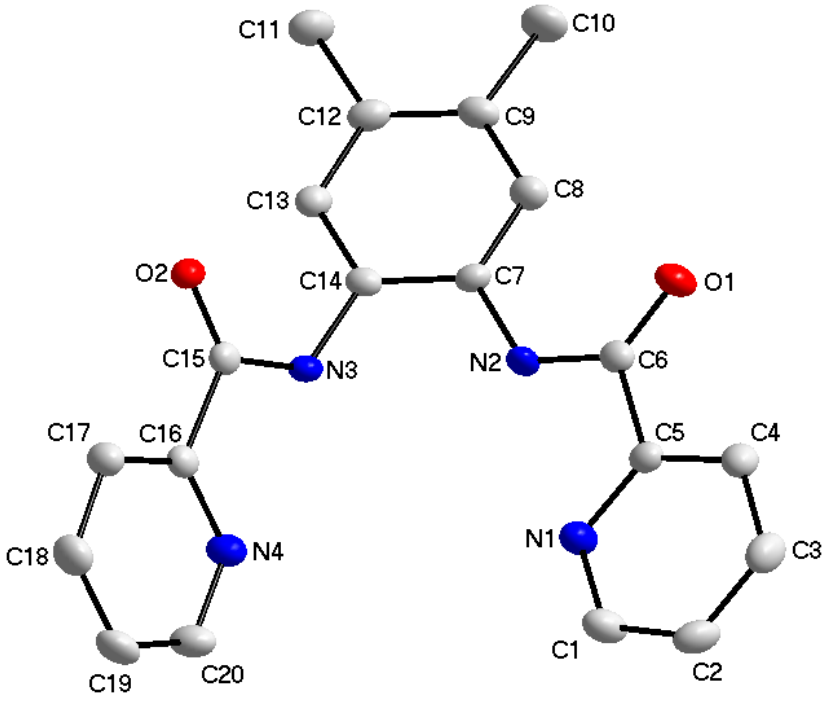

Figure 5.1 Molecular structure of di-Mebpb at 50 % probability level, displaying the numbering scheme. Hydrogen atoms are omitted for clarity

Table 5.3 Selected bond lengths of di-Mebpb

Bonds	Distances (Å)	Bonds	Distances (Å)
C9 – C10	1.509(2)	C6 – O1	1.219(2)
C11 – C12	1.507(2)	C15 – O2	1.2274(19)
C7 – N2	1.410(2)	C6 – C5	1.506(2)
C14 – N3	1.421(2)	C15 – C16	1.505(2)
N2 – C6	1.351(2)	C5 – N1	1.336(2)
N3 – C15	1.342(2)	C16 – N4	1.336(2)

Table 5.4 Selected bond angles of di-Mebpb

Bonds	Angles (°)	Bonds	Angles (°)
C6 – N2 – C7	126.56(14)	N2 – C6 – C5	113.87(14)
C14 – N3 – C15	123.74(14)	N3 – C15 – C16	114.22(14)
O1 – C6 – N2	125.78(15)	C4 – C5 – C6	118.67(15)
O2 – C15 – N3	124.85(15)	C17 – C16 –C15	118.74(14)
O1 – C6 – C5	120.35(15)	N1 – C5 – C6	117.50(14)
O2 – C15 – C16	120.91(14)	N4 – C16 – C15	117.22(14)

Table 5.5 Selected torsion angles of di-Mebpb

Bonds	Torsion angles (°)
N2 – C7 – C14 – N3	0.76(22)
N2 – C6 – C5 – N1	0.14(22)
N3 – C15 – C16 – N4	-2.42(21)

5.3.2 Results and Discussion

The title compound, di-Mebpb, crystallizes in a non-centrosymmetric, monoclinic *Cc* space group, with four molecules in the unit cell. The asymmetric unit consists of one full molecule of the di-Mebpb ligand in which the methyl groups are attached to the phenyl ring in the 4,5-positions and the two picoline type rings are attached at the 1 and 2 positions of the central phenyl ring, respectively.

The N2-C6 and N3-C15 bond distances of 1.351(2) Å and 1.342(2) Å respectively, agree well with similar structures.[2,11] The N2-C7 and N3-C14 bond length of 1.410(2) Å and 1.421(2) Å, respectively as well as C5-C6 and C15-C16 of 1.506(2) Å and 1.505(2) Å are considerated as normal bond distances.

One of the picoline rings is slightly bent out-of-plane (C7-C8-C9-C12-C13-C14), illustrated by the N3-C15-C16-N4 torsion angle of -2.42(21) °. The dihedral angles between the central phenyl ring and the two picoline rings are 57.06(5) ° (Figure 5.2 a) and 22.05(8) °, respectively (Figure 5.2 b) and the dihedral angle between the two picoline rings is calculated as 75.50(5) °.

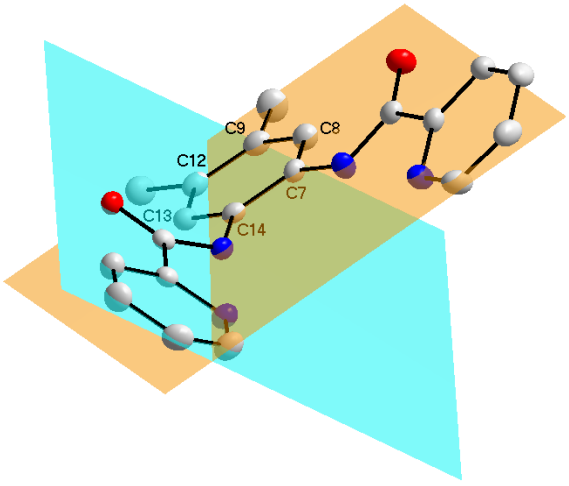

Figure 5.2 a Molecular structure that display the planarity of the central phenyl plane (C7-C8-C9-C12-C13-C14) and one of the picoline type rings at 50 % probability level. Hydrogen atoms are omitted for clarity

[11] Jain, S. L., Bhattacharyya, P., Milton, H. L., Slawin., A. M. Z., Crayston, J. A. & Woollins, J. D., *Dalton Trans.*, pp. 862-871, 2004.

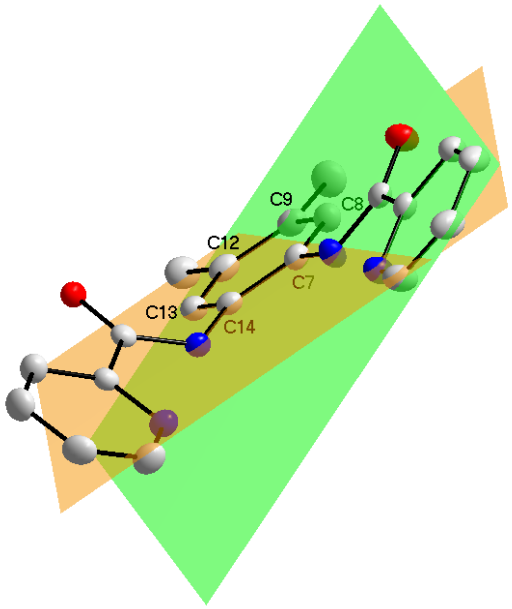

Figure 5.2 b Molecular structure that display the planarity of the central phenyl plane (C7-C8-C9-C12-C13-C14) and one of the picoline type rings at 50 % probability level. Hydrogen atoms are omitted for clarity

The molecules are stabilized by intermolecular N-H...N, C-H...O and N-H...O hydrogen bonding interactions and all these bonding interactions are reported in Table 5.6 and illustrated in Figure 5.3. The molecules pack in a one dimensional chain along the *b*-axis as illustrated in Figure 5.4.

Table 5.6 Specified Hydrogen bonds in di-Mebpb

D-H...A	d(D-H)	d(H...A)	d(D...A)	D-H...A angle
N2-H2'...N1	0.86(2)	2.20(2)	2.6698(19)	114.2(16)
N2-H2'...N3	0.86(2)	2.48(2)	2.777(2)	101.2(15)
N2-H2'...O2[a]	0.86(2)	2.60(2)	3.2112(19)	129.0(17)
N3-H3'...N4	0.86(2)	2.28(2)	2.6670(19)	107.8(15)
C8-H8...O1	0.95	2.31	2.877(2)	117.8
N3-H3'...O2[a]	0.86(2)	2.05(2)	2.8508(19)	155.5(18)
C2-H2...O1[b]	0.95	2.59	3.195(2)	122.0
C3-H3...O2[c]	0.95	2.48	3.160(2)	128.4

Operators for generating equivalent atoms:

[a] x, -y+1, z-1/2, [b] x+1/2, -y+3/2, z-1/2 [c] x+1/2, y+1/2, z

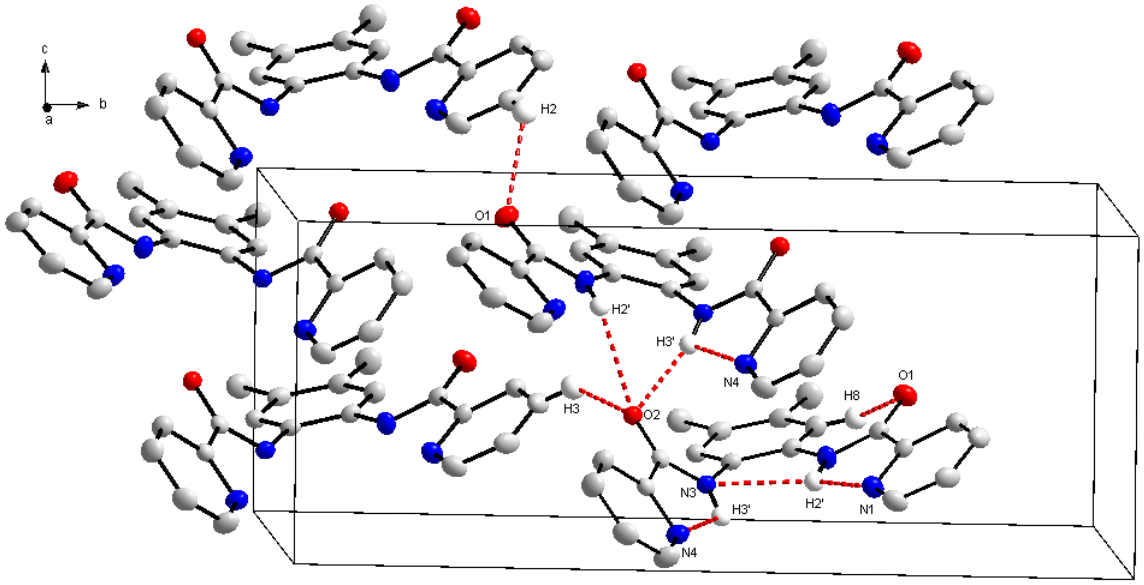

Figure 5.3 Molecular structure of di-Mebpb, displaying inter- and intramolecular interactions at 50 % probability level). Hydrogen atoms that are not part of the interactions are omitted for clarity

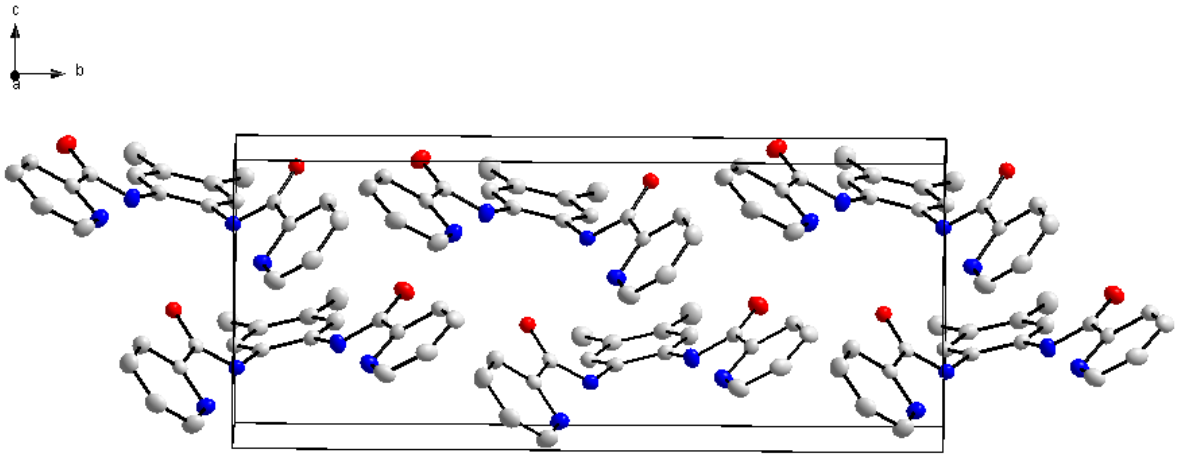

Figure 5.4 Molecular structure of di-Mebpb, displaying the packing along the *b*-axis at 50 % probability level). Hydrogen atoms are omitted for clarity

5.4 Crystal structure of *N,N'*-(1,2-phenylene)bis(pyridine-2-carboxamide)

5.4.1 Introduction

Colourless crystals of the title compound, bpb, were prepared as illustrated in Paragraph 4.3.1. A summary of the crystal data is given in Table 5.1, while the numbering scheme is shown in Figure 5.5. The most important bond lengths, bond angles and torsion angles are reported in Table 5.7, Table 5.8 and Table 5.9, respectively. The positional and thermal parameters are given in the Appendix in Table A.5 and A.6 while all the bond lengths and bond angles are given in Table A.7 and A.8.

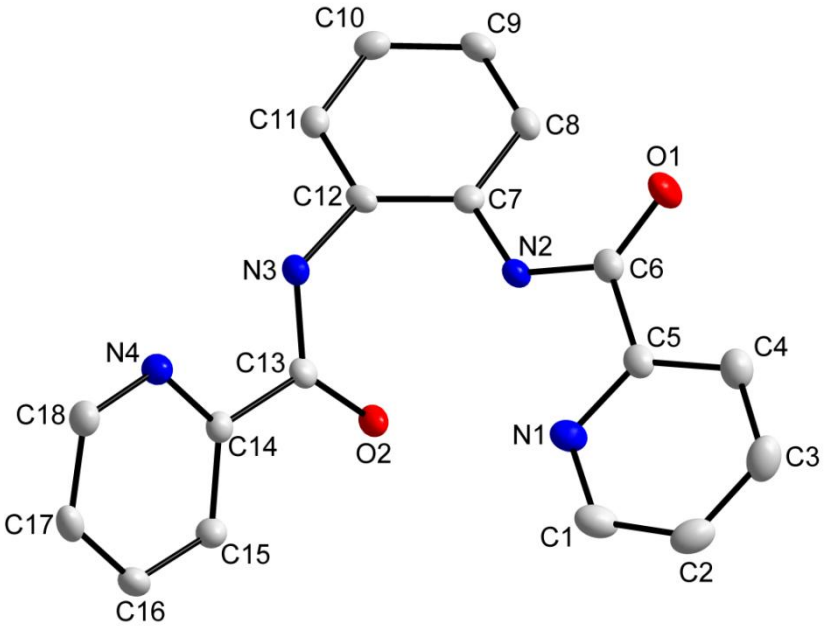

Figure 5.5 Molecular structure of bpb at 50 % probability level, displaying the numbering scheme. Hydrogen atoms are omitted for clarity

Table 5.7 Selected bond lengths of bpb

Bonds	Distances (Å)	Bonds	Distances (Å)
C7 – N2	1.4070(19)	C6 – C5	1.5081(22)
C12 – N3	1.4263(18)	C13 – C14	1.5027(23)
N2 – C6	1.3584(19)	C5 – N1	1.3419(21)
N3 – C13	1.3468(20)	C14 – N4	1.3380(19)
C6 – O1	1.2296(19)		
C13 – O2	1.2326(18)		

Table 5.8 Selected bonds angles of bpb

Bonds	Angles (°)	Bonds	Angles (°)
C6 – N2 – C7	127.24(13)	N2 – C6 –C5	113.56(13)
C12 – N3 – C13	127.16(13)	N3 – C13 –C14	114.54(13)
O1 – C6 – N2	125.63(14)	C6 – C5 – N1	117.31(13)
O2 – C13 –N3	124.07(14)	C13 – C14 – N4	117.15(13)
O1 – C6 – C5	120.81(14)		
O2 –C13 – C14	121.37(14)		

Table 5.9 Selected torsion angles of bpb

Bonds	Torsion angles (°)
N2 – C7 – C12 – N3	1.39(22)
N2 – C6 – C5 – N1	-7.59(20)
N3 – C13 – C14 – N4	-10.06(20)

5.4.2 Results and Discussion

The title compound, bpb, crystallizes in a centrosymmetric, monoclinic $P2_1/c$ space group, with four molecules per unit cell. The asymmetric unit consists of one full molecule of the bpb ligand in which the two picoline type rings are attached at the 1 and 2 positions of the phenyl ring, respectively.

The N2-C6 and N3-C13 bonds, with respective 1.3584(19) Å and 1.3468(20) Å bond distances, are similar to related structures.[1,9] The N2-C7 and N3-C12 bond length of 1.4070(19) Å and 1.4263(18) Å, as well as that of C6-C5 and C13-C14 of 1.5081(22) Å and 1.5027(23) Å are also considered normal when comparing these lengths to similar structures.[1,9]

Both picoline rings are slightly bent out-of-plane (C7-C8-C9-C12-C13-C14), illustrated by the N2-C6-C5-N1 torsion angle of -7.59(20) ° and N3-C13-C14-N4 torsion angle of -10.06(20) °.

The dihedral angle between the central phenyl ring (C7-C8-C9-C12-C13-C14) and the two picoline rings are calculated as 57.82(4) ° (Figure 5.6 a) and 17.96(7) ° (Figure 5.6 b) and the dihedral angle between the two picoline rings is calculated as 64.70(4) °.

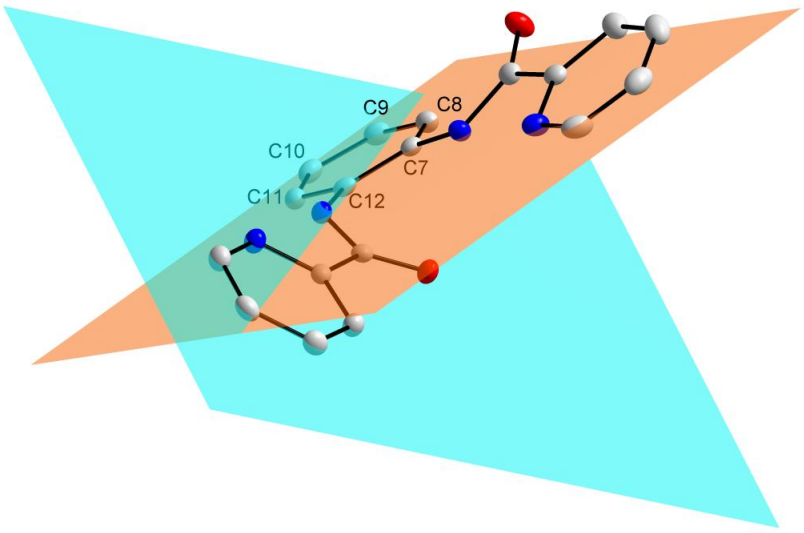

Figure 5.6 a Molecular structure that display the planarity of the central phenyl plane (C7-C8-C9-C12-C13-C14) and one of the picoline types ring at 50 % probability level. Hydrogen atoms are omitted for clarity

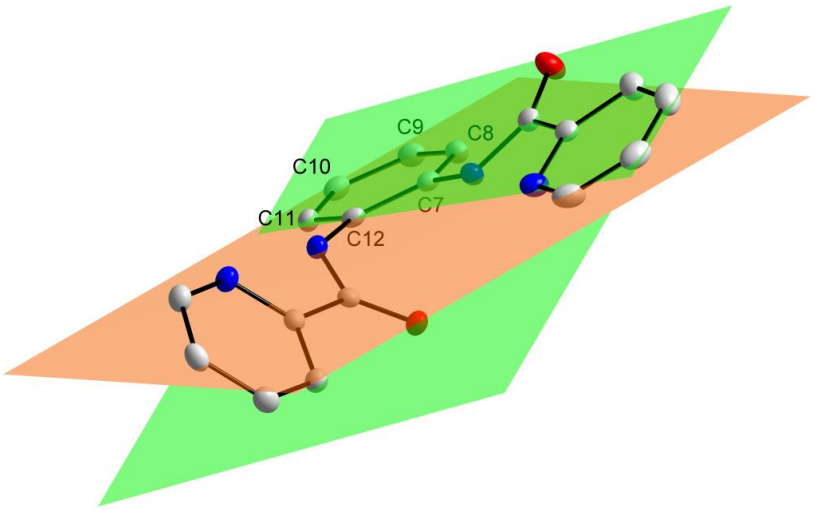

Figure 5.6 b Molecular structure that display the planarity of the central phenyl plane (C7-C8-C9-C12-C13-C14) and one of the picoline type rings at 50 % probability level. Hydrogen atoms are omitted for clarity

Weak intra molecular N-H...O and N-H...N hydrogen bonding interactions as well as intermolecular C-H...O interactions are observed which enhances the stability of the crystal structure. These interactions are listed in Table 5.10 and illustrated in Figure 5.7. The packing diagram displays a tail-to-tail packing fashion along the *a*-axis as illustrated in Figure 5.8.

Table 5.10 The specified Hydrogen bond in bpb

D-H...A	d(D-H)	d(H...A)	d(D...A)	D-H...A angle
N2-H2'...O2	0.901(19)	2.059(19)	2.8126(17)	140.5(16)
N2-H2'...N1	0.901(19)	2.216(18)	2.6720(18)	110.8(14)
N3-H3'...N4	0.88(2)	2.253(19)	2.6813(18)	109.7(15)
C8-H8...O1	0.93	2.36	2.8904(19)	115.7
C11-H11...O2[a]	0.93	2.42	3.1332(18)	133.2

Operators for generating equivalent atoms:

[a]x, y-1, z

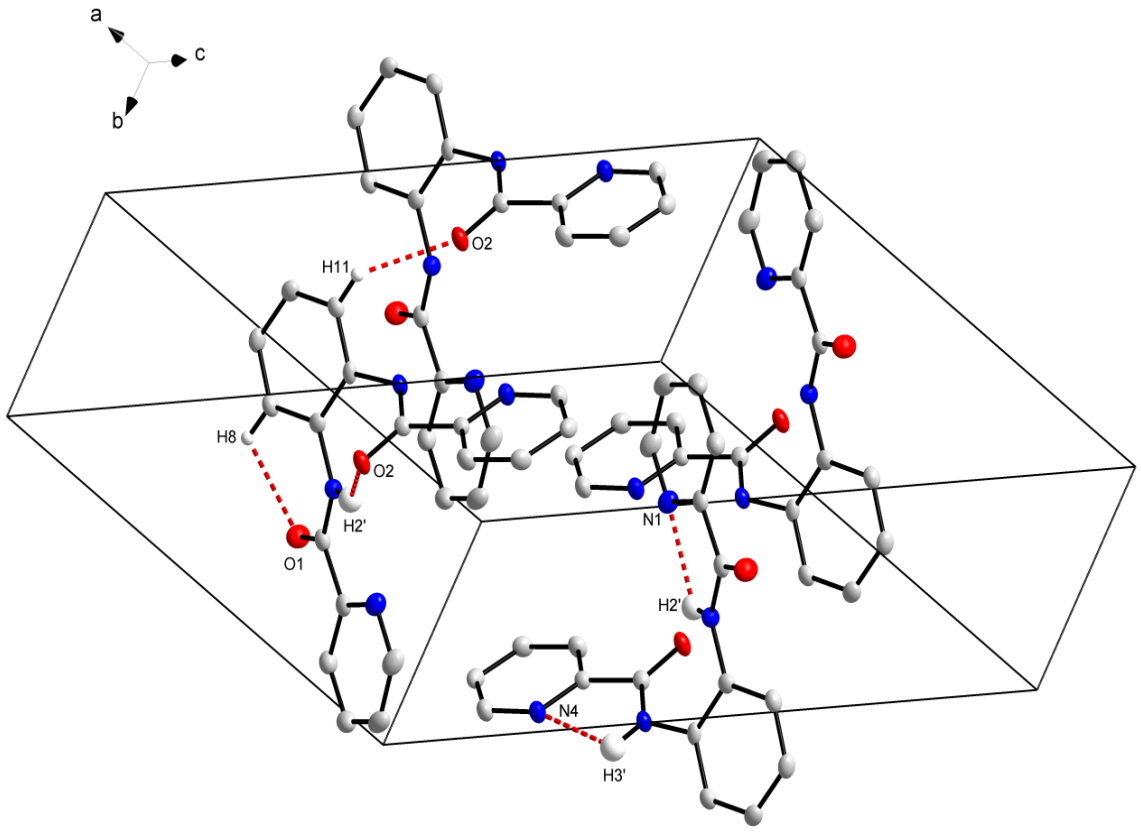

Figure 5.7 Molecular structure of bpb, displaying inter- and intramolecular interactions at 50 % probability level). Hydrogen atoms that are not part of the interactions are omitted for clarity

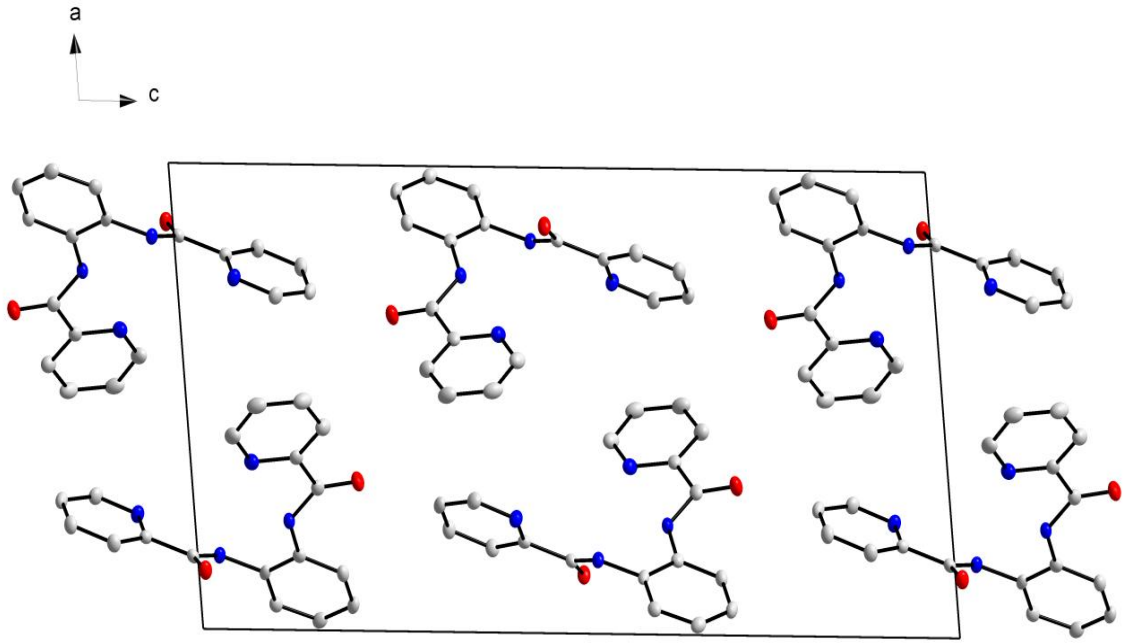

Figure 5.8 Molecular structure of bpb, displaying the packing along the *a*-axis at 50 % probability level). Hydrogen atoms are omitted for clarity

5.5 Discussion

There are only two other structures of similar carboxamide ligands available in literature and these compare well with the crystal structure obtained (Figure 5.1) in this study. Lin *et al.*[2] produced the crystal structure of bpb obtained from reacting 1,2-phenylenediamine and picolinic acid, $C_{18}H_{14}N_4O_2$, and Jain *et al.*[9] synthesized 3,4-Bis(pyridine-2-carboxamido)toluene [(Mebpb)toluene], prepared from 3.4-Diaminotoluene and picolinic acid in toluene.

The selected bonds lengths are summarized in Table 5.11 for comparison and the structure reported by Lin *et al.*[2] and Jain *et al.*[9] are illustrated in Figure 5.9 and Figure 5.10, respectively.

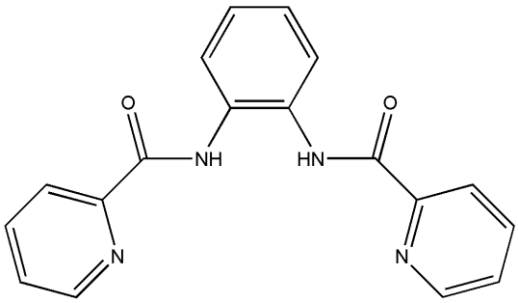

Figure 5.9 Two-dimensional molecular structure of bpb.[2]

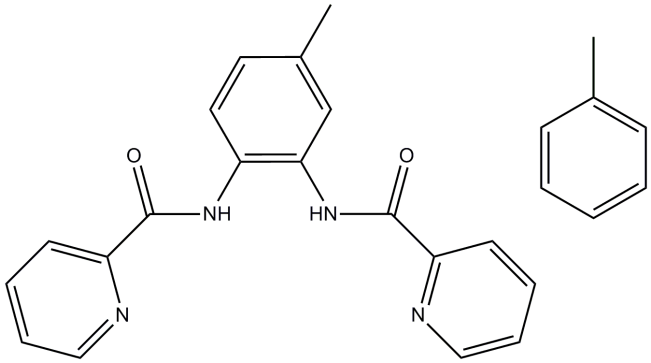

Figure 5.10 Two-dimensional structure of [(Mebpb)toluene][9]

Table 5.11 Comparison of the bond lengths of the crystal structures reported by Lin[2], Jain[9] and the crystal structures obtained in this study

	Selected bond lengths (Å)			
Compounds	**N2-C6**	**N2-C7**	**C14-N3**	**N3-C15**
di-Mebpb	1.351(2)	1.410(2)	1.421(2)	1.342(2)
bpb	1.3584(19)	1.4070(19)	1.4263(18)	1.3468(20)
bpb[2]	1.356(3)	1.406(3)	1.432(3)	1.343(3)
[(Mebpb)toluene][9]	1.352(2)	1.416(2)	1.423(2)	1.347(2)

Care was taken to compare similar bonds throughout

It is clear from Table 5.11 that the bond distances are very similar for all the different types of ligands. The crystal structure of bpb, obtained in this study is similar to that of Lin *et al.*, the only major difference being the temperature at the time of the data collection -173.0 °C *vs.* Lin *et al.*[2] 20.0 °C.

5.6 Crystal structure of [Ga(*N*,*N*′-(1,2-phenylene)bis-(pyridine-2-carboxamide))$(H_2O)_2$]NO_3·CH_3OH

5.6.1 Introduction

Yellow needles of the title compound, [Ga(bpb)$(H_2O)_2$]NO_3·CH_3OH, were obtained according to the synthesis described in Paragraph 4.3.2. The crystal data of the compound is listed in Table 5.2, while the numbering scheme is shown in Figure 5.11. All the selected bond distances, bond angles and torsion angles are listed in Table 5.12, Table 5.13 and Table 5.14, respectively. The positional and thermal parameters are given in the Appendix in Table A.9 and A.10 while all the bond lengths and bond angles are given in Table A.11 and A.12.

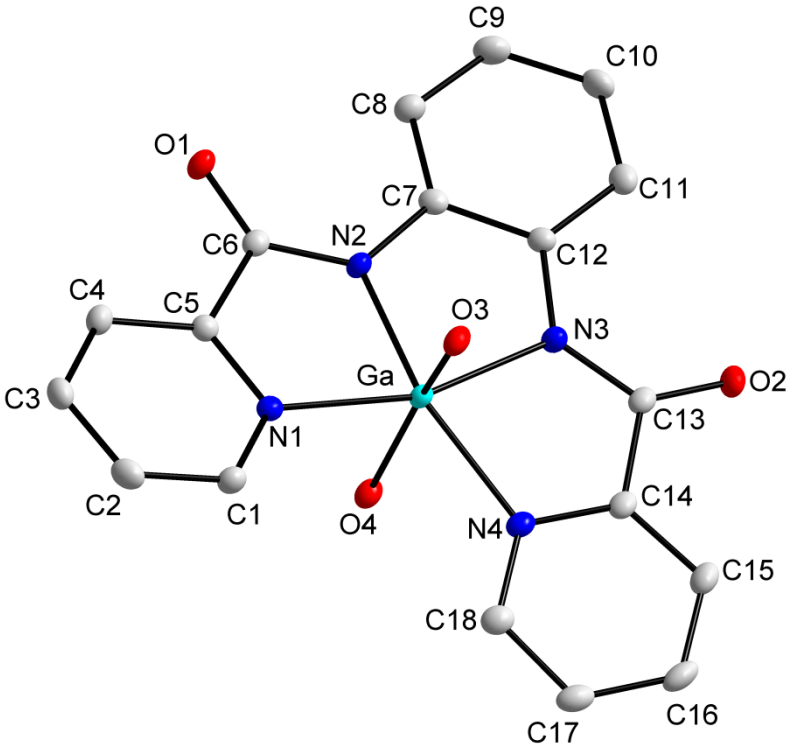

Figure 5.11 Molecular structure of [Ga(bpb)$(H_2O)_2$]$^+$ at 50 % probability level, displaying the numbering scheme. Hydrogen atoms are omitted for clarity

Table 5.12 Selected bond distances of $[Ga(bpb)(H_2O)_2]NO_3 \cdot CH_3OH$

Bonds	Distances (Å)	Bonds	Distances (Å)
Ga – N1	2.0374(5)	N2 – C7	1.4106(4)
Ga – N2	1.9645(4)	N3 – C12	1.4107(4)
Ga – N4	2.0496(5)	N2 – C6	1.3303(4)
Ga – N3	1.9644(4)	N1 – C5	1.3489(3)
Ga – O3	2.0443(4)	N3 – C13	1.3266(4)
Ga – O4	2.0542(4)	N4 – C14	1.3551(3)

Table 5.13 Selected bond angles of $[Ga(bpb)(H_2O)_2]NO_3 \cdot CH_3OH$

Bonds	Angles (°)	Bonds	Angles (°)
N1 - Ga – N2	81.47(1)	N2 – Ga – O3	100.18(1)
N1 – Ga – N4	115.03(1)	N4 – Ga – N3	81.44(1)
N1 – Ga – N3	162.92(2)	N4 – Ga – O4	83.33(1)
N1 – Ga – O4	86.99(1)	N4 – Ga – O3	87.14(1)
N1 – Ga – O3	82.84(1)	N3 – Ga – O4	100.06(1)
N2 – Ga – N4	162. 85(2)	N3 – Ga – O3	94.00(1)
N2 – Ga – N3	82.59(1)	O4 – Ga – O3	161.62(1)
N2 – Ga – O4	93.37(1)		

Table 5.14 Selected torsion angles of $[Ga(bpb)(H_2O)_2]NO_3 \cdot CH_3OH$

Bonds	Torsion angles (°)
N2-C7-C12-N3	4.86(3)
N1-C5-C6-N2	1.58(3)
N3-C13-C14-N4	4.82(3)

5.6.2 Results and Discussion

The title compound, $[Ga(bpb)(H_2O)_2]NO_3 \cdot CH_3OH$, crystallizes in a centrosymmetric, orthorhombic *Pbca* space group, with four molecules per unit cell. The asymmetric unit consists of the Ga(III) complex, a methanol solvent molecule and a nitrate counter ion. In the molecule the Ga(III) metal centre is coordinated to four nitrogen atoms from a bpb tetradentate ligand and two water molecules *trans* to each other to make up a distorted octahedron. This distortion is illustrated by the large bite angle of N1-Ga-N4 (115.03(1) °) and the small bite angle of O4-Ga-O3 (161.62(1) °).

The Ga-N1, Ga-N2, Ga-N3 and Ga-N4 bond distances of 2.0374(5) Å, 1.9645(4) Å, 1.9644(4) Å and 2.0496(5) Å respectively, agree well with similar structures.[12,13,14,15] The Ga-O3 and Ga-O4 bond lengths of 2.0443(4) Å and 2.0542(4) Å respectively, also compare well with similar structures.

The nitrogen atoms, N2 and N3, are situated slightly above and below the phenyl plane (C7-C8-C9-C10-C11-C12), with distances from the plane calculated as N2 = -0.1032(0.0028) Å and N3 = 0.0866(0.0028) Å.

The dihedral angle between the central phenyl ring and the two picoline rings is calculated as 12.40(9) ° (Figure 5.12 a) and 8.73(10) ° (Figure 5.12 b). The dihedral angle between the two picoline rings is calculated as 12.40(9) °.

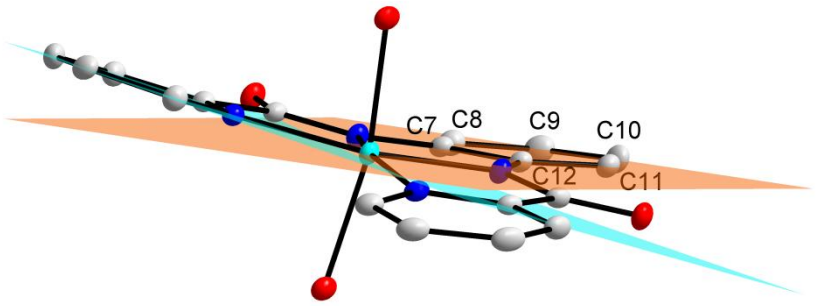

Figure 5.12 a Molecular structure that display the planarity of the central phenyl plane (C7-C8-C9-C10-C11-C12) and one of the picoline type rings at 50 % probability level. Hydrogen atoms are omitted for clarity

[12] Sofetis, A., Raptopoulou, C. P., Terzis, A., Zafiropoulos, T. F., *Inorganica Chimica Acta*, **359**, 3389-3395, 2006.
[13] DiPasquale, A. G. & Mayer, J. M., *J. Am. Chem. Soc.*, **130**, 1812-1813, 2008.
[14] Papaefstathiou, G. S., Sofetis, A., Raptopoulou, C. P., Terzis, A., Spyroulias, G. A., Zafiropoulos, T. F., *J. Molecular Struc.*, **837**, 5-14, 2007.
[15] Heppeler, A., Andrè, J. P., Buschmann, I., Wang, X, Reubi, J-C., Henning, M., Kaden, T. A. & Maecke, H. R., *Chem. Eur. J.*, **14**, 3026-3034, 2008.

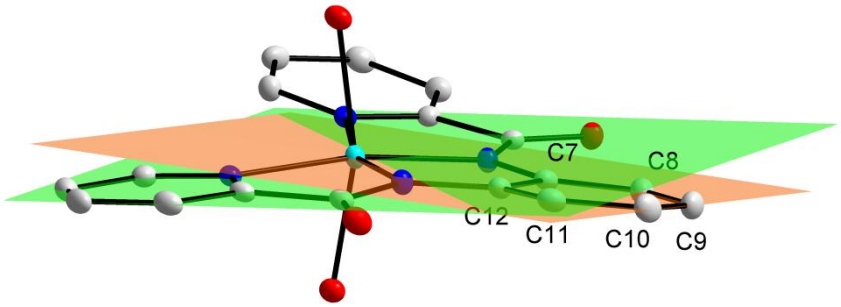

Figure 5.12 b Molecular structure that display the planarity of the central phenyl plane (C7-C8-C9-C10-C11-C12) and one of the picoline type rings at 50 % probability level. Hydrogen atoms are omitted for clarity

Weak O-H...O and C-H...O hydrogen bonding interactions are observed and contribute to the stability of the crystal structure. All the bond distances and angles of these interactions are listed in Table 5.15 and Figure 5.13 illustrates these interactions. The packing diagram of the crystal structure displays a head-to-tail packing fashion in vertical layers along the *b*-axis as illustrated in Figure 5.14.

Table 5.15 Specified hydrogen bonds in $[Ga(bpb)(H_2O)_2]NO_3 \cdot CH_3OH$

D-H...A	d(D-H)	d(H...A)	d(D...A)	D-H...A angle
O5-H5…O7[f]	0.82	2.09	2.904(2)	171.3
O5-H5…O8[f]	0.82	2.35	2.949(2)	130.0
O4-H111…O1[g]	0.77(3)	1.94(3)	2.699(2)	173(3)
O4-H112…O7[g]	0.83(3)	1.91(3)	2.730(2)	169(3)
O3-H113…O5	0.84(3)	1.82(3)	2.652(2)	169(3)
O3-H114…O2[c]	0.77(3)	1.89(3)	2.655(2)	176(3)
C1-H1…O8[b]	0.93	2.38	3.092(2)	133.7
C4-H4…O6	0.93	2.36	3.019(2)	127.9
C8-H8…O1	0.93	2.40	2.977(2)	120.2
C9-H9…O7[a]	0.93	2.59	3.413(3)	147.6
C11-H11…O2	0.93	2.39	2.959(3)	119.4
C15-H15…O8[e]	0.93	2.48	3.100(3)	123.8
C17-C17…O5[d]	0.93	2.39	3.310(3)	168.4
C18-H18…O6[b]	0.93	2.58	3.418(3)	149.4

Operators for generating equivalent atoms:

[a] -x+1, y-1/2, -z+3/2 [b] -x+2, y-1/2, -z+3/2 [c] -x+3/2, y+1/2, z [d] -x+2, -y, -z+1

[e] x, -y+1/2, z-1/2 [f] -x+3/2, -y+1, z-1/2, [g] -x+3/2, y-1/2, z

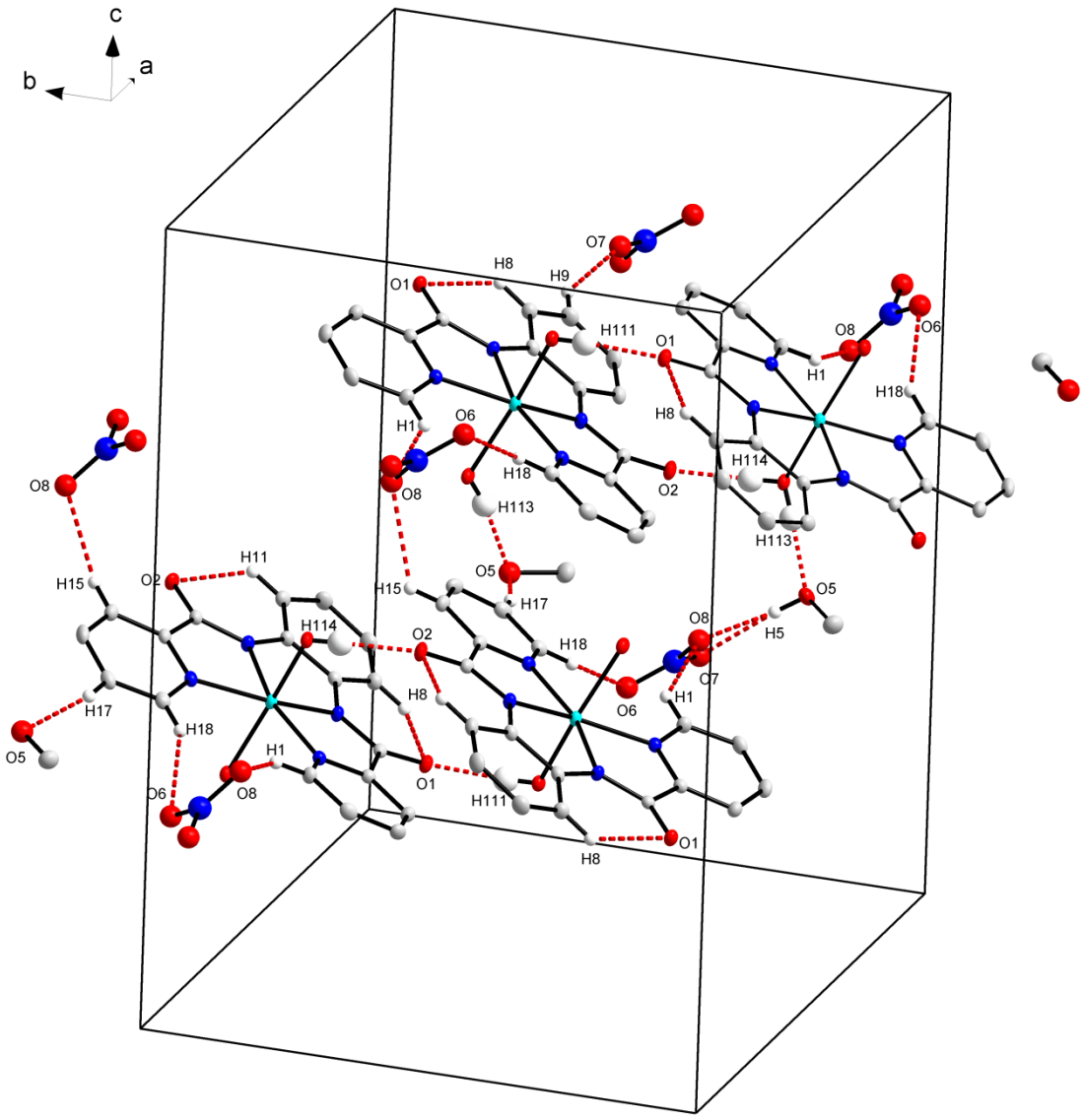

Figure 5.13 Molecular structure of $[Ga(bpb)(H_2O)_2]NO_3 \cdot CH_3OH$, displaying inter- and intramolecular interactions at 50 % probability level). Hydrogen atoms that are not part of the interactions are omitted for clarity

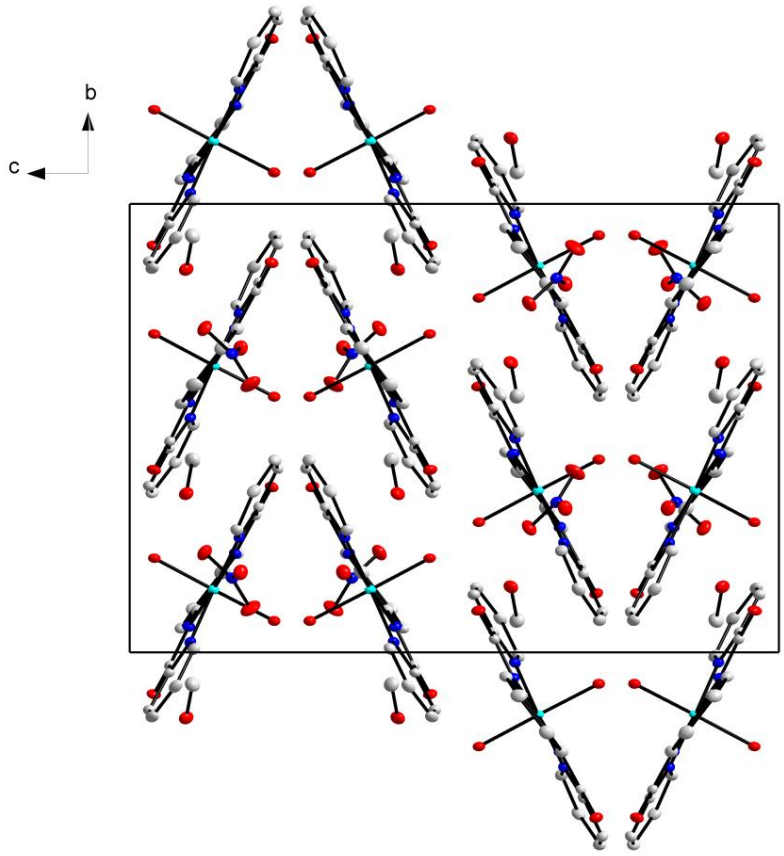

Figure 5.14 Molecular structure of $[Ga(bpb)(H_2O)_2]NO_3 \cdot CH_3OH$, displaying the packing along the *b*-axis at 50 % probability level). Hydrogen atoms are omitted for clarity

5.7 Crystal structure of [Au(*N*,*N'*-(1,2-phenylene)bis-(pyridine-2-carboxamide))]Cl

5.7.1 Introduction

Yellow needles of the title compound, [Au(bpb)]Cl, were obtained and described in Paragraph 4.3.2. The crystal data of the compound is listed in Table 5.2, while the numbering scheme is shown in Figure 5.15. All the selected bond distances, bond angles and torsion angles are listed in Table 5.16, Table 5.17 and Table 5.18, respectively. The positional and thermal parameters are given in the Appendix in Table A.13 and A.14 while all the bond lengths and bond angles are given in Table A.15 and A.16.

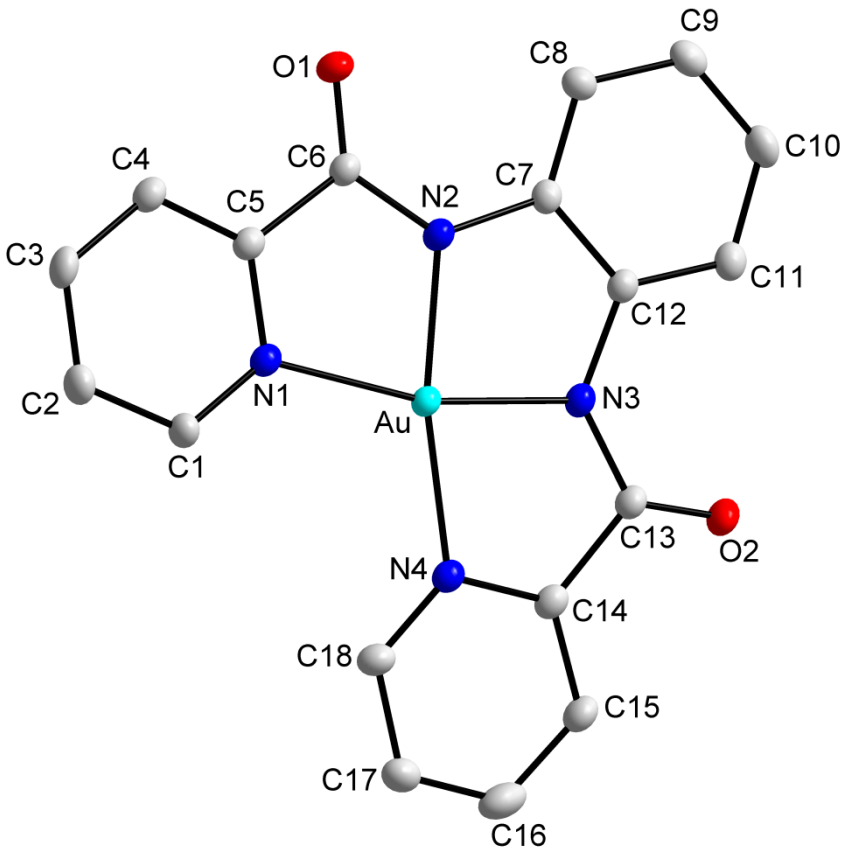

Figure 5.15 Molecular structure of $[Au(bpb)]^{+}$ at 50 % probability level, displaying the numbering scheme. Hydrogen atoms are omitted for clarity

Table 5.16 Selected bond distances of [Au(bpb)]Cl

Bonds	Distances (Å)	Bonds	Distances (Å)
Au – N1	2.046(5)	N2 – C6	1.356(8)
Au – N2	1.948(6)	N1 – C5	1.363(9)
Au – N4	2.052(6)	N3 – C13	1.356(8)
Au – N3	1.946(5)	N4 – C14	1.364(9)
N2 – C7	1.420(8)		
N3 – C12	1.435(9)		

Table 5.17 Selected bond angles of [Au(bpb)]Cl

Bonds	Angles (°)
N3 – Au – N2	84.3(2)
N3 – Au – N1	165.9(2)
N2 – Au – N1	81.8(2)
N3 – Au – N4	81.9(2)
N2 – Au – N4	165.8(2)
N1 – Au – N4	111.9(2)

Table 5.18 Selected torsion angles of [Au(bpb)]Cl

Bonds	Torsion angles (°)
N2-C7-C12-N3	0.94(83)
N1-C5-C6-N2	3.75(88)
N3-C13-C14-N4	2.84(93)

5.7.2 Results and Discussion

The title compound, [Au(bpb)]Cl, crystallizes in a centrosymmetric, triclinic *P*ī space group, with two molecules per unit cell. The asymmetric unit consists of the Au(III) complex and a chlorine atom as a counter ion. In the molecule the Au(III) metal centre is coordinated to four nitrogen atoms from a bpb tetradentate ligand to make up a slightly distorted planar geometry. This distortion is illustrated by the bond angles of N-Au-N ranging from 81.8(2) ° to 111.9(2) °.

The Au-N1, Au-N2, Au-N3 and Au-N4 bond distances of 2.046(5) Å, 1.948(6) Å, 1.9646(5) Å and 2.052(6) Å respectively, agree well with a similar structure.[16]

The molecule structure is nearly planar with the gold deviating 0.0518(3) Å from the N1-N2-N3-N4 plane, illustrated in Figure 5.16.

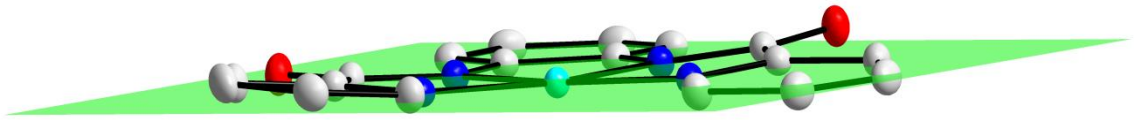

Figure 5.16 Molecular structure of $[Au(bpb)]^+$ displaying the planarity of the complex at 50 % probability level. Hydrogen atoms are omitted for clarity

Weak C-H...Cl and C-H...O hydrogen bonding interactions are observed and contribute to the stability of the crystal structure. All the bond distances and angles of these interactions are listed in Table 5.19 and Figure 5.17 illustrates these interactions. The packing diagram of the crystal structure displays a head-to-tail packing fashion when viewed along the *c*-axis, illustrated in Figure 5.18.

[16] Shachter, A. M., Fleischer, E. B. & Haltiwanger, R. C., *Acta Cryst.*, **C43**, 1876-1878, 1987.

Table 5.19 Specified hydrogen bonds in [Au(bpb)]Cl

D-H...A	d(D-H)	d(H...A)	d(D...A)	D-H...A angle
C1-H1...Cl1[a]	0.93	2.66	3.488(8)	149.3
C3-H3...Cl1[b]	0.93	2.80	3.596(7)	144.1
C4-H4...O1[c]	0.93	2.29	3.117(8)	147.3
C8-H8...O1	0.93	2.39	2.962(9)	119.9
C11-H11...O2	0.93	2.39	2.975(9)	120.7
C11-H11...O2[d]	0.93	2.49	3.264(8)	140.8
C8-H18...Cl1[a]	0.93	2.65	3.469(9)	147.2

Operators for generating equivalent atoms:

[a] –x+1, -y, -z+1 [b] -x+1, y, z [c] -x+2, -y+1, -z [d] -x, -y, -z

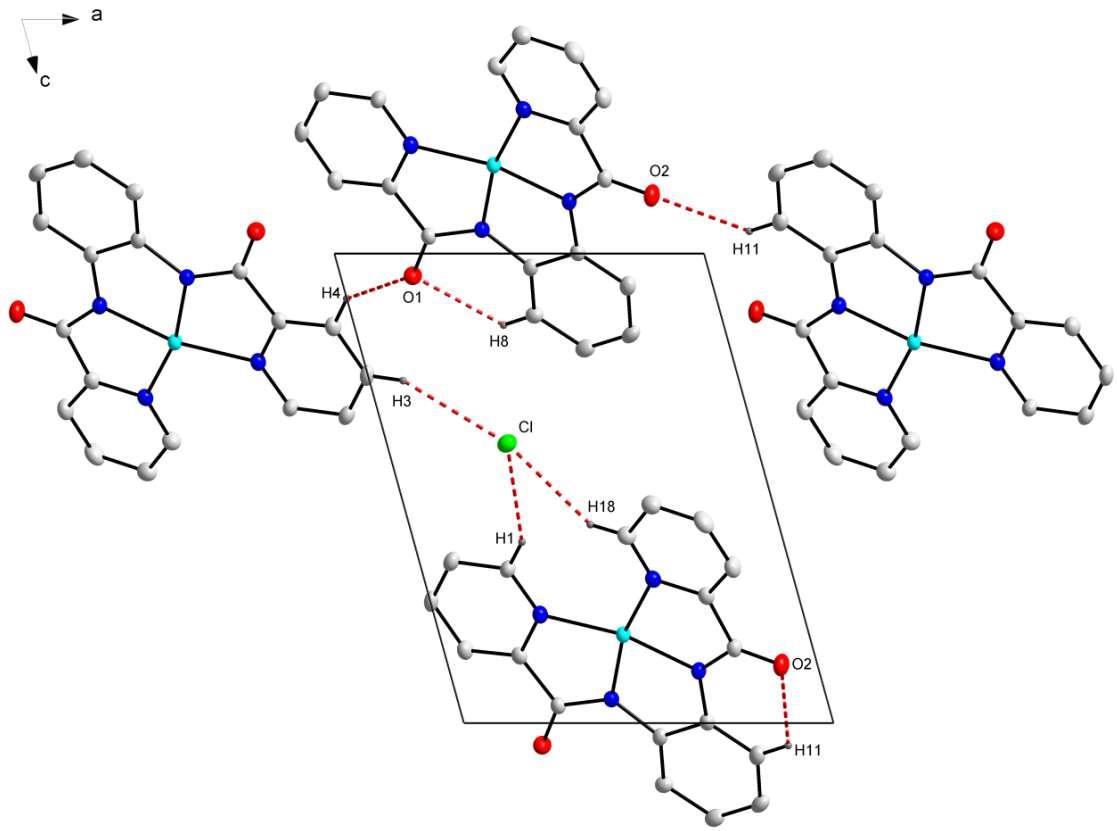

Figure 5.17 Molecular structure of [Au(bpb)]Cl, displaying inter- and intramolecular interactions at 50 % probability level). Hydrogen atoms that are not part of the interactions are omitted for clarity

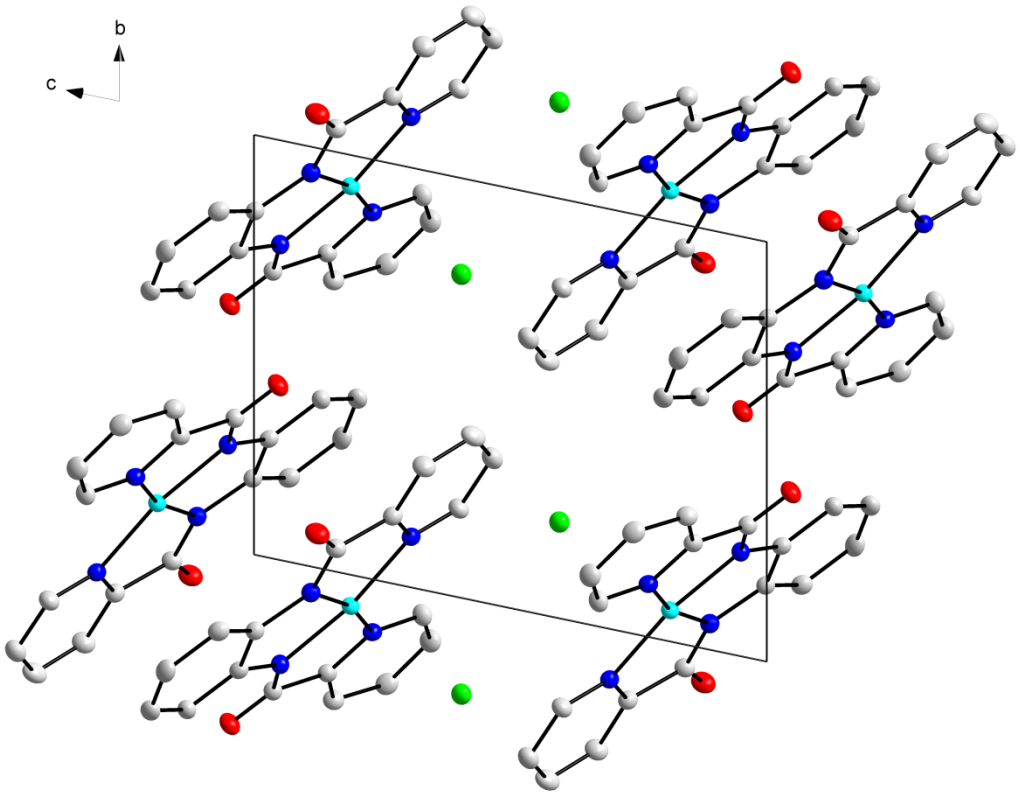

Figure 5.18 Molecular structure of [Au(bpb)]Cl, displaying the packing along the *c*-axis at 50 % probability level). Hydrogen atoms are omitted for clarity

5.8 Discussion

There are four other crystal structures with very similar properties to the gallium complex available in literature. Sofetis *et al.*[10] synthesized $[Ga(dmbpy)_2(H_2O)_2](NO_3)_3$ from $Ga(NO_3)_3 \cdot 9H_2O$ and 4,4'-dimethylbipyridine (dmbpy). DiPasquale *et al.*[11] synthesized gallium tetraphenylporphyrin, $[(TPP)Ga(OH_2)_2]ClO_4$, from gallium(III) perchlorate hydrate and 5,10,15,20-tetraphenylporphin. Papaefstathiou *et al.*[12] synthesized $[Ga_2(OH)_2(H_2O)_2(terpy)_2](NO_3)_4$ from $Ga(NO_3)_3 \cdot 9H_2O$ and 2,2':6',2''-terpyridine (terpy) and Heppeler *et al.*[13] synthesized $[Ga(H_2dota)]^+Cl^-$ from $Ga(NO_3)_3 \cdot 9H_2O$ and 1,4,7,10-tetraazacyclododecane-1,4,7,10-teraacetic acid (DOTA).

The selected bond distances which were compared for all the different gallium complexes are reported in Table 5.20 and the structures reported by Sofetis *et al.*[10], DiPasquale *et al.*[11], Papaefstathiou *et al.*[12] and Heppeler *et al.*[13] are illustrated in Figure 5.19, Figure 5.20, Figure 5.21 and Figure 5.22, respectively.

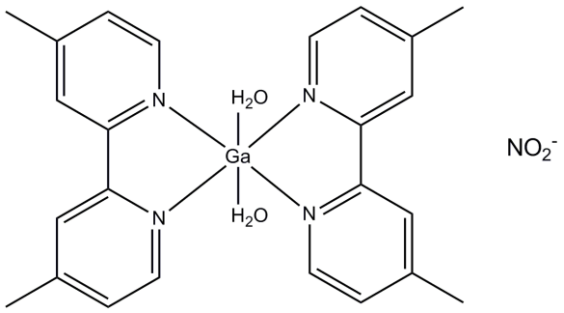

Figure 5.19 Two-dimensional molecular structure of $[Ga(dmbpy)_2(H_2O)_2](NO_3)_3$[10]

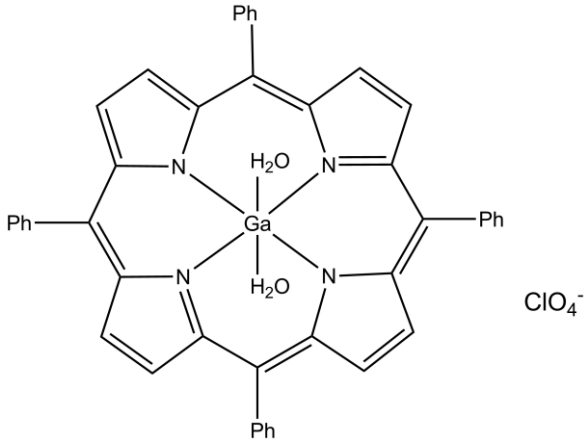

Figure 5.20 Two-dimensional molecular structure of $[(TPP)Ga(OH_2)_2]ClO_4$[11]

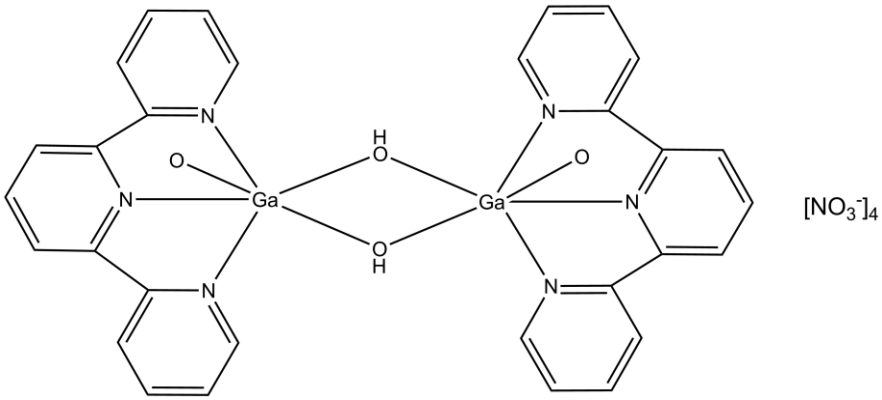

Figure 5.21 Two-dimensional molecular structure of $[Ga_2(OH)_2(H_2O)_2(terpy)_2](NO_3)_4$[12]

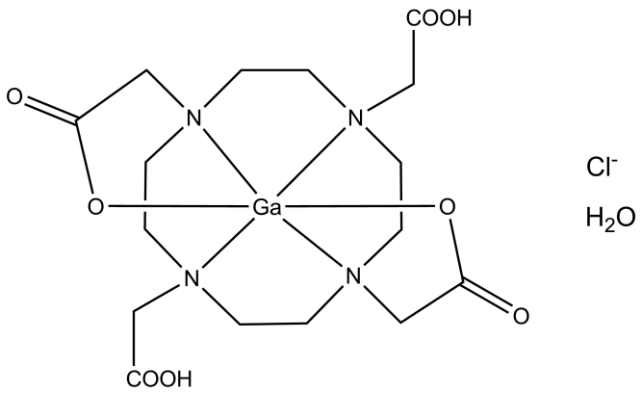

Figure 5.22 Two-dimensional molecular structure of $[Ga(H_2dota)]^+Cl^-$ [13]

Table 5.20 Comparison of the bond lengths of the crystal structures reported by Sofetis[10], DiPasquale[11], Papaefstathiou[12], Heppeler[13] and the crystal structure obtained in this study

	Bond distances (Å)					
Complex	**Ga-N1**	**Ga-N2**	**Ga-N3**	**Ga-N4**	**Ga-O3**	**Ga-O4**
$[Ga(bpb)(H_2O)_2]NO_3 \cdot CH_3OH$	2.037(5)	1.965(4)	1.964(4)	2.050(5)	2.044(4)	2.054(4)
$[Ga(dmbpy)_2(H_2O)_2](NO_3)_3$ [10]	2.056(3)		2.046(2)		1.956(2)	
$[(TPP)Ga(OH_2)_2]ClO_4$ [11]	2.021(2)	2.004(1)	2.004(1)	2.021(2)	2.091(2)	
$[Ga_2(OH)_2(H_2O)_2(terpy)_2]^+$ [12]	2.089(2)	2.028(2)	2.117(2)		1.972(2)	1.893(2)
$[Ga(H_2dota)]^+Cl^-$ [13]	2.152(50)		2.111(8)		1.927(19)	

From the table above, it can be seen that the Ga-N2 and Ga-N3 bonding distances in $[Ga(bpb)(H_2O)_2]NO_3 \cdot CH_3OH$ are slightly shorter than what is expected normally for these complexes. This might be due to the general rigidity of the tetradentate ligand which imposes this structural requirement on the central ion.

The complex synthesized by Sofetis *et al.*[10] consists of a oxygen atom and three nitrogen atoms of two 4,4'-dimethylbipyridine ligands in the equatorial plane and a oxygen atom and a nitrogen atom of one 4,4'-dimethylbipyridine ligand in the axial plane. The complex synthesized by Papaefstathiou *et al.*[12] consists of three nitrogen atoms of the 2,2':6',2''-terpyridine ligand and one oxygen atom of a aqua ligand in the equatorial plane and two oxygen atoms of the aqua ligands in the axial plane. Heppeler *et al.*[13] synthesized $[Ga(H_2dota)]^+Cl^-$ where the equatorial plane comprises of two nitrogen atoms of the DOTA ring and two oxygen atoms of the four pendant carboxylic acid groups. The axial plane comprises of the remaining two transannular nitrogen atoms of the DOTA ring. The gallium(III) complex synthesized in this study, $[Ga(bpb)(H_2O)_2]NO_3 \cdot CH_3OH$, consists of

four nitrogen atoms of the bpb ligand in the equatorial plane and two oxygen atoms of the two aqua ligands in the axial plane.

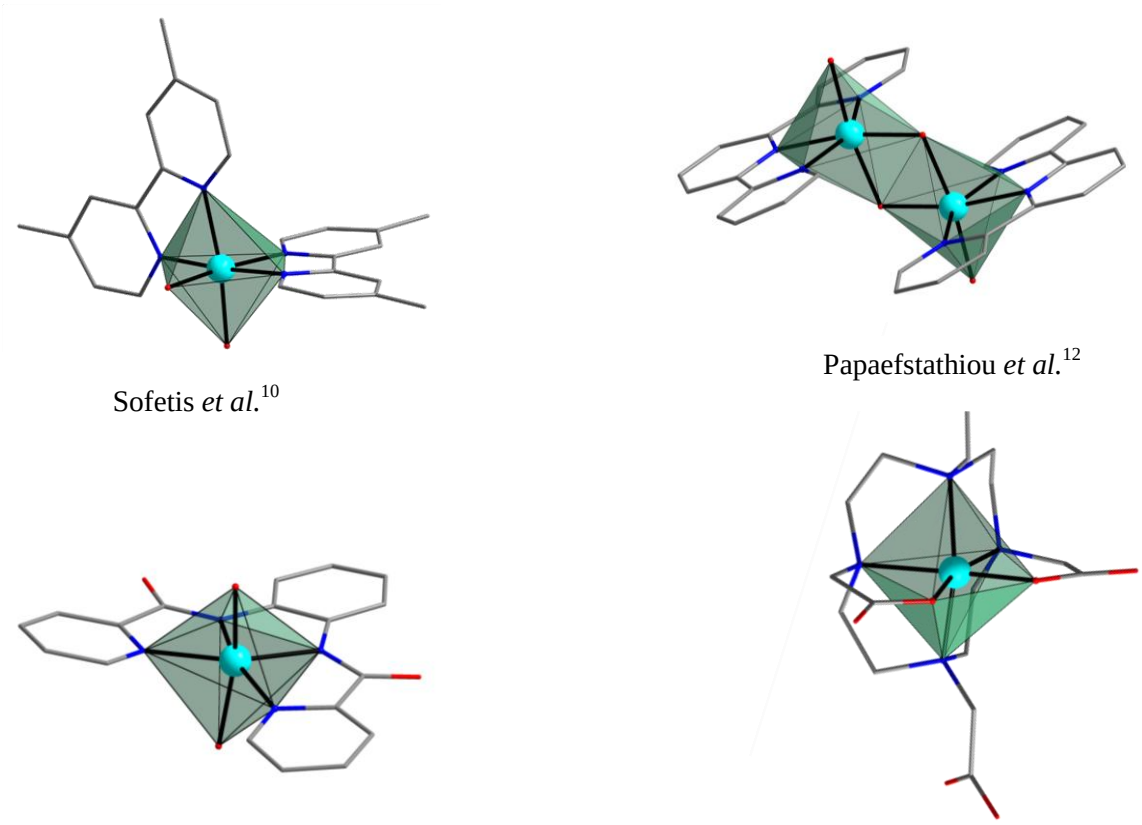

Sofetis *et al.*[10]

Papaefstathiou *et al.*[12]

Study

Heppeler *et al.*[13]

Figure 5.23 Polyhedra illustration of the distortions away from ideal octahedral geometries

It is known from related complexes that these types of gallium complexes coordinates in an octahedral fashion, where the metal is bonded to nitrogen and oxygen atoms. Slight distortions away from ideal octahedral geometries are evident. These distortions are best illustrated by Figure 5.23. The degree of distortion is quantified by the deviation of the axial angle of the octahedral polyhedrons constructed. Deviations from the ideal octahedral geometries are listed in Table 5.21 in terms of axial angles.

Table 5.21 Comparison of the axial bond angles of crystal structures reported by Sofetis[10], DiPasquale[11], Papaefstathiou[12], Heppeler[13] and the crystal structure obtained in this study to illustrate the degree of distortion

Complex	Axial angle (°) O-Ga-O (N)*
$[Ga(bpb)(H_2O)_2]NO_3 \cdot CH_3OH$	161.62(1)
$[Ga(dmbpy)_2(H_2O)_2](NO_3)_3$[10]	171.4(1)
$[Ga_2(OH)_2(H_2O)_2(terpy)_2] (NO_3)_4$[12]	170.90(1)
$[Ga(H_2dota)]^+Cl^-$[13]	157.1(2)

*Axial angles of atoms O-Ga-O or O-Ga-N or N-Ga-N

There is only one crystal structure with similar properties to the gold complex synthesized in this study available in literature. Shachter *et al.*[16] synthesized (5,10,15,20-Teraphenylporphinato)gold(III) Tetrachloroaurate(III) from gold(III) chloride and 5,10,15,20-tetraphenylporphin (TPP), see Figure 5.24.

The selected bond distances which were compared are reported in Table 5.21.

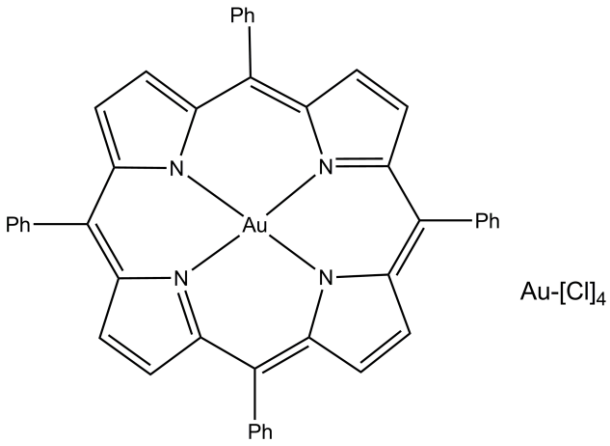

Figure 5.24 Two-dimensional molecular structure of $[AuTPP]AuCl_4$[16]

Table 5.21 Comparison of the bond lengths of the crystal structure reported by Shachter[16] and the crystal structure obtained in this study, [Au(bpb)]Cl

	Bond distances (Å)			
Complex	**Au-N1**	**Au-N2**	**Au-N3**	**Au-N4**
[Au(bpb)]Cl	2.046(5)	1.948(6)	1.946(5)	2.052(6)
$[AuTPP]AuCl_4$[16]	2.029(7)	2.004(6)		

From Table 5.16 it is clear that the respective Au-N bond distances of the gold(III) complex obtained in this study and the gold complex from literature are very similar. Once again the tetradentate ligand imposes the structural rigidity on the gold atom as observed in the shorter Au-N2 and Au-N3 distances in [Au(bpb)]Cl. It is known from related literature complexes that these types of gold complexes bind in a square planar fashion, where the metal is bonded to four nitrogen atoms as could be seen in Figure 5.16.

5.9 Conclusion

During the course of this study, two ligands and two metal compounds have been synthesized and characterized by X-Ray diffractometry. One of these compounds, bpb, have already been published by Lin *et al.*[2] There is a very limited amount of structural crystal data available in literature for the complexes synthesized in this project.

In general, it was observed that the tetradentate ligands investigated crystallize in the absence of any solvent or counter ions in the unit cell. The gallium(III) complex crystallizes in a distorted octahedral fashion with the presence of a methanol as solvent and a nitrate counter ion and the gold(III) complex crystallizes in a distorted square planar fashion with a chlorine counter ion.

The reactivity towards methanol substitution of the gallium complex, *trans*-$[Ga(bpb)(CH_3OH)_2]^+$, is discussed in Chapter 6 with 4-methylpyridine as entering ligand.

6 Kinetic Study of the Methanol Substitution in *trans*-$[Ga(bpb)(CH_3OH)_2]^+$

6.1 Introduction

This chapter describes the methanol substitution from *trans*-$[Ga(bpb)(CH_3OH)_2]^+$ by 4-methylpyridine.

Chemical kinetics comprises the study of the rates of chemical reactions, which involves a precise measurement of a range of concentrations of an entering ligand over time at a precise temperature. Most of the kinetic studies on gallium(III) in literature involve the formation of complexes with different multidentate ligands with a special focus to study the pH dependence of these reactions.[1,2,3,4] Our literature search did not reveal any studies of complexes nearly resembling *trans*-$[Ga(bpb)(CH_3OH)_2]^+$ where only two possible positions on the Ga(III) complex is available for substitution. However, some related work were performed on cobalt(III) porphyrin complexes and will be discussed briefly in the following paragraphs.

Ashley *et al.*[5] studied the kinetics of the reaction of (*meso*-Tetrakis(*p*-sulfonatophenyl)porphyrinato)diaquocolbaltate(III) with pyridine as entering ligand in a aqueous solution at different pH. It was found that the aqua substitution with pyridine points towards a dissociative mechanism and that the effect of a *trans*-hydoxo ligand had a marked

[1] Kubicek, V., Havlickova, J., Kotek, J., Tircso, G., Hermann, P., Toth, E. & Lukes, I., *Inorg. Chem.*, **49**, 10960-10969, 2010.
[2] Corigli, R., Secco, F. & Venturini, M., *Inorg. Chem.*, **21**, 2992-2998, 1982.
[3] Simecek, J., Schulz, M., Notni, J., Plutnar, J., Kubicek, V., Halickova, J. & Hermann, P., *Inorg. Chem.*, **51**, 577-590, 2012.
[4] Jarjayes, O., Hamman, S., Sarrazin F., Benaissa, T & Beguin, C. G., *New J. Chem.*, 361-366, 1998.
[5] Ashley, K. R. & Leipoldt, J. G., *Inorg. Chem.*, **20**, 2326-2333, 1981.

increase on the rate of substitution (at higher pH). Overall, the study leads to very complicated kinetics which was made more difficult by the formation of hydroxo-briged species at higher pH.

It is well known that Gallium(III) ions are very susceptible to the formation of hydroxo bridged polymeric species in aqueous solution and this was also found for *trans*-$[Ga(bpb)(CH_3OH)_2]^+$ during our preliminary kinetic studies.[1,2,3,4] In order to circumvent the associated problems which naturally is associated with a pH dependence study, it was decided to investigate the substitution reactions of coordinated methanol in *trans*-$[Ga(bpb)(CH_3OH)_2]^+$ instead. Kinetic studies that follow the ligand substitution reactions of model or potential radiopharmaceuticals are very important in order to understand the intimate mechanism that guide these reactions and to ensure fast and complete synthesis of potential radiopharmaceuticals. These types of investigations also give an indication of the rate of ligand substitution, the biodistribution of the agent, in vivo stability and also the excretion of the radioactive agent.

6.2 Experimental

All the reagents and chemicals used were of analytical grade. The gallium(III) methanol solvento complex, *trans*-$[Ga(bpb)(CH_3OH)_2]^+$, was prepared as described in Paragraph 4.3.2 and the ligand 4-methylpyridine (4-mepy) were used as received from Sigma Aldrich. The solvent (MeOH) was dried (by the use of Calcium Hydrate and distillation over 24 hours) prior to use. Kinetic measurements were performed on a Varian Cary 50 Conc UV/Vis spectrophotometer and the temperature control of the reaction solutions was maintained to within ± 0.1 °C by means of a circulating water bath.

The kinetics involves the scanning of a sample over a certain time period at a range of preset wavelengths to determine absorption changes in this range. The samples were a mixture of a metal complex, *trans*-$[Ga(bpb)(CH_3OH)_2]^+$, in solution and a ligand (4-methylpyridine) in solution with known concentrations. The software program Scientist[6] from Micromath was used to fit the data.

Stability tests for both the complex and the ligand in solution were examined in this kinetic study. The solutions were scanned over a period of 3 days, to establish that the reagents

[6] MicroMath Scientist for Windows. Version 2.01. Copyright © 1986-1995, MicroMath Inc.

themselves do not undergo changes in solution such as decomposition or polymerisation. No decomposition or interactions were observed for the starting reagents in methanol over this period of time.

For the kinetic study, the metal solution was prepared-throughout the study at a final concentration of 1.0×10^{-4} M in MeOH, whereas the ligand solutions was prepared to range from 0.1 M to 1.0 M, to fit *pseudo* first-order conditions. Fresh samples were prepared each time for every kinetic experiment to ensure that the concentrations stay precise and accurate.

6.3 Results and Discussion

6.3.1 Proposed Reaction Mechanism

In order to get a better understanding of the mechanism of methanol substitution in *trans*-$[Ga(bpb)(CH_3OH)_2]^+$ a few preliminary experiments were first performed. These are listed below:

- Firstly, our preliminary investigation suggested that there is a fast reaction taking place immediately upon mixing, see Figure 6.1. Unfortunately, all our attempts to follow these reactions on a stopped-flow spectrophotometer under our reaction conditions were unsuccessful, and indicated that it was probably occurring faster than what the limitations of our equipment holds at this stage or that the absorption range is simply too small for proper detection.
- A second, slower reaction was observed and monitored on a UV/Vis spectrophotometer, see Figure 6.2. Figure 6.2 is a representation of a typical UV/Vis spectrum of the absorbance *vs.* wavelength at 2 minute time intervals of the substitution reaction in MeOH at 25.0 °C. From this graph the disappearance of the peaks at 362 nm could be observed.
- The choice of 4-methylpyridine as entering ligand was a deliberate one. The photons of the methyl substituent can be used very effectively as a ^{1}H NMR probe in cases like these where all the protons of the coordinated tetradentate ligand are aromatic and fall in similar regions as those of the entering ligand.

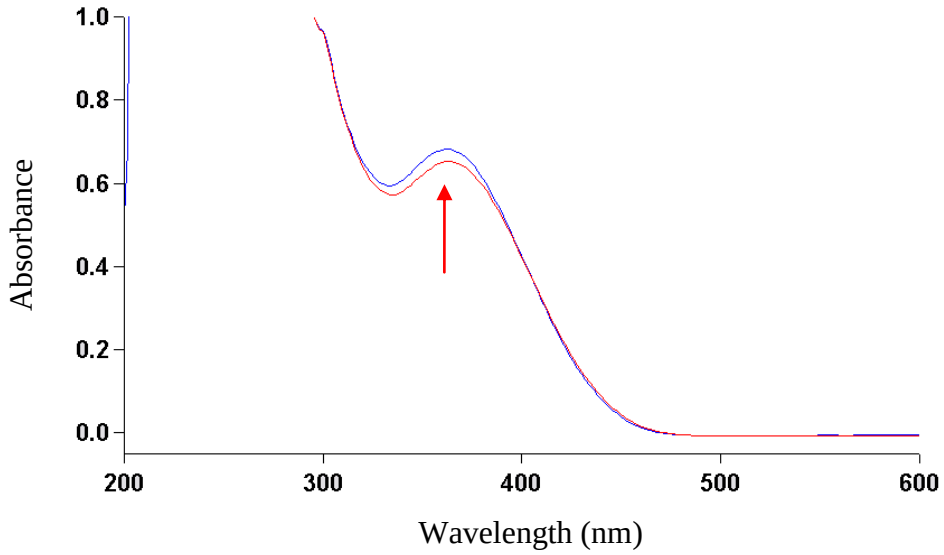

Figure 6.1 UV/Vis Spectrum illustrating the fast observed reaction immediately upon mixing, [*trans*-[Ga(bpb)$(CH_3OH)_2]^+$] ($1x10^{-4}$ M) with [4-methylpyridine] (0.1 M) at 25.0 °C. Scan of [*trans*-[Ga(bpb)$(CH_3OH)_2]^+$] ($1x10^{-4}$ M) before mix (red line) and scan of [*trans*-[Ga(bpb)$(CH_3OH)_2]^+$] ($1x10^{-4}$ M) with [4-methylpyridine] (0.1 M) immediately after mixing (blue line)

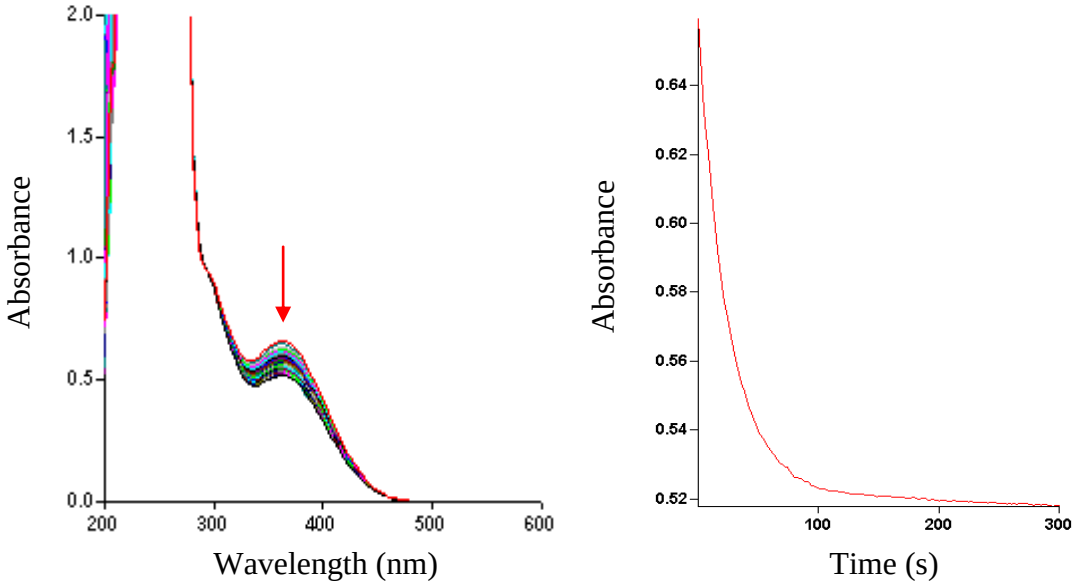

Figure 6.2 UV/Vis Spectrum for the reaction between [*trans*-[Ga(bpb)$(CH_3OH)_2]^+$] ($1x10^{-4}$ M) and [4-methylpyridine] (0.1 M) at 25.0 °C. *(left)* Wavelength scans over time (total time 5h); *(right)* Absorbance *vs.* time trace at 362nm

- In order to verify the coordination of 4-mepy to the gallium complex, solutions of *trans*-[Ga(bpb)$(CH_3OH)_2]^+$ and 4-methylpyridine (ratio 1:10) were added together and the substitution reaction was followed on ^{1}H NMR by obtaining NMR spectra at 20 minute intervals for 5 hours. The results obtained are shown in Figure 6.3. These experiments were complicated by the low solubility of the metal complex in MeOH, making the detection of new metal species very difficult. In spite of this the formation of a peak at 2.513 ppm were detected immediately after mixing, possibly pointing to the formation of a Ga-4-mepy species (**a** in Figure 6.3). This peak shifts with time to 2.516 ppm, possibly indicating that a second species is formed with time (**b** in Figure 6.3).

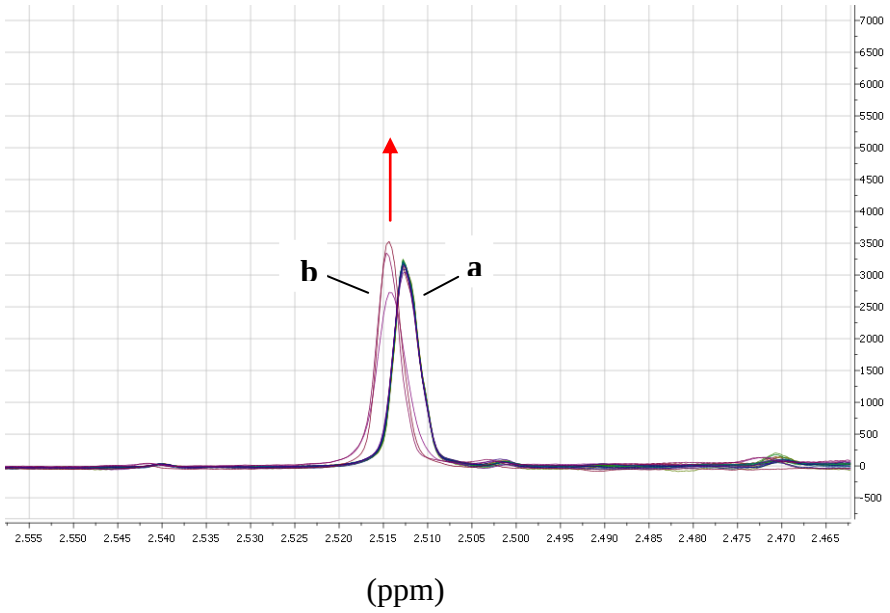

Figure 6.3 ^{1}H NMR spectrum showing the formation of Ga-4-mepy species (**a**) and second species formed (**b**) from [*trans*-[Ga(bpb)$(CH_3OH)_2]^+$**]** (1 x 10^{-4} M) with [4-mepy] (0.1 M)

- The synthesis and characterisation of the starting material *trans*-[Ga(bpb)$(CH_3OH)_2]^+$ was fully discussed in Paragraph 4.3.2. The final product was successfully formed and characterized by IR, UV/Vis and ^{1}H NMR and indicated that both of the methanol ligands were substituted under our reaction conditions.
- Preliminary fits of the kinetic data obtained for the slow reaction yielded non-linear plots of k_{obs} *vs.* [4-mepy], indicating that the substitution of the methanol is not a simple equilibrium reaction, but that the formation of an intermediate is expected.

Taking the above into consideration a possible reaction scheme for the substitution of both the methanol ligands by 4-mepy from *trans*-$[Ga(bpb)(CH_3OH)_2]^+$ is presented in Scheme 6.1. According to Scheme 6.1 the first reaction involves a fast substitution of a 4-mepy ligand which could not be followed on the stopped-flow devise as explained earlier. This reaction is completely separable from the second, slower reaction step which involves the formation of an outer sphere intermediate (K_2 step), followed by a slow, rate determining step (k_3 step) where 4-mepy enters the coordination sphere.

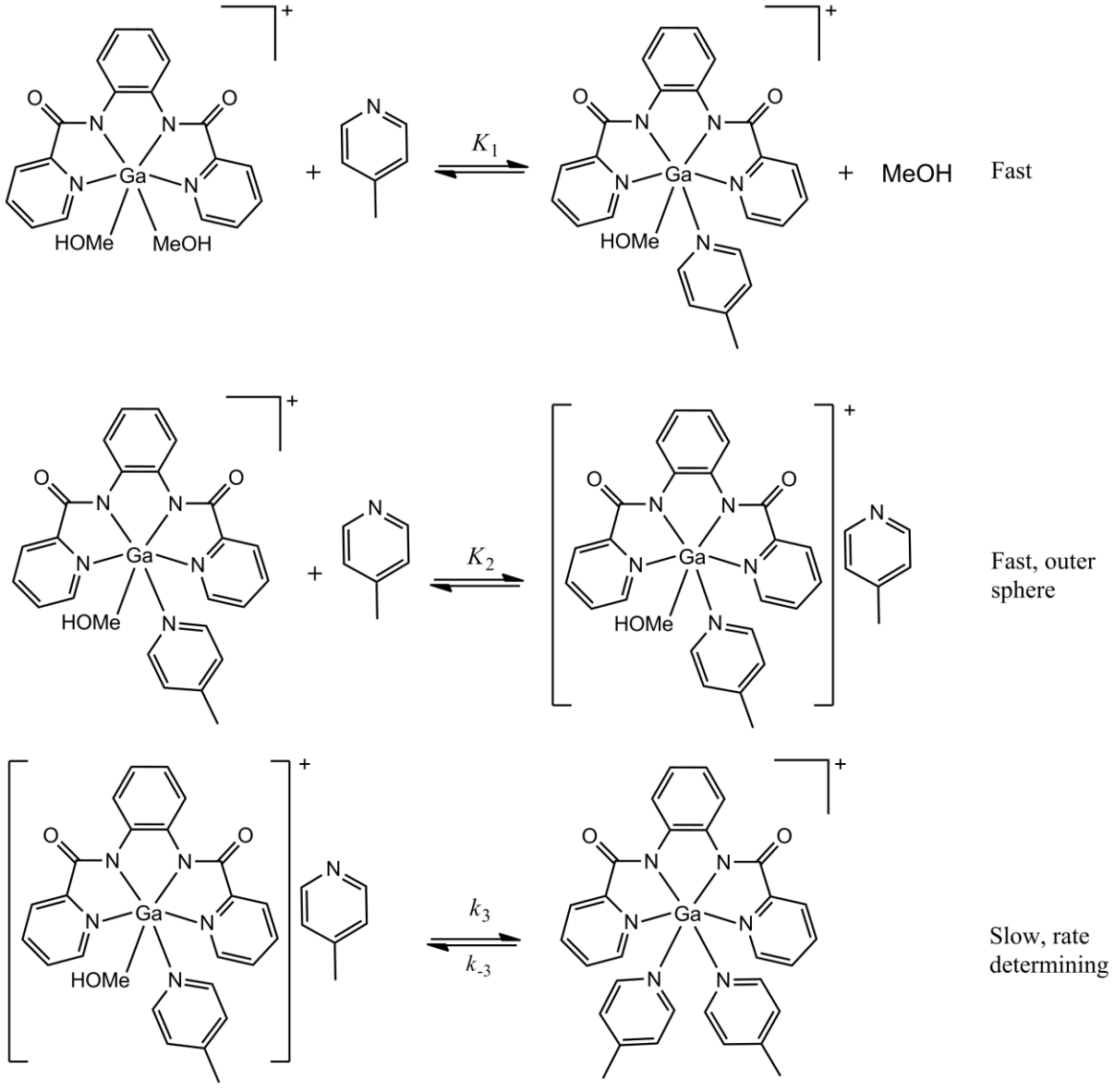

Scheme 6.1 Proposed reaction scheme for the methanol substitution by 4-mepy in *trans*-$[Ga(bpb)(CH_3OH)_2]^+$

6.3.2 Discussion

In order to verify that the observed slow reaction involves only one reaction, the preliminary kinetic data was fitted to a one step kinetic profile as in Eq. 6.1 (see Figure 6.4).

$$A_{obs} = A_1 - (A_1 - A_0)e^{-k_{obs}.t} \quad \text{... Eq. 6.1}$$

with A_{obs} = the observed absorbance, A_0 = initial absorbance, A_1 = the final absorbance and $k_{obs1/2}$ = the observed rate constant.

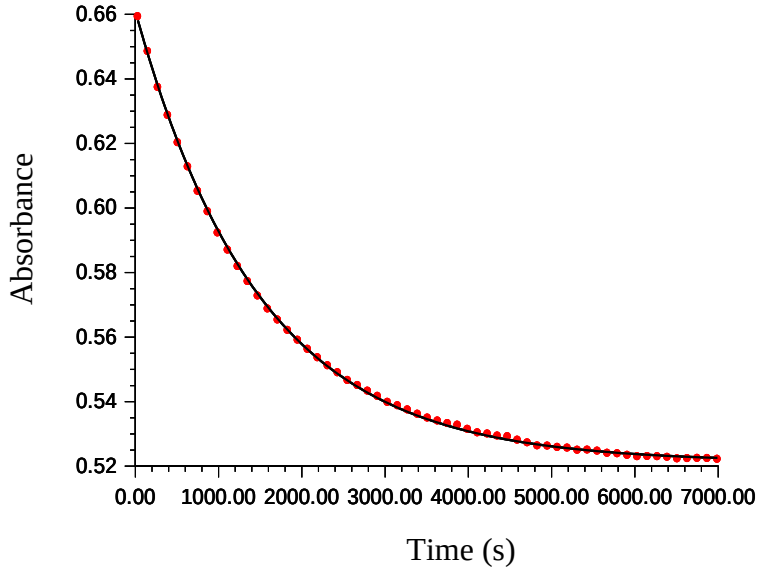

Figure 6.4 Data of **[***trans*-[Ga(bpb)$(CH_3OH)_2]^+$] ($1x10^{-4}$ M) and [4-mepy] (0.1 M) in MeOH fitted to a one step *pseudo* first-order reaction model at 25.0 °C and λ = 362 nm

Fits to equations related to two consecutive step reactions were not successful, suggesting that only one reaction step is occurring here.

As mentioned earlier, plots of k_{obs} *vs.* [4-mepy] yielded non-linear graphs. Equation 6.2 can be derived from Scheme 6.1 and taking into consideration the previous discussions and the fact that the first step in the scheme (K_1 step) is very fast and completely separable from the second step.

$$k_{obs} = \frac{k_3 K_2[4-mepy]}{1+K_2[4-mepy]} + k_{-3} \quad \text{... Eq. 6.2}$$

Figure 6.5 provide plots of k_{obs} *vs.* [4-mepy] at temperatures 15.0 °C, 25.0 °C, 35.0 °C and 45.0 °C.

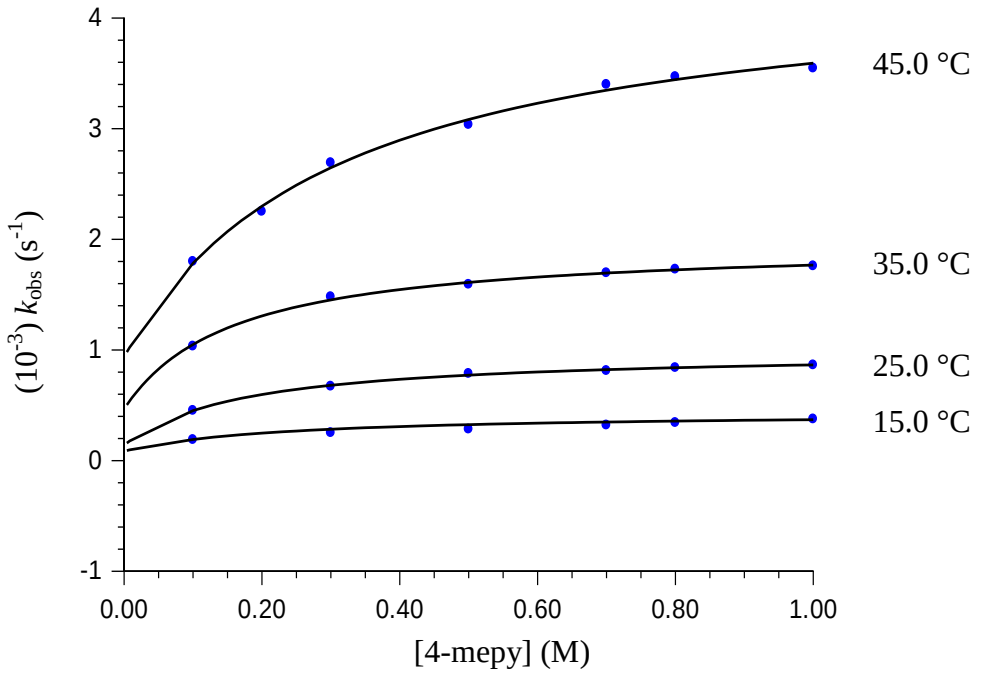

Figure 6.5 Plot of k_{obs} *vs.* [4-mepy] for the slow substitution reaction between [*trans*-[Ga(bpb)(CH_3OH)(4-mepy)]$^+$] and [4-mepy] in MeOH at different temperatures, [Ga(bpb)($CH_3OH)_2$]$^+$ = 1 x 10^{-4} M, λ = 362 nm

The values of k_3, k_{-3} and K_2 obtained from the data fitted to Eq. 6.2 are given in Table 6.1. In order to obtain an idea of the overall equilibrium constant, $K_{overall}$, govering this reaction the values of the final absorbance *vs.* [4-mepy] at 25.0 °C (Figure 6.6, Eq. 6.3) were fitted to Eq. 6.3, see also Table 6.1.

$$A_{obs} = \frac{A_0 + A_1 K_1 [4-mepy]}{1 + K[4-mepy]} \quad \text{... Eq. 6.3}$$

with A_{obs} = observed absorbance, A_0 = initial absorbance, A_1 = the final absorbance and K = equilibrium constant.

The equilibrium constant, K_3, can be determined from Eq. 6.4.

$$K_3 = \frac{k_3}{k_{-3}} \quad \text{... Eq. 6.4}$$

Table 6.1 Rate constants for the slow reaction between [*trans*-[Ga(bpb)(CH_3OH)(4-mepy)]$^+$] and 4-mepy

Rate constants	15.0 °C	25.0 °C	35.0 °C	45.0 °C
k_3 (s^{-1})	3.5(1) x 10^{-4}	8.5(1) x 10^{-4}	1.5(1) x 10^{-3}	3.5(1) x 10^{-3}
k_{-3} (s^{-1})	9(3) x 10^{-5}	1.4(1) x 10^{-4}	4.7(2) x 10^{-4}	9.4(2) x 10^{-4}
K_2 (M^{-1})	4.4(1)	5.8(1)	6.3(4)	3.2(8)
K_3 (M^{-1})	3.9(1)	6.1(1)	3.2(2)	3.7(2)
$K_{overall}$ (M^{-1})		44(2)		

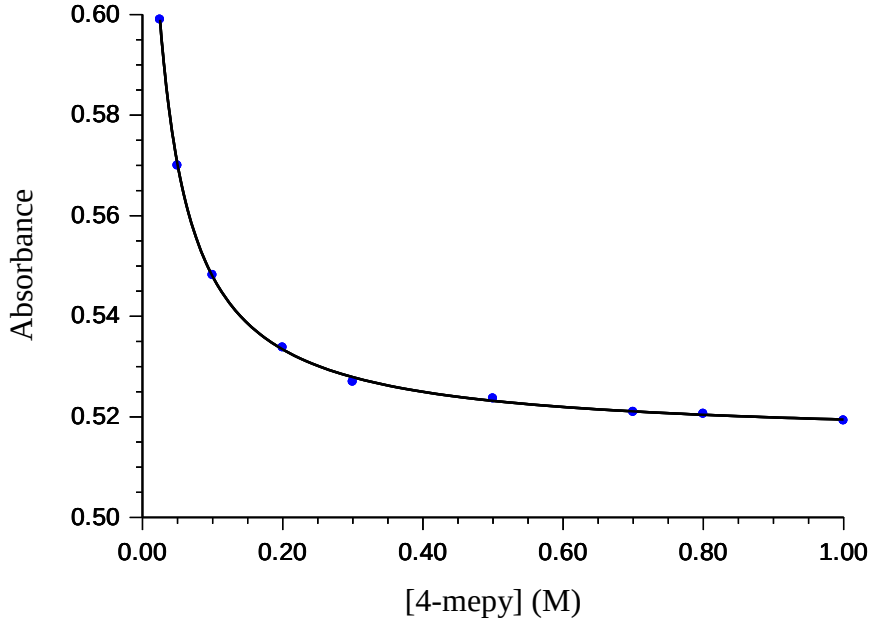

Figure 6.6 Spectrophotometric determination of $K_{overall}$ by plotting the final absorbance vs. [4-mepy] at 25.0 °C

It is evident from the results given in Table 6.1 that the fits of the data to Eq. 6.2 are in good agreement with the rate law (Scheme 6.1).

Figures 6.7 and 6.8 show the Eyring plots of the data obtained by fitting the k_3 and k_{-3} data to Eq. 6.5, see Table 6.2. The Eyring equation is given in Eq. 6.5.

$$\ln\frac{k}{T} = \frac{-\Delta H^{\neq}}{RT} + \ln\frac{k_B}{h} + \frac{\Delta S^{\neq}}{R} \qquad \text{... Eq. 6.5}$$

with $\Delta H^{\neq}$ = enthalpy of activation, $\Delta S^{\neq}$ = entropy of activation, R = gas constant and k_B = Boltzman constant.

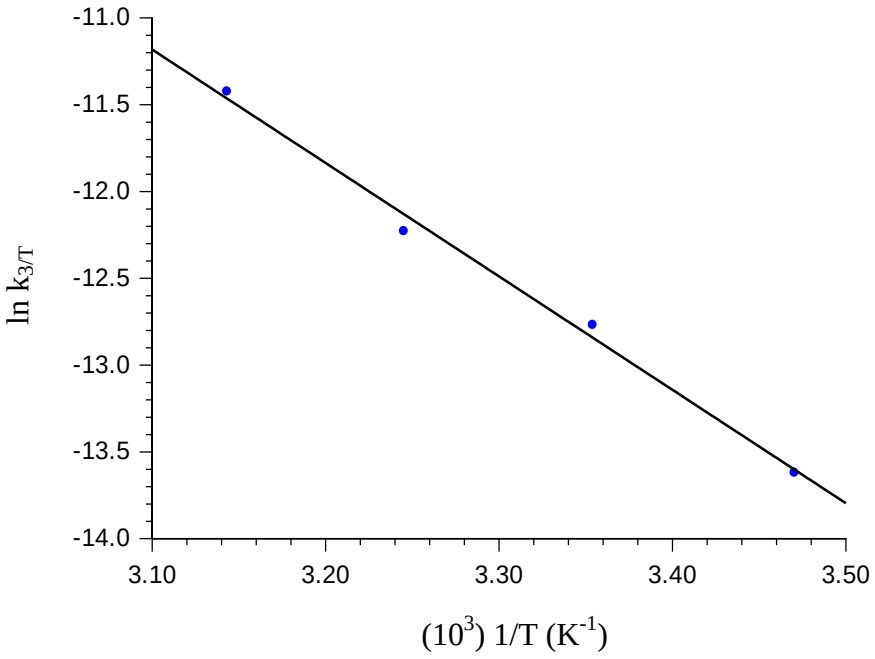

Figure 6.7 Eyring plot according to Eq. 6.5, of the k_3 rate constant for the substitution reaction between [*trans*-[Ga(bpb)(CH_3OH)(4-mepy)]$^+$] and 4-mepy at a temperature range of 288.15 – 318.15 K

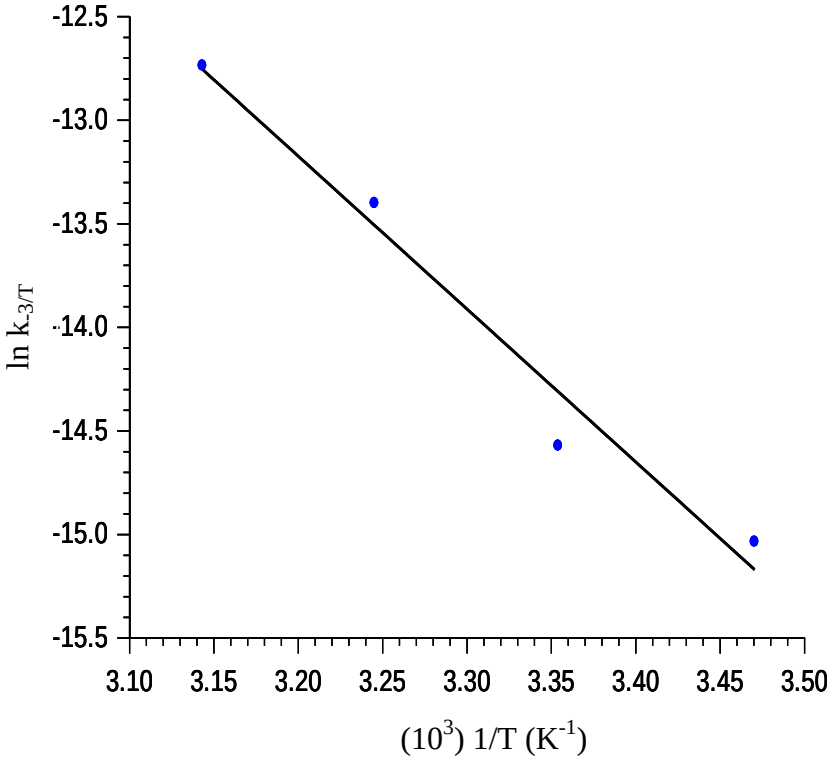

Figure 6.8 Eyring plot according to Eq. 6.5, of the k_{-3} rate constant for the substitution reaction between [*trans*-[Ga(bpb)(CH_3OH)(4-mepy)]$^+$] and 4-mepy at a temperature range of 288.15 – 318.15 K

Table 6.2 Activation parameters for the slow reaction between [*trans*-[Ga(bpb)(CH_3OH)(4-mepy)]$^+$] and 4-mepy

Rate constants	$\Delta H^{\neq}$ (kJ.mol^{-1})	$\Delta S^{\neq}$ (J K^{-1}.mol^{-1})
k_3 (s^{-1})	54(3)	-122(10)
k_{-3} (s^{-1})	61(8)	-110(25)

6.4 Conclusion

The kinetic study of the substitution reaction between [*trans*-[Ga(bpb)($CH_3OH)_2$]$^+$] and 4-mepy yielded very interesting results despite the difficulties associated with insolubility of the metal species and our inability to follow the fast observed reaction successfully.

The rate constant for the second substitution step, k_3, is slower than what was expected, taking into consideration that the rate of water exchange on $[Ga(H_2O)_6]^{3+}$ is quite fast ($9.56 \pm 0.30 \times 10^2$ s^{-1}). This is somewhat puzzling point since one would expect 4-mepy to labilise the *trans*-methanol substitution, making the k_3 step even faster.[5] A possible explanation for this could be that the tetradentate bpb ligand donates so much electron density to the central metal ion that further substitution by soft, electron rich ligands is slowed down.

The values of the equilibrium constants, K_2 and K_3, are quite low (5.8(1) and 6(1) M^{-1}) at 25.0 °C and might provide some proof for the statement in the previous paragraph. The overall equilibrium constant, $K_{overall}$ (= $K_1 \times K_2 \times K_3$), was determined as 44(2) M^{-1}. Given the fact that the values for K_2 and K_3 are known, an estimate of K_1 can be obtained (~1 M^{-1}). This is also enexpectedly low, but possibly indicates that the tetradentate ligand satisfies the electron density needs of the metal ion.

The large negative $\Delta S^{\neq}$ value obtained for the forward reaction (k_3), points strongly towards an associative mechanism for the MeOH substitution with a monodentate ligand, 4-mepy. This is not what is expected for octahedral substitution reactions, and given that the fact that the backwards step, k_{-3}, also gives a negative value for $\Delta S^{\neq}$, suggests that one cannot make too much of these values. High pressure kinetics is required to fully understand the intimate mechanism at play here.

The two compounds, di-Mebpb and $[Ga(bpb)(H_2O)_2]NO_3 \cdot CH_3OH$ that was successfully synthesized and characterized by IR, ^{1}H NMR, ^{13}C NMR, elemental analysis and X-Ray crystallography analysis was sent for *in vitro* cancer testing and is discussed in detail in Chapter 7.

7 *In Vitro* Cancer Testing of Selected Compounds

7.1 Introduction

A proposal of a quantitative colorimetric assay for mammalian cell survival and cell proliferation was conducted by Mosmann in 1983. This colorimetric assay reduces the tetrazolium salt MTT (3-(4,5-dimethylthazol-2-yl)-2,5-diphenyl tetrazolium bromide) by mitochondrial reductase to produce a purple formazan product (Figure 7.1). Where the assay measures the cell respiration and the number of living cells present in the culture is determined by the amount of formazan produced.

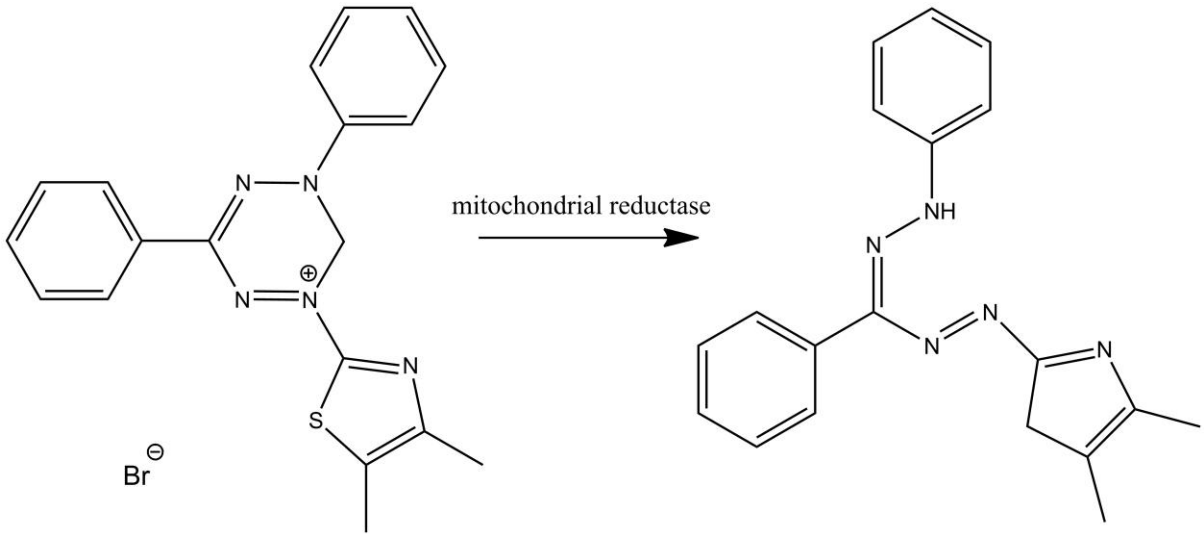

Figure 7.1 Reduction of MTT to produce a blue formazan product[1]

The colorimetric assay offers various advantages in speed, cost, simplicity, safety over conventional cell counting assays, has fewer steps to produce, uses fewer materials and does not carry the added burden of radioactive waste disposal.[1] Thus in general, the assay can be

[1] Mosmann, T., *Journal of Immunological Methods*, **65**, 55-63, 1983.

applied in the assessment of viability and proliferation of cells and the reason for its effectiveness in the determination of cytotoxicity of potential medical agents and toxic material is because these agents would either stimulate or inhibit cell viability and growth.

The MTT assay protocol is based on the addition of MTT solution to the cell cultures in 94 well flat bottom tissue culture plates called microplates, followed by four hour incubation to allow the formazan crystals to accumulate. The insoluble formazan is dissolved in either dimethyl sulfoxide, an acidified ethanol solution or a solution of the detergent sodium dodecyl sulphate in diluted hydrochloric acid and quantified by an ELISA plate reader at 500 – 600 nm.[2]

The toxicity of two selected compounds, *N*,*N'*-(4,5-Diemethyl-1,2-phenylene)bis(pyridine-2-carboxamide) (di-Mebpb) and [Ga(*N*,*N'*-(1,2-phenylene)bis(pyridine-2-carboxamide))$(H_2O)_2$]$NO_3 \cdot CH_3OH$, ([Ga(bpb)$(H_2O)_2$]$NO_3 \cdot CH_3OH$) in an *in vitro* cell culture were investigated by using the MTT (3-(4,5-dimethylthazol-2-yl)-2,5-diphenyl tetrazolium bromide) assay protocol.

These compounds were tested on oesophageal cancer cell lines.

7.2 Experimental

The oesophageal cancer cell lines were obtained from the University of the Cape Town, where the cells were cultured as usual and subjected to a "treatment". Usually the cell lines are carefully transferred to a 96-well plate for the treatment. After the treatment period, the MTT assay is used to check cell survival, viability or proliferation. The MTT assay can be metabolized by all living cells; therefore it can be used with all the different cancer cell types.

The general procedure entails the removal of the cells from the medium, followed by rinsing with trypsin and trypsinize. The trypsin is quenched and the cells are centrifuged to spin down the cells. The cells are re-suspended in a fresh medium followed by a final cell count determination (~1500 cells per 90 µl). In triplicate, 90 µl of the cell suspension are pipette into a microplate well. Three blank wells are also included were it contains only medium without cells. The cells are then incubated for 24 hours at 37.0 °C to allow cells to settle. The compounds were prepared at different concentrations ranging from 1 x 10^{-4} µM – 1000 µM. The compounds (10 µl) were added to the cells and incubated for 48 hours at 37.0 °C.

[2] Cory, A. H., Owne, T. C., Barltrop, J. A., Cory, J. G., *Cancer Communications*, **3**, **7**, 207-212, 1991.

After the treatment period the MTT reagent (Roche Diagnostics) (10 µl) was then added to each well and incubated for a further 4 hours at 37.0 °C. Solubilisation solution (100 µl) was then added to the wells followed by incubation for 16 hours at 37.0 °C. The plates were then quantified by using an ELISA plate reader at 595 nm.

7.3 Results and Discussion

According to the Food and drug administration (FDA), IC_{50} represents the concentration of a particular drug that is required for 50 % inhibition, *in vitro*. The determined IC_{50} values of the two compounds that were tested on oesophageal cancer cell lines, with an incubation period of approximately 6 days are reported in Table 7.1, Figure 7.2 and Figure 7.3, respectively.

Table 7.1 The two compounds and their respective IC_{50} values on oesophageal cancer cell lines

Compound	**IC_{50} value (µM)**
di-Mebpb	3.796
$[Ga(bpb)(H_2O)_2]NO_3 \cdot CH_3OH$	2.285

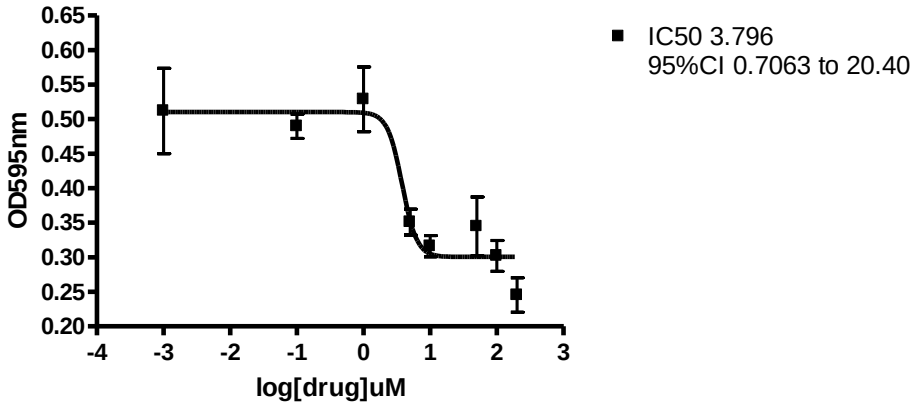

Figure 7.2 Graph that illustrates the determination of the IC_{50} value of di-Mebpb

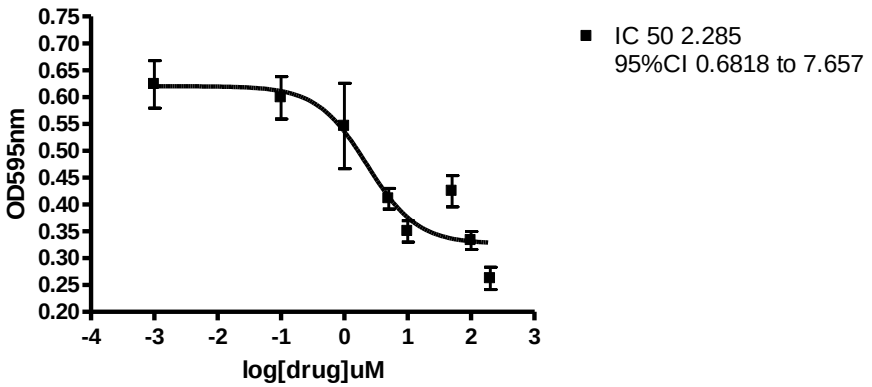

Figure 7.3 Graph that illustrates the determination of the IC_{50} value of $[Ga(bpb)(H_2O)_2]NO_3 \cdot CH_3OH$

Generally, IC_{50} values are used for ranking purposes within one compound series or binned into classes exhibiting, a low (IC_{50} > 10 µM), moderate (1 µM < IC_{50} > 10 µM) and high (IC_{50} < 1 µM) risk potential. The two compounds that were tested in this study shows a moderate reactivity towards inhibition, but it is still not enough to be considered as an active substance for inhibition, with respective IC values of 3.796 µM and 2.285 µM.

7.4 Conclusion

From the above IC_{50} results it is clear that none of the two compounds tested, show a high risk of toxicity to the selected cancer cell line (oesophageal cancer). However by linking the two compounds to a radioactive nuclide, the toxicity could be enhanced or explored as potential imaging agents.

8 Evaluation of the Study

8.1 Introduction

In this chapter a summary of the results obtained together with the scientific importance of the project is briefly discussed. A few possibilities for further investigation in the future are also briefly outlined.

8.2 Success of the Study

This study aimed to synthesize new tetradentate carboxamide ligands and to investigate their coordination to gallium(III) and gold(III), which could give more insight into the behaviour of radiopharmaceuticals for cancer treatment.

Seven compounds, (two ligands and five metal complexes) were successfully synthesized and characterized by IR, ^{1}H NMR, ^{13}C NMR, UV/Vis spectrometry, elemental analysis. The two ligands, di-Mebpb and bpb, and two metal complexes, $[Ga(bpb)(H_2O)_2]NO_3 \cdot CH_3OH$ and [Au(bpb)]Cl, were characterized by X-Ray diffraction. The gallium(III) complex crystallized in a distorted octahedral formation while the gold(III) complex crystallized in a distorted square planar formation.

The kinetic study to follow the rate at which methanol is substituted from a *trans*-$[Ga(bpb)(CH_3OH)_2]^+$ complex with 4-methylpyridine as entering ligand revealed that two distinguishable reaction steps occurred in MeOH as solvent. The equilibrium constant, K_1, for the first methanol substitution was calculated as ~1 M^{-1} and the equilibrium constants, K_2 and K_3, were determined as 5.8(1) M^{-1} and 6(1) M^{-1}, respectively at 25.0 °C. The rate constant for the second substitution step, k_3, was determined as 8.5(1) x 10^{-4} (s^{-1}) which is much slower than what was expected at 25.0 °C. The activation parameters was determined for the forward reaction (k_3), which suggests that an associative mechanism for the MeOH substitution with 4-mepy as entering ligand is taking place.

The ligand and the metal complex, di-Mebpb and $[Ga(bpb)(H_2O)_2]NO_3 \cdot CH_3OH$ that were tested on oesophageal cancer cell lines showed moderate toxicity towards inhibition, however it was not reactive enough to be considered as active substance for inhibition.

8.3 Future Research

From the results obtained, various focus areas for further investigations have been identified. Future research may include the following:

- Synthesis of more different tetradentate carboxamide ligands.
- Coordinate these ligands successfully to gallium(III) and gold(III).
- A complete kinetic investigation of the reaction between *trans*-$[Ga(bpb)(CH_3OH)_2]^+$ and 4-mepy using a stopped-flow spectrophotometer at low temperatures.
- High pressure kinetic studies to investigate the intimate mechanism of this reaction.
- Further cell studies on all of the compounds that were successfully synthesized.

Appendix A

Table A.1 Fractional atomic coordinates and isotropic or equivalent isotropic displacement parameters (Å^2) for di-Mebpb. $U_{(eq)}$ is defined as one third of the trace of the orthogonalized U^{ij} tensor

Atom	***x***	***y***	***z***	U_{iso}*/U_{eq}
C6	0.77131(13)	0.70520(9)	0.3849(2)	0.0204(3)
C10	0.34827(15)	0.64314(11)	0.4195(3)	0.0336(4)
H10A	0.2857	0.6104	0.4193	0.05
H10B	0.3246	0.6815	0.3361	0.05
H10C	0.3713	0.6629	0.5373	0.05
H10D	0.3688	0.6927	0.4424	0.05
H10E	0.3298	0.6217	0.5257	0.05
H10F	0.2831	0.6403	0.3245	0.05
C11	0.33503(15)	0.48994(11)	0.3373(3)	0.0313(4)
H11A	0.3459	0.4411	0.3025	0.047
H11B	0.2703	0.5102	0.2592	0.047
H11C	0.3218	0.4908	0.4583	0.047
H11D	0.2794	0.5204	0.3775	0.047
H11E	0.355	0.4512	0.4208	0.047
H11F	0.3035	0.4706	0.2217	0.047
C15	0.77150(13)	0.44582(8)	0.2917(2)	0.0202(2)
N2	0.73461(11)	0.64533(7)	0.2985(2)	0.0221(3)
N3	0.72056(11)	0.50299(7)	0.21172(19)	0.0190(3)
O1	0.72183(10)	0.73844(7)	0.48200(17)	0.0277(3)
O2	0.74071(9)	0.41395(6)	0.41242(15)	0.0202(2)
H2'	0.7803(17)	0.6283(10)	0.237(3)	0.027(5)
H3'	0.7438(16)	0.5199(10)	0.122(3)	0.024(5)
C1	1.03548(14)	0.71236(10)	0.2222(2)	0.0283(4)
H1	1.0731	0.6853	0.1474	0.034
C2	1.08852(15)	0.77174(10)	0.3009(2)	0.0293(4)
H2	1.1603	0.7852	0.2795	0.035
C3	1.03552(16)	0.81103(10)	0.4107(2)	0.0289(4)
H3	1.07	0.8521	0.4668	0.035
C4	0.93064(15)	0.78956(9)	0.4380(2)	0.0249(4)
H4	0.8918	0.8154	0.5134	0.03
C5	0.88403(13)	0.72965(9)	0.3529(2)	0.0197(3)
C7	0.63512(12)	0.60847(8)	0.3093(2)	0.0192(3)
C8	0.54288(15)	0.64111(9)	0.3586(2)	0.0241(3)
H8	0.5468	0.6899	0.3874	0.029
C9	0.44549(13)	0.60415(9)	0.3667(2)	0.0243(4)
C12	0.43827(14)	0.53253(9)	0.3249(2)	0.0235(3)

C13	0.53017(14)	0.50011(9)	0.2728(2)	0.0215(3)
H13	0.5258	0.4515	0.2421	0.026
C14	0.62761(12)	0.53699(8)	0.2646(2)	0.0189(3)
C16	0.87530(13)	0.42368(9)	0.2250(2)	0.0189(3)
C17	0.93911(15)	0.36937(9)	0.3085(2)	0.0255(4)
H17	0.9157	0.344	0.4012	0.031
C18	1.03894(15)	0.35268(10)	0.2530(3)	0.0295(4)
H18	1.0859	0.316	0.3079	0.035
C19	1.06792(15)	0.39063(10)	0.1168(2)	0.0283(4)
H19	1.1357	0.3806	0.0764	0.034
C20	0.99767(15)	0.44332(10)	0.0395(3)	0.0301(4)
H20	1.0181	0.4685	−0.056	0.036
N1	0.93415(12)	0.69083(8)	0.2456(2)	0.0248(3)
N4	0.90251(12)	0.46069(8)	0.09200(19)	0.0245(3)

Table A.2 Atomic displacement parameters (Å^2) of di-Mebpb

Atom	U^{11}	U^{22}	U^{33}	U^{12}	U^{13}	U^{23}
C6	0.0205(7)	0.0210(8)	0.0200(8)	0.0032(6)	0.0050(6)	0.0032(6)
C10	0.0211(8)	0.0387(10)	0.0437(12)	0.0041(7)	0.0132(8)	−0.0001(9)
C11	0.0227(8)	0.0378(10)	0.0351(10)	−0.0060(7)	0.0102(8)	−0.0020(8)
C15	0.0209(4)	0.0201(5)	0.0205(4)	−0.0022(3)	0.0064(4)	−0.0014(4)
N2	0.0184(7)	0.0206(7)	0.0304(8)	0.0008(5)	0.0124(6)	−0.0027(6)
N3	0.0181(6)	0.0214(7)	0.0192(7)	−0.0007(5)	0.0081(5)	0.0004(6)
O1	0.0252(6)	0.0322(7)	0.0283(7)	0.0007(5)	0.0117(5)	−0.0061(6)
O2	0.0209(4)	0.0201(5)	0.0205(4)	−0.0022(3)	0.0064(4)	−0.0014(4)
C1	0.0238(8)	0.0362(10)	0.0265(9)	−0.0018(7)	0.0088(7)	−0.0063(8)
C2	0.0253(9)	0.0384(11)	0.0253(9)	−0.0092(7)	0.0078(7)	0.0008(8)
C3	0.0343(10)	0.0279(9)	0.0243(9)	−0.0102(7)	0.0043(8)	−0.0031(8)
C4	0.0291(9)	0.0253(8)	0.0215(8)	−0.0022(7)	0.0079(7)	−0.0008(7)
C5	0.0196(7)	0.0191(8)	0.0213(8)	0.0005(6)	0.0061(6)	0.0034(6)
C7	0.0168(7)	0.0215(8)	0.0202(8)	−0.0008(6)	0.0060(6)	0.0027(6)
C8	0.0212(7)	0.0253(8)	0.0268(9)	0.0037(7)	0.0072(7)	0.0020(7)
C9	0.0196(8)	0.0314(9)	0.0232(8)	0.0047(7)	0.0070(7)	0.0027(7)
C12	0.0174(7)	0.0329(9)	0.0205(8)	−0.0024(7)	0.0041(6)	0.0035(7)
C13	0.0217(7)	0.0238(8)	0.0196(8)	−0.0022(6)	0.0055(6)	−0.0005(6)
C14	0.0173(7)	0.0240(8)	0.0158(8)	0.0020(6)	0.0044(6)	0.0014(6)
C16	0.0188(7)	0.0188(7)	0.0190(7)	−0.0015(6)	0.0035(6)	−0.0040(6)
C17	0.0262(8)	0.0248(8)	0.0274(9)	0.0022(7)	0.0097(7)	0.0020(7)
C18	0.0271(9)	0.0278(9)	0.0346(10)	0.0079(7)	0.0079(8)	0.0012(8)
C19	0.0210(8)	0.0356(10)	0.0302(9)	0.0049(7)	0.0096(7)	−0.0046(8)
C20	0.0274(9)	0.0375(10)	0.0282(9)	0.0030(7)	0.0128(8)	0.0046(8)
N1	0.0218(7)	0.0269(7)	0.0275(8)	−0.0029(6)	0.0089(6)	−0.0051(6)
N4	0.0231(7)	0.0290(8)	0.0227(7)	0.0031(6)	0.0080(6)	0.0027(6)

Table A.3 Geometric parameters (Å) for di-Mebpb

Bond	Distance (Å)	Bond	Distance (Å)
C6-O1	1.219(2)	C1-H1	0.95
C6-N2	1.351(2)	C2-C3	1.375(3)
C6-C5	1.506(2)	C2-H2	0.95
C10-C9	1.509(2)	C3-C4	1.388(2)
C10-H10A	0.98	C3-H3	0.95
C10-H10B	0.98	C4-C5	1.381(2)
C10-H10C	0.98	C4-H4	0.95
C10-H10D	0.98	C5-N1	1.336(2)
C10-H10E	0.98	C7-C8	1.391(2)
C10-H10F	0.98	C7-C14	1.397(2)
C11-C12	1.507(2)	C8-C9	1.384(2)
C11-H11A	0.98	C8-H8	0.95
C11-H11B	0.98	C9-C12	1.394(2)
C11-H11C	0.98	C12-C13	1.395(2)
C11-H11D	0.98	C13-C14	1.384(2)
C11-H11E	0.98	C13-H13	0.95
C11-H11F	0.98	C16-N4	1.336(2)
C15-O2	1.2274(19)	C16-C17	1.377(2)
C15-N3	1.342(2)	C17-C18	1.392(2)
C15-C16	1.505(2)	C17-H17	0.95
N2-C7	1.410(2)	C18-C19	1.374(3)
N2-H2'	0.86(2)	C18-H18	0.95
N3-C14	1.421(2)	C19-C20	1.378(3)
N3-H3'	0.86(2)	C19-H19	0.95
C1-N1	1.338(2)	C20-N4	1.333(2)
C1-C2	1.382(3)	C20-H20	0.95

Table A.4 Geometric parameters (°) for di-Mebpb

Bond	Angle (°)	Bond	Angle (°)
O1-C6-N2	125.78(16)	C15-N3-H3'	119.0(13)
O1-C6-C5	120.35(15)	C14-N3-H3'	117.3(13)
N2-C6-C5	113.87(14)	N1-C1-C2	123.65(17)
C9-C10-H10A	109.5	N1-C1-H1	118.2
C9-C10-H10B	109.5	C2-C1-H1	118.2
H10A-C10-H10B	109.5	C3-C2-C1	118.80(16)
C9-C10-H10C	109.5	C3-C2-H2	120.6
H10A-C10-H10C	109.5	C1-C2-H2	120.6
H10B-C10-H10C	109.5	C2-C3-C4	118.66(16)
C9-C10-H10D	109.5	C2-C3-H3	120.7
H10A-C10-H10D	141.1	C4-C3-H3	120.7
H10B-C10-H10D	56.3	C5-C4-C3	118.40(16)
H10C-C10-H10D	56.3	C5-C4-H4	120.8

C9-C10-H10E	109.5	C3-C4-H4	120.8
H10A-C10-H10E	56.3	N1-C5-C4	123.82(14)
H10B-C10-H10E	141.1	N1-C5-C6	117.49(14)
H10C-C10-H10E	56.3	C4-C5-C6	118.67(15)
H10D-C10-H10E	109.5	C8-C7-C14	118.66(14)
C9-C10-H10F	109.5	C8-C7-N2	122.39(15)
H10A-C10-H10F	56.3	C14-C7-N2	118.93(14)
H10B-C10-H10F	56.3	C9-C8-C7	121.53(15)
H10C-C10-H10F	141.1	C9-C8-H8	119.2
H10D-C10-H10F	109.5	C7-C8-H8	119.2
H10E-C10-H10F	109.5	C8-C9-C12	120.01(15)
C12-C11-H11A	109.5	C8-C9-C10	118.66(16)
C12-C11-H11B	109.5	C12-C9-C10	121.33(16)
H11A-C11-H11B	109.5	C9-C12-C13	118.41(15)
C12-C11-H11C	109.5	C9-C12-C11	121.62(16)
H11A-C11-H11C	109.5	C13-C12-C11	119.96(16)
H11B-C11-H11C	109.5	C14-C13-C12	121.65(15)
C12-C11-H11D	109.5	C14-C13-H13	119.2
H11A-C11-H11D	141.1	C12-C13-H13	119.2
H11B-C11-H11D	56.3	C13-C14-C7	119.73(14)
H11C-C11-H11D	56.3	C13-C14-N3	120.85(14)
C12-C11-H11E	109.5	C7-C14-N3	119.42(13)
H11A-C11-H11E	56.3	N4-C16-C17	123.97(15)
H11B-C11-H11E	141.1	N4-C16-C15	117.22(14)
H11C-C11-H11E	56.3	C17-C16-C15	118.74(14)
H11D-C11-H11E	109.5	C16-C17-C18	118.08(16)
C12-C11-H11F	109.5	C16-C17-H17	121
H11A-C11-H11F	56.3	C18-C17-H17	121
H11B-C11-H11F	56.3	C19-C18-C17	118.40(17)
H11C-C11-H11F	141.1	C19-C18-H18	120.8
H11D-C11-H11F	109.5	C17-C18-H18	120.8
H11E-C11-H11F	109.5	C18-C19-C20	119.32(16)
O2-C15-N3	124.85(15)	C18-C19-H19	120.3
O2-C15-C16	120.91(14)	C20-C19-H19	120.3
N3-C15-C16	114.22(14)	N4-C20-C19	123.20(17)
C6-N2-C7	126.56(14)	N4-C20-H20	118.4
C6-N2-H2'	113.8(13)	C19-C20-H20	118.4
C7-N2-H2'	119.5(13)	C5-N1-C1	116.67(14)
C15-N3-C14	123.74(14)	C20-N4-C16	117.01(15)

Table A.5 Fractional atomic coordinates and isotropic or equivalent isotropic displacement parameters (Å^2) for bpb. $U_{(eq)}$ is defined as one third of the trace of the orthogonalized U^{ij} tensor

Atom	***x***	***y***	***z***	U_{iso}*/U_{eq}
C1	0.41519(13)	1.0991(3)	0.05811(8)	0.0255(4)
H1	0.4093	1.1193	0.0169	0.031
C2	0.48085(13)	1.2602(3)	0.09302(8)	0.0265(4)
H2	0.5169	1.3869	0.0756	0.032
C3	0.49167(14)	1.2290(3)	0.15407(8)	0.0273(4)
H3	0.5357	1.3341	0.1786	0.033
C4	0.43618(13)	1.0393(3)	0.17839(8)	0.0237(4)
H4	0.4427	1.0132	0.2194	0.028
C5	0.37055(12)	0.8889(3)	0.14002(7)	0.0178(3)
C6	0.30620(12)	0.6859(3)	0.16555(7)	0.0185(3)
C7	0.15978(12)	0.3840(3)	0.13439(7)	0.0159(3)
C8	0.12247(13)	0.3464(3)	0.19041(7)	0.0185(3)
H8	0.1434	0.4543	0.2212	0.022
C9	0.05485(13)	0.1513(3)	0.20103(7)	0.0199(3)
H9	0.0317	0.1280	0.2389	0.024
C10	0.02168(13)	−0.0092(3)	0.15536(7)	0.0195(3)
H10	−0.0222	−0.1426	0.1626	0.023
C11	0.05440(12)	0.0308(3)	0.09879(7)	0.0175(3)
H11	0.0303	−0.0740	0.0678	0.021
C12	0.12263(12)	0.2252(3)	0.08758(6)	0.0156(3)
N1	0.35977(11)	0.9157(2)	0.08044(6)	0.0216(3)
N2	0.23404(10)	0.5730(2)	0.12435(6)	0.0167(3)
O1	0.32088(9)	0.6349(2)	0.21895(5)	0.0256(3)
H2'	0.2305(15)	0.634(3)	0.0871(9)	0.032(5)
H3'	0.1758(16)	0.105(4)	0.0121(9)	0.036(5)
C13	0.15595(12)	0.4384(3)	−0.00626(7)	0.0159(3)
C14	0.19571(12)	0.3954(3)	−0.06667(7)	0.0155(3)
C18	0.28234(13)	0.1486(3)	−0.12885(7)	0.0207(3)
H18	0.3175	0.0027	−0.1356	0.025
C17	0.27216(13)	0.3171(3)	−0.17461(7)	0.0199(3)
H17	0.2999	0.2849	−0.2110	0.024
C16	0.21985(13)	0.5340(3)	−0.16500(7)	0.0208(3)
H16	0.2106	0.6500	−0.1950	0.025
C15	0.18140(13)	0.5757(3)	−0.10968(7)	0.0198(3)
H15	0.1469	0.7211	−0.1016	0.024
N3	0.15854(10)	0.2415(2)	0.02912(6)	0.0166(3)
N4	0.24471(11)	0.1828(2)	−0.07547(6)	0.0190(3)
O2	0.12616(9)	0.64081(18)	0.00891(5)	0.0201(3)

Table A.6 Atomic displacement parameters (Å^2) of bpb

Atom	U^{11}	U^{22}	U^{33}	U^{12}	U^{13}	U^{23}
C1	0.0208(8)	0.0313(9)	0.0244(9)	0.0035(7)	0.0019(7)	0.0081(7)
C2	0.0203(8)	0.0222(9)	0.0376(11)	0.0011(7)	0.0058(7)	0.0053(7)
C3	0.0208(8)	0.0282(9)	0.0333(10)	−0.0028(7)	0.0052(7)	−0.0091(7)
C4	0.0219(8)	0.0274(9)	0.0222(9)	0.0009(7)	0.0032(7)	−0.0050(7)
C5	0.0157(7)	0.0203(8)	0.0174(8)	0.0053(6)	0.0016(6)	−0.0017(6)
C6	0.0187(8)	0.0198(8)	0.0170(8)	0.0047(6)	0.0024(6)	−0.0026(6)
C7	0.0155(7)	0.0153(7)	0.0167(8)	0.0036(6)	0.0007(6)	0.0012(6)
C8	0.0208(8)	0.0208(8)	0.0139(8)	0.0038(6)	0.0008(6)	−0.0018(6)
C9	0.0219(8)	0.0239(8)	0.0144(8)	0.0041(7)	0.0047(6)	0.0035(6)
C10	0.0199(8)	0.0169(8)	0.0221(9)	0.0025(6)	0.0045(6)	0.0038(6)
C11	0.0185(7)	0.0167(7)	0.0172(8)	0.0034(6)	0.0010(6)	−0.0022(6)
C12	0.0163(7)	0.0184(7)	0.0123(7)	0.0066(6)	0.0033(6)	0.0019(6)
N1	0.0200(7)	0.0243(7)	0.0203(7)	0.0012(6)	0.0006(6)	0.0041(6)
N2	0.0191(7)	0.0183(7)	0.0124(7)	0.0002(5)	0.0007(5)	0.0006(5)
O1	0.0286(6)	0.0317(7)	0.0156(6)	−0.0050(5)	−0.0018(5)	0.0008(5)
C13	0.0148(7)	0.0183(7)	0.0140(8)	0.0020(6)	−0.0012(6)	−0.0009(6)
C14	0.0142(7)	0.0166(7)	0.0155(8)	0.0004(6)	0.0006(6)	−0.0021(6)
C18	0.0225(8)	0.0203(8)	0.0196(8)	0.0021(6)	0.0043(6)	−0.0038(6)
C17	0.0209(8)	0.0246(8)	0.0148(8)	−0.0044(6)	0.0040(6)	−0.0042(6)
C16	0.0261(9)	0.0204(8)	0.0159(8)	−0.0023(7)	0.0017(7)	0.0026(6)
C15	0.0245(8)	0.0167(7)	0.0180(8)	0.0031(6)	0.0011(6)	0.0001(6)
N3	0.0196(7)	0.0167(7)	0.0137(7)	0.0032(5)	0.0027(5)	−0.0020(5)
N4	0.0227(7)	0.0175(7)	0.0172(7)	0.0035(5)	0.0043(5)	−0.0004(5)
O2	0.0266(6)	0.0179(5)	0.0159(6)	0.0069(5)	0.0023(5)	−0.0019(4)

Table A.7 Geometric parameters (Å) for bpb

Bond	Distance (Å)	Bond	Distance (Å)
C1-N1	1.338(2)	C10-C11	1.386(2)
C1-C2	1.383(2)	C10-H10	0.9300
C1-H1	0.9300	C11-C12	1.390(2)
C2-C3	1.377(2)	C11-H11	0.9300
C2-H2	0.9300	C12-N3	1.4263(18)
C3-C4	1.384(2)	N2-H2'	0.901(19)
C3-H3	0.9300	C13-O2	1.2326(17)
C4-C5	1.388(2)	C13-N3	1.3468(19)
C4-H4	0.9300	C13-C14	1.503(2)
C5-N1	1.342(2)	C14-N4	1.3380(19)
C5-C6	1.508(2)	C14-C15	1.388(2)
C6-O1	1.2296(18)	C18-N4	1.337(2)
C6-N2	1.3584(19)	C18-C17	1.385(2)
C7-C8	1.394(2)	C18-H18	0.9300
C7-N2	1.4070(19)	C17-C16	1.381(2)

C7-C12	1.410(2)	C17-H17	0.9300
C8-C9	1.385(2)	C16-C15	1.388(2)
C8-H8	0.9300	C16-H16	0.9300
C9-C10	1.386(2)	C15-H15	0.9300
C9-H9	0.9300	N3-H3'	0.88(2)

Table A.8 Geometric parameters (°) for bpb

Bond	**Angle (°)**	**Bond**	**Angle (°)**
N1-C1-C2	123.54(16)	C10-C11-H11	119.5
N1-C1-H1	118.2	C12-C11-H11	119.5
C2-C1-H1	118.2	C11-C12-C7	119.71(13)
C3-C2-C1	118.61(16)	C11-C12-N3	116.96(13)
C3-C2-H2	120.7	C7-C12-N3	123.15(13)
C1-C2-H2	120.7	C1-N1-C5	117.08(14)
C2-C3-C4	119.10(16)	C6-N2-C7	127.24(13)
C2-C3-H3	120.5	C6-N2-H2'	115.6(12)
C4-C3-H3	120.5	C7-N2-H2'	117.0(12)
C3-C4-C5	118.34(16)	O2-C13-N3	124.08(14)
C3-C4-H4	120.8	O2-C13-C14	121.37(13)
C5-C4-H4	120.8	N3-C13-C14	114.54(13)
N1-C5-C4	123.31(15)	N4-C14-C15	123.63(14)
N1-C5-C6	117.32(13)	N4-C14-C13	117.16(13)
C4-C5-C6	119.37(14)	C15-C14-C13	119.20(13)
O1-C6-N2	125.63(15)	N4-C18-C17	124.00(14)
O1-C6-C5	120.82(14)	N4-C18-H18	118.0
N2-C6-C5	113.55(13)	C17-C18-H18	118.0
C8-C7-N2	121.42(13)	C16-C17-C18	118.44(14)
C8-C7-C12	118.42(14)	C16-C17-H17	120.8
N2-C7-C12	120.16(13)	C18-C17-H17	120.8
C9-C8-C7	121.21(14)	C17-C16-C15	118.77(14)
C9-C8-H8	119.4	C17-C16-H16	120.6
C7-C8-H8	119.4	C15-C16-H16	120.6
C8-C9-C10	120.11(14)	C14-C15-C16	118.42(14)
C8-C9-H9	119.9	C14-C15-H15	120.8
C10-C9-H9	119.9	C16-C15-H15	120.8
C11-C10-C9	119.44(14)	C13-N3-C12	127.16(13)
C11-C10-H10	120.3	C13-N3-H3'	115.5(13)
C9-C10-H10	120.3	C12-N3-H3'	116.8(13)
C10-C11-C12	121.04(14)	C18-N4-C14	116.72(13)

Table A.9 Fractional atomic coordinates and isotropic or equivalent isotropic displacement parameters (Å^2) for [Ga(bpb)$(H_2O)_2$]$NO_3 \cdot CH_3OH$. $U_{(eq)}$ is defined as one third of the trace of the orthogonalized U^{ij} tensor

Atom	***x***	***y***	***z***	U_{iso}*/U_{eq}
Ga	0.808064(12)	0.139608(14)	0.629235(10)	0.01043(6)
C9	0.47570(13)	0.17845(15)	0.64236(11)	0.0179(4)
H9	0.4233	0.2049	0.6563	0.021
C18	0.96560(12)	0.00752(14)	0.59880(10)	0.0150(4)
H18	0.9989	0.0540	0.6223	0.018
C3	0.94516(12)	0.42838(14)	0.72384(10)	0.0160(4)
H3	0.9684	0.4861	0.7428	0.019
O1	0.67808(8)	0.36880(9)	0.71863(7)	0.0143(3)
C14	0.83171(12)	−0.04560(13)	0.56082(10)	0.0130(4)
C4	0.85763(12)	0.41045(14)	0.72785(10)	0.0142(4)
H4	0.8216	0.4556	0.7498	0.017
C16	0.95553(13)	−0.14333(14)	0.53473(10)	0.0177(4)
H16	0.9809	−0.1983	0.5138	0.021
N1	0.87618(10)	0.25607(11)	0.66879(8)	0.0114(3)
N2	0.71143(9)	0.22050(11)	0.66260(8)	0.0117(3)
C2	0.99748(12)	0.35960(14)	0.69141(10)	0.0159(4)
H2	1.0562	0.3711	0.6873	0.019
N4	0.88086(10)	0.02333(11)	0.59329(8)	0.0121(3)
C17	1.00512(13)	−0.07552(14)	0.57073(10)	0.0171(4)
H17	1.0639	−0.0855	0.5760	0.020
C15	0.86735(13)	−0.12857(14)	0.53015(10)	0.0162(4)
H15	0.8329	−0.1740	0.5067	0.019
N3	0.71524(10)	0.05731(11)	0.59095(8)	0.0123(3)
C5	0.82473(12)	0.32450(14)	0.69870(10)	0.0115(4)
C8	0.55157(12)	0.22103(14)	0.66568(10)	0.0149(4)
H8	0.5498	0.2761	0.6948	0.018
C11	0.55544(12)	0.05427(14)	0.57948(10)	0.0152(4)
H11	0.5563	−0.0010	0.5505	0.018
C1	0.96107(12)	0.27338(14)	0.66520(10)	0.0139(4)
H1	0.9963	0.2261	0.6445	0.017
C6	0.72857(12)	0.30585(13)	0.69477(10)	0.0114(4)
C10	0.47747(12)	0.09687(14)	0.59856(11)	0.0172(4)
H10	0.4263	0.0705	0.5818	0.021
C12	0.63199(12)	0.09450(13)	0.60373(10)	0.0119(4)
C7	0.62993(12)	0.18166(14)	0.64566(10)	0.0126(4)
C13	0.73553(12)	−0.02903(13)	0.56177(10)	0.0127(4)
O2	0.68658(8)	−0.09332(9)	0.53717(7)	0.0162(3)
O4	0.82517(9)	0.07009(11)	0.72250(8)	0.0141(3)
O3	0.83291(9)	0.20989(11)	0.53798(8)	0.0146(3)
O7	0.74058(9)	0.67844(10)	0.82921(7)	0.0187(3)
N5	0.81998(10)	0.66554(12)	0.84255(9)	0.0146(3)

O6	0.86044(10)	0.59799(11)	0.81393(8)	0.0281(4)
O5	0.79217(9)	0.14606(10)	0.41291(8)	0.0192(3)
H5	0.7785	0.1968	0.3921	0.029
O8	0.85548(9)	0.72241(11)	0.88457(7)	0.0210(3)
C20	0.72758(14)	0.07132(16)	0.40326(11)	0.0230(5)
H20A	0.7494	0.0077	0.4178	0.035
H20B	0.7122	0.0681	0.3555	0.035
H20C	0.6778	0.0880	0.4301	0.035
H113	0.8146(16)	0.186(2)	0.5007(15)	0.036(8)
H111	0.8200(17)	0.013(2)	0.7220(14)	0.037(8)
H114	0.8250(17)	0.267(2)	0.5377(14)	0.037(8)
H112	0.8005(18)	0.097(2)	0.7554(17)	0.056(10)

Table A.10 Atomic displacement parameters ($Å^2$) of $[Ga(bpb)(H_2O)_2]NO_3 \cdot CH_3OH$

Atom	U^{11}	U^{22}	U^{33}	U^{12}	U^{13}	U^{23}
Ga	0.00956(10)	0.00788(10)	0.01384(11)	0.00019(8)	−0.00010(8)	−0.00151(8)
C9	0.0119(9)	0.0186(9)	0.0231(11)	0.0010(8)	0.0016(8)	0.0027(8)
C18	0.0155(9)	0.0141(9)	0.0154(10)	0.0005(7)	0.0019(8)	0.0032(8)
C3	0.0183(10)	0.0126(9)	0.0169(10)	−0.0029(8)	−0.0046(8)	−0.0003(8)
O1	0.0145(7)	0.0104(6)	0.0181(7)	0.0003(5)	0.0024(5)	−0.0024(5)
C14	0.0172(9)	0.0094(8)	0.0124(9)	0.0011(7)	0.0000(7)	0.0019(7)
C4	0.0170(9)	0.0117(9)	0.0140(10)	0.0000(7)	−0.0002(8)	−0.0013(8)
C16	0.0234(10)	0.0124(9)	0.0172(10)	0.0063(8)	0.0053(8)	0.0014(8)
N1	0.0115(7)	0.0102(7)	0.0124(8)	0.0000(6)	−0.0007(6)	0.0009(6)
N2	0.0111(7)	0.0094(7)	0.0147(8)	0.0007(6)	0.0007(6)	−0.0018(6)
C2	0.0127(9)	0.0162(9)	0.0187(10)	−0.0037(8)	−0.0016(8)	0.0039(8)
N4	0.0131(8)	0.0099(7)	0.0132(8)	0.0012(6)	0.0012(6)	0.0016(6)
C17	0.0169(9)	0.0163(9)	0.0181(10)	0.0048(8)	0.0028(8)	0.0048(8)
C15	0.0229(10)	0.0105(9)	0.0152(10)	0.0011(8)	−0.0002(8)	0.0000(7)
N3	0.0109(7)	0.0100(7)	0.0160(9)	−0.0005(6)	−0.0001(6)	−0.0009(6)
C5	0.0119(9)	0.0115(8)	0.0113(9)	−0.0008(7)	0.0001(7)	0.0013(7)
C8	0.0139(9)	0.0138(9)	0.0169(10)	0.0010(7)	0.0011(8)	0.0004(8)
C11	0.0174(9)	0.0112(8)	0.0169(10)	−0.0024(7)	−0.0023(8)	0.0015(8)
C1	0.0133(9)	0.0124(9)	0.0161(10)	0.0012(7)	0.0006(8)	−0.0007(8)
C6	0.0133(9)	0.0102(8)	0.0108(9)	0.0001(7)	0.0010(7)	0.0017(7)
C10	0.0123(9)	0.0163(9)	0.0231(11)	−0.0032(8)	−0.0041(8)	0.0016(8)
C12	0.0111(9)	0.0105(8)	0.0142(9)	−0.0005(7)	−0.0007(7)	0.0021(7)
C7	0.0120(9)	0.0112(8)	0.0144(10)	−0.0009(7)	−0.0009(7)	0.0032(7)
C13	0.0161(9)	0.0100(8)	0.0120(9)	0.0013(7)	0.0000(7)	0.0014(7)
O2	0.0189(7)	0.0098(6)	0.0198(7)	−0.0021(6)	−0.0034(6)	−0.0022(5)
O4	0.0171(7)	0.0097(7)	0.0154(7)	0.0004(5)	0.0010(6)	−0.0002(6)
O3	0.0197(7)	0.0086(7)	0.0154(8)	0.0009(6)	−0.0001(6)	−0.0005(6)
O7	0.0124(7)	0.0229(7)	0.0208(8)	0.0021(6)	−0.0022(6)	−0.0014(6)
N5	0.0161(8)	0.0124(7)	0.0152(8)	0.0004(6)	0.0024(7)	0.0014(6)
O6	0.0232(8)	0.0235(8)	0.0376(10)	0.0078(7)	−0.0007(7)	−0.0140(7)

O5	0.0216(7)	0.0159(7)	0.0202(8)	0.0020(6)	−0.0054(6)	0.0026(6)
O8	0.0198(8)	0.0227(8)	0.0205(8)	−0.0043(6)	−0.0012(6)	−0.0072(6)
C20	0.0254(11)	0.0213(10)	0.0224(11)	−0.0027(9)	−0.0031(9)	−0.0019(9)

Table A.11 Geometric parameters (Å) for $[Ga(bpb)(H_2O)_2]NO_3 \cdot CH_3OH$

Bond	Distance (Å)	Bond	Distance (Å)
Ga-N3	1.9644(16)	C2-C1	1.384(3)
Ga-N2	1.9645(15)	C2-H2	0.9300
Ga-N1	2.0374(16)	C17-H17	0.9300
Ga-O3	2.0441(15)	C15-H15	0.9300
Ga-N4	2.0495(16)	N3-C13	1.326(2)
Ga-O4	2.0542(15)	N3-C12	1.411(2)
C9-C10	1.386(3)	C5-C6	1.520(3)
C9-C8	1.388(3)	C8-C7	1.385(3)
C9-H9	0.9300	C8-H8	0.9300
C18-N4	1.341(2)	C11-C12	1.390(3)
C18-C17	1.384(3)	C11-C10	1.392(3)
C18-H18	0.9300	C11-H11	0.9300
C3-C2	1.382(3)	C1-H1	0.9300
C3-C4	1.386(3)	C10-H10	0.9300
C3-H3	0.9300	C12-C7	1.424(3)
O1-C6	1.243(2)	C13-O2	1.246(2)
C14-N4	1.355(2)	O4-H111	0.77(3)
C14-C15	1.378(3)	O4-H112	0.83(3)
C14-C13	1.514(3)	O3-H113	0.84(3)
C4-C5	1.382(3)	O3-H114	0.77(3)
C4-H4	0.9300	O7-N5	1.275(2)
C16-C17	1.382(3)	N5-O6	1.235(2)
C16-C15	1.390(3)	N5-O8	1.246(2)
C16-H16	0.9300	O5-C20	1.432(2)
N1-C1	1.344(2)	O5-H5	0.8200
N1-C5	1.349(2)	C20-H20A	0.9600
N2-C6	1.330(2)	C20-H20B	0.9600
N2-C7	1.411(2)	C20-H20C	0.9600

Table A.12 Geometric parameters (°) for $[Ga(bpb)(H_2O)_2]NO_3 \cdot CH_3OH$

Bond	Angle (°)	Bond	Angle (°)
N3-Ga-N2	82.59(7)	C14-C15-H15	120.5
N3-Ga-N1	162.92(6)	C16-C15-H15	120.5
N2-Ga-N1	81.47(7)	C13-N3-C12	127.02(16)
N3-Ga-O3	94.00(7)	C13-N3-Ga	118.44(13)
N2-Ga-O3	100.18(6)	C12-N3-Ga	114.28(12)
N1-Ga-O3	82.85(6)	N1-C5-C4	121.51(17)

N3-Ga-N4	81.44(7)	N1-C5-C6	116.85(16)
N2-Ga-N4	162.85(6)	C4-C5-C6	121.53(17)
N1-Ga-N4	115.02(7)	C7-C8-C9	120.11(18)
O3-Ga-N4	87.15(6)	C7-C8-H8	119.9
N3-Ga-O4	100.06(6)	C9-C8-H8	119.9
N2-Ga-O4	93.36(6)	C12-C11-C10	119.91(18)
N1-Ga-O4	86.98(6)	C12-C11-H11	120.0
O3-Ga-O4	161.62(6)	C10-C11-H11	120.0
N4-Ga-O4	83.33(6)	N1-C1-C2	121.87(17)
C10-C9-C8	120.52(18)	N1-C1-H1	119.1
C10-C9-H9	119.7	C2-C1-H1	119.1
C8-C9-H9	119.7	O1-C6-N2	129.18(18)
N4-C18-C17	122.23(18)	O1-C6-C5	119.53(16)
N4-C18-H18	118.9	N2-C6-C5	111.26(16)
C17-C18-H18	118.9	C9-C10-C11	120.29(18)
C2-C3-C4	119.31(18)	C9-C10-H10	119.9
C2-C3-H3	120.3	C11-C10-H10	119.9
C4-C3-H3	120.3	C11-C12-N3	126.23(17)
N4-C14-C15	121.58(18)	C11-C12-C7	119.50(17)
N4-C14-C13	116.93(16)	N3-C12-C7	114.27(16)
C15-C14-C13	121.46(17)	C8-C7-N2	125.92(17)
C5-C4-C3	119.08(18)	C8-C7-C12	119.52(17)
C5-C4-H4	120.5	N2-C7-C12	114.57(16)
C3-C4-H4	120.5	O2-C13-N3	128.42(18)
C17-C16-C15	119.38(18)	O2-C13-C14	119.94(16)
C17-C16-H16	120.3	N3-C13-C14	111.64(16)
C15-C16-H16	120.3	Ga-O4-H111	115(2)
C1-N1-C5	119.28(16)	Ga-O4-H112	115(2)
C1-N1-Ga	128.66(13)	H111-O4-H112	113(3)
C5-N1-Ga	111.95(12)	Ga-O3-H113	120.3(19)
C6-N2-C7	127.39(16)	Ga-O3-H114	115(2)
C6-N2-Ga	118.40(13)	H113-O3-H114	109(3)
C7-N2-Ga	114.12(12)	O6-N5-O8	121.12(16)
C3-C2-C1	118.88(18)	O6-N5-O7	120.17(16)
C3-C2-H2	120.6	O8-N5-O7	118.71(15)
C1-C2-H2	120.6	C20-O5-H5	109.5
C18-N4-C14	119.03(16)	O5-C20-H20A	109.5
C18-N4-Ga	129.59(13)	O5-C20-H20B	109.5
C14-N4-Ga	111.37(12)	H20A-C20-H20B	109.5
C16-C17-C18	118.66(18)	O5-C20-H20C	109.5
C16-C17-H17	120.7	H20A-C20-H20C	109.5
C18-C17-H17	120.7	H20B-C20-H20C	109.5
C14-C15-C16	119.01(18)		

Table A.13 Fractional atomic coordinates and isotropic or equivalent isotropic displacement parameters (Å^2) for [Au(bpb)]Cl. $U_{(eq)}$ is defined as one third of the trace of the orthogonalized U^{ij} tensor

Atom	***x***	***y***	***z***	U_{iso}*/U_{eq}
Au	0.5027 (2)	0.07438(2)	0.188549(19)	0.04473(11)
Cl1	0.3252(3)	0.2295(2)	0.40445(19)	0.0648(4)
N1	0.7122(6)	0.1259(6)	0.2307(5)	0.0484(11)
N2	0.5837(6)	0.2491(6)	0.0513(5)	0.0492(11)
N3	0.3261(6)	0.0628(6)	0.1116(6)	0.0489(11)
N4	0.3809(6)	−0.1198(6)	0.3068(5)	0.0479(11)
O2	0.0980(6)	−0.0810(6)	0.1238(6)	0.0678(13)
O1	0.8043(6)	0.4160(6)	−0.0467(5)	0.0623(12)
C18	0.4210(10)	−0.2116(8)	0.4008(7)	0.0607(16)
H18	0.5117	−0.1845	0.4243	0.073
C17	0.3308(10)	−0.3471(10)	0.4650(8)	0.0692(18)
H17	0.3582	−0.4072	0.5330	0.083
C16	0.2015(10)	−0.3920(10)	0.4280(10)	0.075(2)
H16	0.1446	−0.4858	0.4665	0.090
C15	0.1573(9)	−0.2946(9)	0.3318(9)	0.0666(18)
H15	0.0658	−0.3194	0.3084	0.080
C14	0.2496(8)	−0.1601(8)	0.2707(7)	0.0546(15)
C13	0.2123(8)	−0.0550(8)	0.1605(7)	0.0538(14)
C12	0.3410(7)	0.1817(8)	0.0027(6)	0.0490(12)
C11	0.2309(8)	0.2008(8)	−0.0685(7)	0.0572(15)
H11	0.1400	0.1337	−0.0479	0.069
C10	0.2587(10)	0.3225(10)	−0.1718(8)	0.0657(18)
H10	0.1862	0.3357	−0.2210	0.079
C9	0.3925(10)	0.4235(9)	−0.2018(7)	0.0626(17)
H9	0.4079	0.5054	−0.2697	0.075
C8	0.5051(9)	0.4037(8)	−0.1307(6)	0.0547(14)
H8	0.5958	0.4710	−0.1518	0.066
C7	0.4795(7)	0.2823(7)	−0.0285(6)	0.0470(12)
C6	0.7317(7)	0.3156(7)	0.0375(6)	0.0498(13)
C5	0.7993(8)	0.2457(8)	0.1442(7)	0.0503(13)
C4	0.9421(8)	0.3062(8)	0.1562(7)	0.0572(15)
H4	1.0000	0.3882	0.0966	0.069
C3	0.9976(8)	0.2420(9)	0.2591(8)	0.0626(17)
H3	1.0915	0.2830	0.2700	0.075
C2	0.9128(9)	0.1180(9)	0.3441(8)	0.0641(17)
H2	0.9510	0.0717	0.4113	0.077
C1	0.7670(9)	0.0617(9)	0.3284(7)	0.0583(16)
H1	0.7081	−0.0211	0.3865	0.070

Table A.14 Atomic displacement parameters (Å^2) of [Au(bpb)]Cl

Atom	U^{11}	U^{22}	U^{33}	U^{12}	U^{13}	U^{23}
Au	0.03943(15)	0.04651(15)	0.04852(17)	−0.00414(9)	−0.01321(10)	−0.00795(10)
Cl1	0.0715(11)	0.0650(10)	0.0608(10)	0.0038(8)	−0.0249(9)	−0.0100(8)
N1	0.042(2)	0.051(3)	0.054(3)	−0.001(2)	−0.014(2)	−0.013(2)
N2	0.046(3)	0.051(3)	0.047(3)	−0.004(2)	−0.012(2)	−0.005(2)
N3	0.039(2)	0.055(3)	0.057(3)	−0.005(2)	−0.018(2)	−0.012(2)
N4	0.043(2)	0.048(2)	0.052(3)	−0.0031(19)	−0.010(2)	−0.011(2)
O2	0.052(3)	0.066(3)	0.089(4)	−0.014(2)	−0.032(3)	−0.007(3)
O1	0.059(3)	0.062(3)	0.060(3)	−0.017(2)	−0.015(2)	0.003(2)
C18	0.064(4)	0.053(3)	0.058(4)	−0.009(3)	−0.009(3)	−0.004(3)
C17	0.067(4)	0.066(4)	0.067(5)	0.001(3)	−0.016(4)	0.000(4)
C16	0.059(4)	0.060(4)	0.088(6)	−0.016(3)	0.000(4)	0.002(4)
C15	0.050(3)	0.066(4)	0.080(5)	−0.013(3)	−0.015(3)	−0.008(4)
C14	0.048(3)	0.056(4)	0.059(4)	−0.004(3)	−0.010(3)	−0.016(3)
C13	0.046(3)	0.053(3)	0.060(4)	−0.005(2)	−0.013(3)	−0.010(3)
C12	0.043(3)	0.054(3)	0.051(3)	0.002(2)	−0.011(2)	−0.015(3)
C11	0.051(3)	0.060(4)	0.066(4)	0.006(3)	−0.021(3)	−0.017(3)
C10	0.068(4)	0.080(5)	0.059(4)	0.016(4)	−0.031(4)	−0.020(4)
C9	0.071(4)	0.059(4)	0.058(4)	0.014(3)	−0.022(3)	−0.008(3)
C8	0.058(3)	0.056(3)	0.048(3)	0.004(3)	−0.015(3)	−0.006(3)
C7	0.046(3)	0.044(3)	0.054(3)	0.003(2)	−0.017(2)	−0.012(2)
C6	0.043(3)	0.052(3)	0.055(3)	−0.003(2)	−0.012(3)	−0.012(3)
C5	0.042(3)	0.053(3)	0.056(4)	0.002(2)	−0.011(3)	−0.015(3)
C4	0.046 (3)	0.058(3)	0.068(4)	−0.008(3)	−0.014(3)	−0.014(3)
C3	0.042 (3)	0.075(4)	0.080(5)	−0.001(3)	−0.026(3)	−0.025(4)
C2	0.056(4)	0.076(4)	0.067(4)	0.003(3)	−0.028(3)	−0.014(4)
C1	0.051(3)	0.068(4)	0.057(4)	−0.003(3)	−0.019(3)	−0.007(3)

Table A.15 Geometric parameters (Å) for [Au(bpb)]Cl

Bond	Distance (Å)	Bond	Distance (Å)
Au-N3	1.946(5)	C15-H15	0.9300
Au-N2	1.948(6)	C14-C13	1.510(11)
Au-N1	2.046(5)	C12-C11	1.383(9)
Au-N4	2.052(6)	C12-C7	1.409(8)
N1-C1	1.341(9)	C11-C10	1.397(11)
N1-C5	1.363(9)	C11-H11	0.9300
N2-C6	1.356(8)	C10-C9	1.381(12)
N2-C7	1.420(8)	C10-H10	0.9300
N3-C13	1.356(8)	C9-C8	1.400(10)
N3-C12	1.435(9)	C9-H9	0.9300
N4-C18	1.327(9)	C8-C7	1.388(9)
N4-C14	1.364(9)	C8-H8	0.9300
O2-C13	1.199(8)	C6-C5	1.503(10)

O1-C6	1.204(8)	C5-C4	1.384(9)
C18-C17	1.390(11)	C4-C3	1.394(11)
C18-H18	0.9300	C4-H4	0.9300
C17-C16	1.369(13)	C3-C2	1.373(12)
C17-H17	0.9300	C3-H3	0.9300
C16-C15	1.385(13)	C2-C1	1.411(10)
C16-H16	0.9300	C2-H2	0.9300
C15-C14	1.384(10)	C1-H1	0.9300

Table A.16 Geometric parameters (°) for [Au(bpb)]Cl

Bond	**Angle (°)**	**Bond**	**Angle (°)**
N3-Au-N2	84.3(2)	C11-C12-C7	120.8(6)
N3Au-N1	165.9(2)	C11-C12-N3	124.5(6)
N2-Au-N1	81.8(2)	C7-C12-N3	114.7(5)
N3-Au-N4	81.9(2)	C12-C11-C10	118.8(7)
N2-Au-N4	165.8(2)	C12-C11-H11	120.6
N1-Au-N4	111.9(2)	C10-C11-H11	120.6
C1-N1-C5	119.7(6)	C9-C10-C11	120.8(7)
C1-N1-Au	129.2(5)	C9-C10-H10	119.6
C5-N1-Au	111.0(4)	C11-C10-H10	119.6
C6-N2-C7	128.2(6)	C10-C9-C8	120.6(7)
C6-N2-Au	118.7(5)	C10-C9-H9	119.7
C7-N2-Au	113.0(4)	C8-C9-H9	119.7
C13-N3-C12	128.4(5)	C7-C8-C9	119.2(6)
C13-N3-Au	118.8(5)	C7-C8-H8	120.4
C12-N3-Au	112.8(4)	C9-C8-H8	120.4
C18-N4-C14	119.5(6)	C8-C7-C12	119.8(6)
C18-N4-Au	129.3(5)	C8-C7-N2	124.9(6)
C14-N4-Au	110.9(5)	C12-C7-N2	115.2(5)
N4-C18-C17	121.6(7)	O1-C6-N2	127.0(6)
N4-C18-H18	119.2	O1-C6-C5	122.5(6)
C17-C18-H18	119.2	N2-C6-C5	110.5(6)
C16-C17-C18	119.8(8)	N1-C5-C4	121.5(7)
C16-C17-H17	120.1	N1-C5-C6	117.8(6)
C18-C17-H17	120.1	C4-C5-C6	120.6(7)
C17-C16-C15	118.6(7)	C5-C4-C3	118.9(7)
C17-C16-H16	120.7	C5-C4-H4	120.5
C15-C16-H16	120.7	C3-C4-H4	120.5
C14-C15-C16	119.8(7)	C2-C3-C4	119.6(6)
C14-C15-H15	120.1	C2-C3-H3	120.2
C16-C15-H15	120.1	C4-C3-H3	120.2
N4-C14-C15	120.6(7)	C3-C2-C1	119.2(7)
N4-C14-C13	117.6(6)	C3-C2-H2	120.4
C15-C14-C13	121.8(7)	C1-C2-H2	120.4
O2-C13-N3	127.5(7)	N1-C1-C2	120.9(7)

O2-C13-C14	121.8(6)	N1-C1-H1	119.5
N3-C13-C14	110.7(6)	C2-C1-H1	119.5

Appendix B

B.1 Supplementary data of the methanol substitution from *trans*-$[Ga(bpb)(CH_3OH)_2]^+$ by 4-methylpyridine

Table B.1 Data collected on the CARY for slow reaction between [*trans*-$[Ga(bpb)(CH_3OH)(4\text{-mepy})]^+$] and 4-mepy

[4-mepy] (M)	**15.0 °C** k_{obs} **(x 10^{-4}) (s^{-1})**	**25.0 °C** k_{obs} **(x 10^{-4}) (s^{-1})**	**35.0 °C** k_{obs} **(x 10^{-3}) (s^{-1})**	**45.0 °C** k_{obs} **(x 10^{-3}) (s^{-1})**
0.1	1.90	4.54	1.04	1.80
0.2	2.52			2.25
0.3	2.86	6.73	1.48	2.69
0.5	3.22	7.88	1.59	3.04
0.7	3.44	8.14	1.70	3.40
0.8		8.4	1.73	3.47
1.0	3.76	8.65	1.76	3.55

Table B.2 ln(k/T) and 1/T values for the forward and reverse reaction, as used for the Eyring plot

1/T (K^{-1})	**Ln(k_3/T)**	**Ln(k_{-3}/T)**
0.003143	-11.4235	-12.7360
0.003245	-12.2286	-13.3998
0.003354	-12.7683	-14.5717
0.00347	-13.6200	-15.0354